National Aeronautics and Space Administration
Headquarters
Washington, D.C.

14 February 1966

GCA CORPORATION
GCA TECHNOLOGY DIVISION
Bedford, Massachusetts

LABORATORY AND THEORETICAL INVESTIGATION OF CHEMICAL RELEASE EXPERIMENT

Quarterly Progress Report No. 1

Covering the Period
8 October 1965 - 8 January 1966

Contract No. NASW-1341

TABLE OF CONTENTS

LIST OF ILLUSTRATIONS (continued)

LIST OF ILLUSTRATIONS

LIST OF ILLUSTRATIONS (continued)

I INTRODUCTION

This is the first quarterly report, October 8, 1965 to January 8, 1966 under contract NASW-1341, "Laboratory and Theoretical Investigations of Chemical Release Experiments."

A. WORK SUMMARY

During this initial quarter the following work was performed.

1. Experimental

a. Chemiluminescence Measurements

(1) There was completed and analyzed measurements of the Chemiluminous reactions between (a) atmospheric constituents of (i) atomic oxygen (ii) ozone and (iii) atomic nitrogen and (b) organo-metallic compounds such as (i) trimethyl bismuth (ii) trimethyl phosphorous and (iii) dimethyl mercury and (iv) diethyl cadmium. Some extremely interesting relations for the chemiluminous reaction of the entire class of organometallic compounds (including those previously measured) were found. This work is described in Section II A.

(2) There has been initiated a program of absolute calibration of the chemiluminescence reactions. A setup has been constructed for this purpose using an NBS standard lamp. The setup involves using previously obtained chemiluminescent spectra integrated against the photomultiplier sensitivity and comparing these results with the intensity due to the standard source integrated against the photomultiplier spectral sensitivity.

The basic problem was that of comparing effectively a point source (the standard lamp) against a volume source (the chemiluminescent emitting region). This was solved by removing both sources to distances from the photomultiplier much greater than the linear dimensions of the emitting region. The results will be reported upon in the next quarterly report.

b. De-Activation Experiment

The problem of measuring the deactivation of $O(^1D)$ excited atomic oxygen by molecular oxygen has been completely analyzed. This has for its purpose the elucidation of one of the problems involved in the 6300Å atmospheric emission caused by the release of molecular oxygen in the upper atmosphere. Further, the apparatus for making the measurement in several alternative fashions has been set up and several initial runs made. This is described in Section II B.

2. Theoretical

As a concomitant part of the fluorescent study program a study was completed on the morphology of spherically symmetric fluorescent clouds in the intermediate range of optical thickness, $\tau = 1$ to 20. The concept here was to obtain realistic first approximations through a geometrical approach. It developed that the model used was applicable to other types of atmospheric clouds. Not only isotropic scattering phase functions such as that typical of atomic resonance clouds but also non-isotropic such as typical of Rayleigh scattering clouds and even Mie scattering particulate clouds are also subsumed under this model. This is discussed in Section III.

B. FISCAL SUMMARY - OCTOBER 8 - JANUARY 2

Labor Breakdown

Category	Hours	No. of People in Category
Principal Scientist	186	2
Senior Scientist	558	3
Scientist	2	1
Technician "A"	48	3
Technical Typist	0	1
Total Hours	694	

Cost Breakdown

Labor	$5190.00
Indirect Expenses	0
Materials,Supplies,Equipment	1824.00
Travel	0
Total to date including overhead	$15.500.00

C. TRAVEL SUMMARY

No trips taken this quarter.

II REPORT ON EXPERIMENTAL WORK

A. ORGANOMETALLIC CHEMILUMINESCENCE

It has been concluded from our previous extensive survey of the gas phase chemiluminous reactions of several groups of compounds with atomic oxygen, atomic nitrogen and ozone that the reactions of the organometallic compounds in general produce more intense chemiluminescence. Therefore, the reactions of some more organometallic compounds, e.g., trimethyl bismuth, trimethyl phosphorus, dimethyl mercury and diethyl cadmium have been investigated. Table 1 shows the salient features of our survey of the chemiluminous reactions of the organometallic compounds. The metallic components of the organometallic compounds studied by us are closely related to their positions in the periodic table.

2nd B Group - Zinc, Cadmium and Mercury

3rd A Group - Boron and Aluminum

4th A Group - Germanium

5th A Group - Phosphorous, Antimony and Bismuth

Some similiarities in the spectra of the chemiluminescence produced by the reactions of the organometallic compounds of the metals belonging to the same group have been found. The organometallic compounds of the remaining groups of the periodic table are either not available or do not have high enough vapor pressure, and therefore are not suitable for the chemical release study in the upper atmosphere.

TABLE 1

CHEMILUMINESCENT REACTIONS OF ORGANOMETALLICS
WITH ATMOSPHERIC CONSTITUENTS
(SPECTRAL FEATURES)

Reactant	Atomic Oxygen	Atomic Nitrogen	Ozone
Trimethyl Bismuth	Large number of bands between 3400 and 3700Å some may be BiO bands	CN red and violet systems CH and NH bands	Large number of bands between 5000 and 6900Å possibly OH band at 3060Å
Trimethyl Phosphorus	Continuum between 3700 and 6800Å, OH bands and possibly PO bands	CN red and violet systems, CH and NH bands	Continuum between 3800 and 6800Å possibly OH band at 3060Å
Dimethyl Mercury	Broad emission on 4020Å and OH band at 3060Å	CN red and violet systems CH and NH bands	Faint glow
Dietyhl Cadmium	Continuum between 3800 and 6800Å and OH band at 3060Å	CN red and violet systems CH and NH bands	----------
Triethyl Boron	BO and BO_2 bands	CN red and violet systems CH and NH bands	BO_2 bands
Trimethyl Aluminum	Continuum	CN red and violet systems CH and NH bands	Continuum
Trimethyl Antimony	α and β systems of SbO	CN red and violet systems	----------
Diethyl Zinc	Continuum	CN red and violet systems	Faint glow

However, the present study gives a fairly complete survey of the gas phase reactions of the organometallic compounds with atomic oxygen, atomic nitrogen and ozone. The recent results obtained during this quarter are summarized here.

1. Atomic Oxygen

The relative intensity and spectral features of chemiluminous reactions of atomic oxygen are given in Table 2. The spectra of chemiluminescence produced during the reactions of the organometallic compounds studied during the present quarter are shown in Figures 1 through 4. The spectrum (Figure 1) of the chemiluminescence produced during the reaction of trimethyl bismuth and atomic oxygen consists of a very large number of bands. Some of the observed peaks may be identified with the known bands of BiO[1]. The identification of the remaining bands is being attempted by photographing the spectra with larger dispersion and resolution. It may be noted that the spectrum of chemiluminescence produced during the reaction of trimethyl antimony and atomic oxygen also consists[2] of a large number of bands belonging to the α and β systems of SbO.

Another compound of the same group studied by us is trimethyl phosphorous. The spectrum (Figure 2) of the chemiluminescence produced during its reaction with atomic oxygen consists of a continuum starting at about 3800Å with increasing intensity up to about 7000Å. There is an indication of the presence of some bands at about 3000Å,

TABLE 2

REACTIONS WITH ATOMIC OXYGEN

		Spectral Features	
Reactant	Intensity	Bands	Continuum
Trimethyl Bismuth	17	BiO bands and unknown bands	----------
Trimethyl Phosphorus	26	OH band (3060Å) PO Band (3300Å)	(3700 - 6800Å)
Dimethyl Mercury	5	OH band (3060Å) Broad band (4020Å)	----------
Diethyl Cadmium	2	OH band (3060Å)	(3800 - 6800Å)

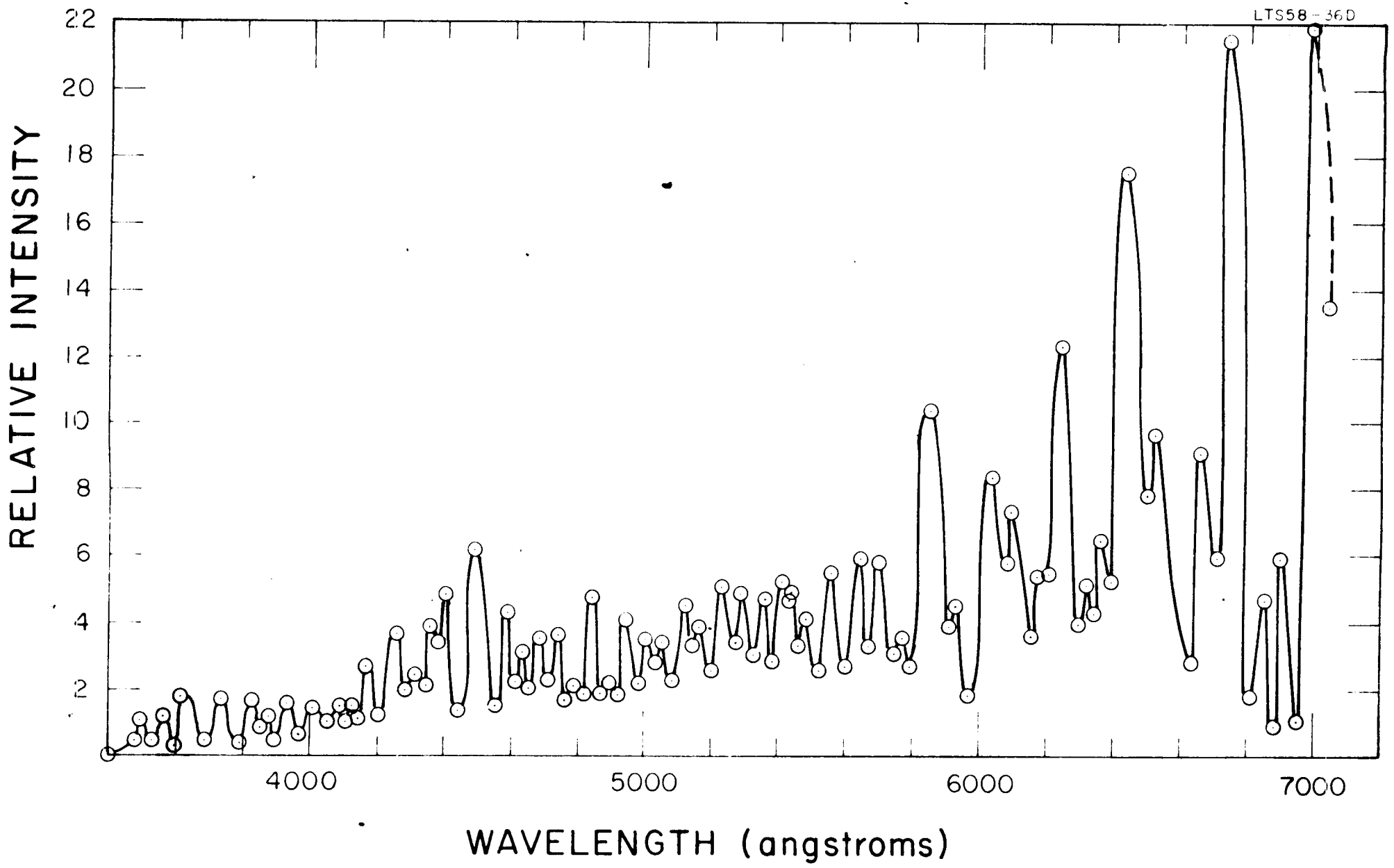

Figure 1. Spectrum of chemiluminescent reaction of atomic oxygen with trimethyl bismuth.

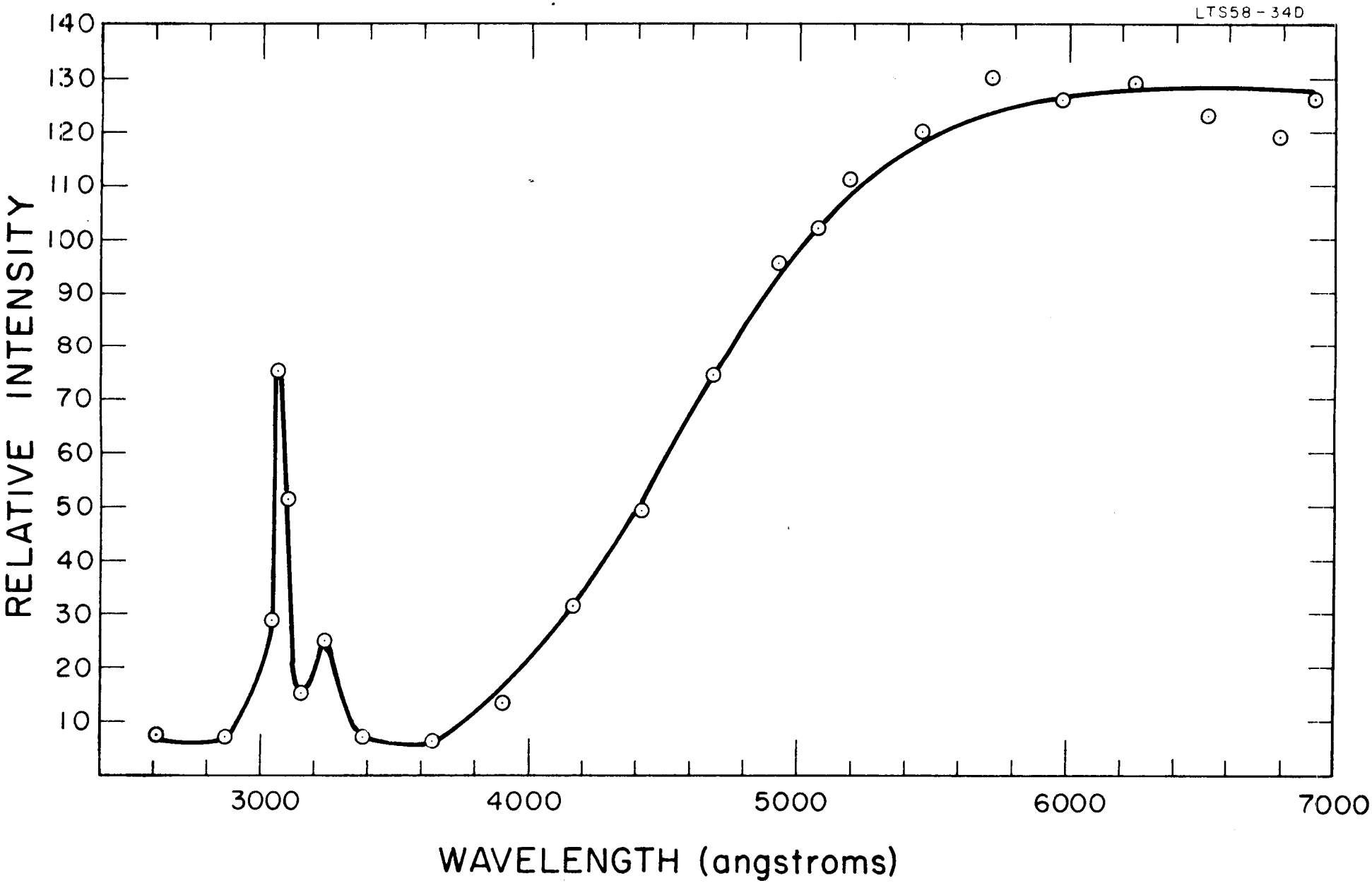

Figure 2. Spectrum of chemiluminescent reaction of atomic oxygen with trimethyl phosphine.

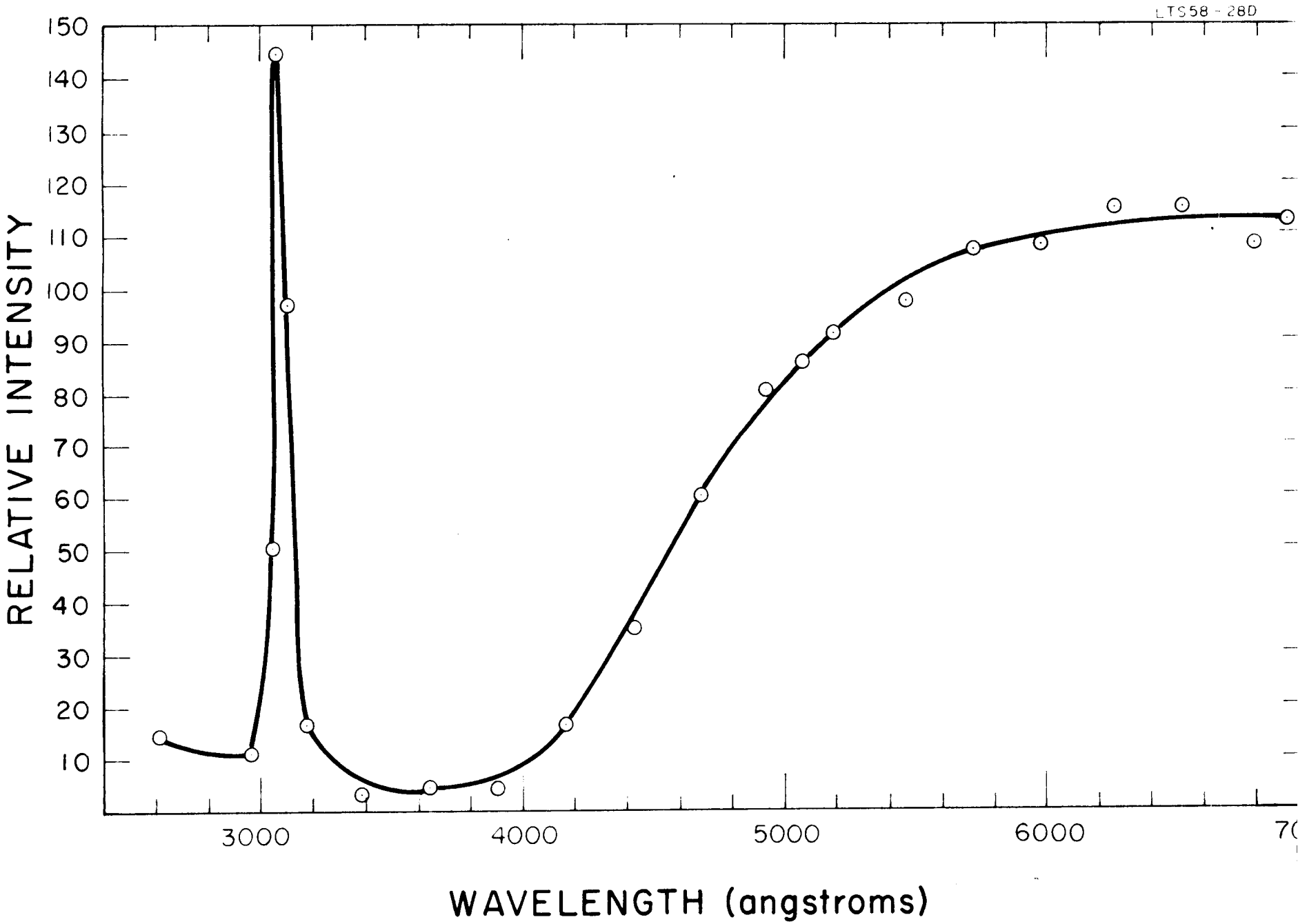

Figure 3. Spectrum of chemiluminescent reaction of atomic oxygen with diethyl cadmium.

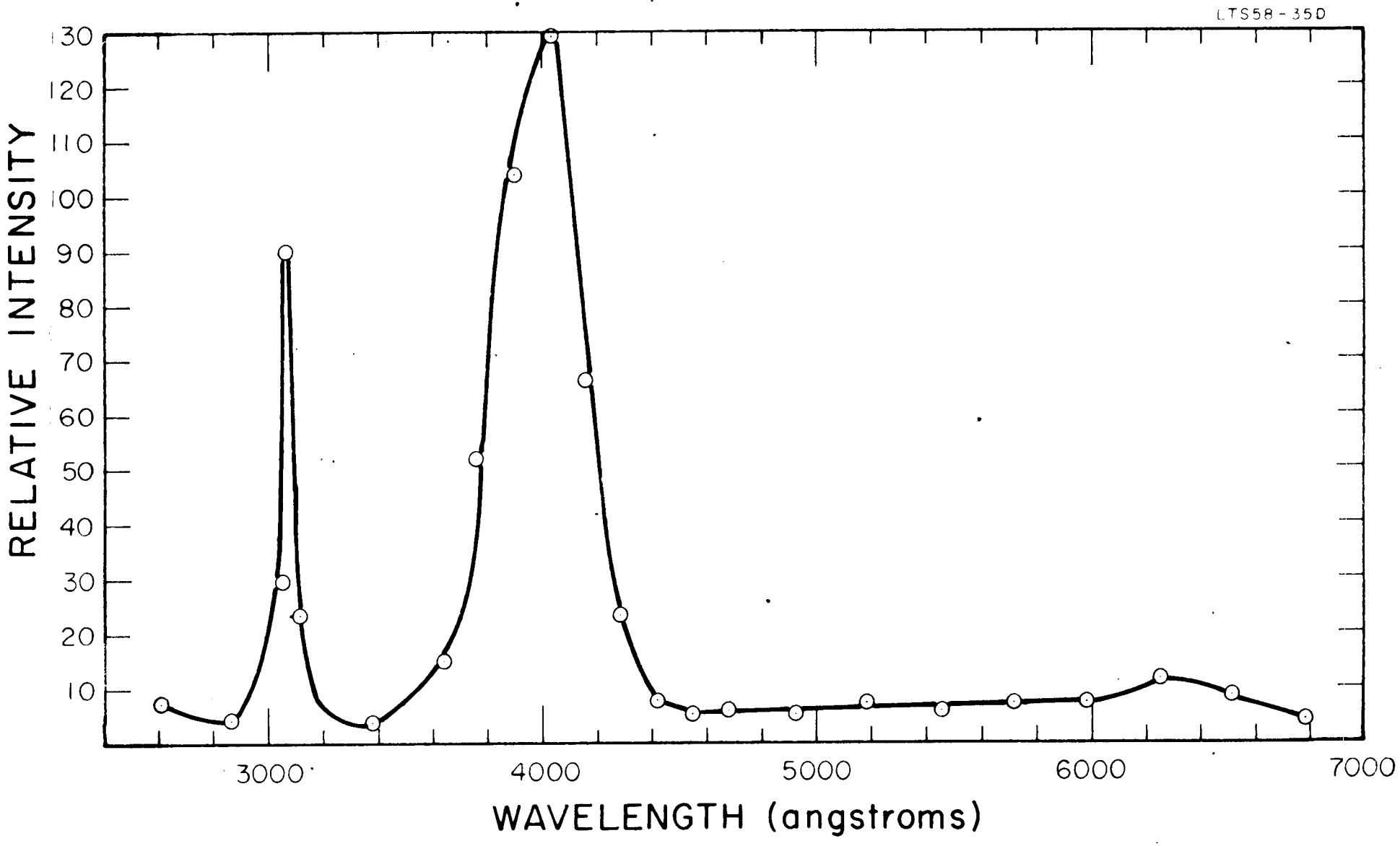

Figure 4. Spectrum of chemiluminescent reaction of atomic oxygen with dimethyl mercury.

which may be due to the OH band at 3060Å. A second peak at about 3250Å may be due to the presence of the β system of PO. According to Pearse and Gaydon[1] the strong bands of the β system of PO lie between 4360 and 3218Å.

The intensities of the chemiluminescence produced during the reactions of dimethyl mercury and the diethyl cadmium are much less than the previous two compounds. The spectrum (Figure 3) of the chemiluminescence produced during the reaction of diethyl cadmium and atomic oxygen consists of predominantly an OH band at about 3060Å and a continuum starting from 3800Å and extending to 7000Å. The spectrum (Figure 4) of the chemiluminescence produced during the reaction between dimethyl mercury and atomic oxygen consists mainly of the OH band at 3060Å and a broad band at about 4000Å. However, no definite information regarding the HgO and CdO spectrum is available.

2. Atomic Nitrogen

Table 3 shows the relative intensity and spectral features of the chemiluminescence produced during the gas phase reactions of organometallic compounds with atomic nitrogen. The spectra of the chemiluminescence produced during these reactions mainly consist of the red and violet systems of CN and some CH and NH bands. The corrected spectra of the compounds studied during the present quarter are shown in Figures 5 through 8. It may be noted that the spectral profiles are different for the different compounds. Some unidentified bands have also been observed.

TABLE 3

REACTIONS WITH ATOMIC NITROGEN

Reactant	Intensity	Spectral Features & Relative Intensity*			
		CN Red (500-6800Å)	CN Violet (3000-4200Å)	CH (4300Å)	NH (3360Å)
Trimethyl Bismuth	60	150	>350	100	100
Trimethyl Phosphorus	60	120	>150	35	20
Dimethyl Mercury	90	50	>150	25	<10
Diethyl Cadmium	17	>160	110	40	25

*The relative intensity indicated is the peak intensity of the strongest band of the system as compared to other bands in the same spectrum.

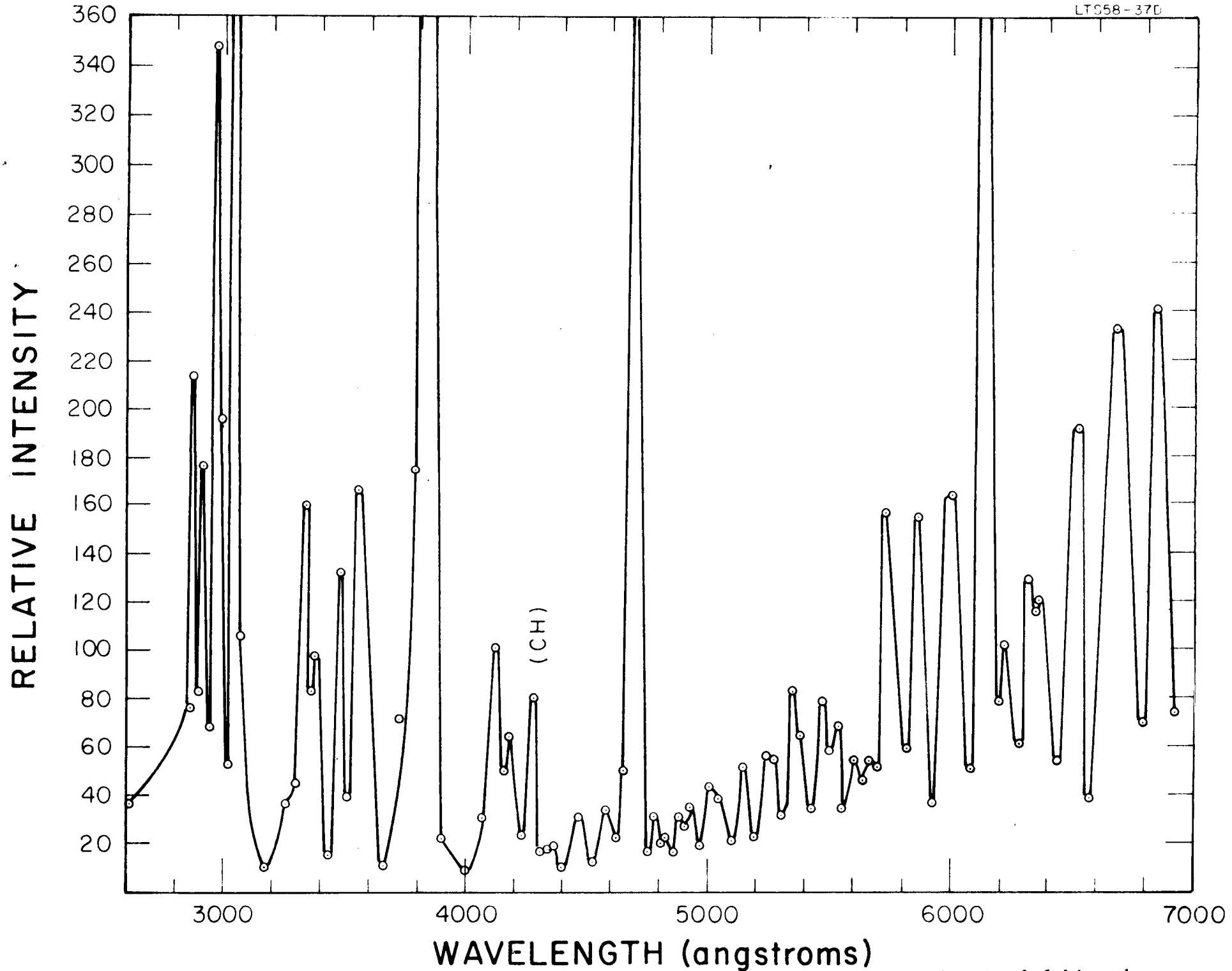

Figure 5. Spectrum of chemiluminescent reaction of atomic nitrogen with trimethyl bismuth.

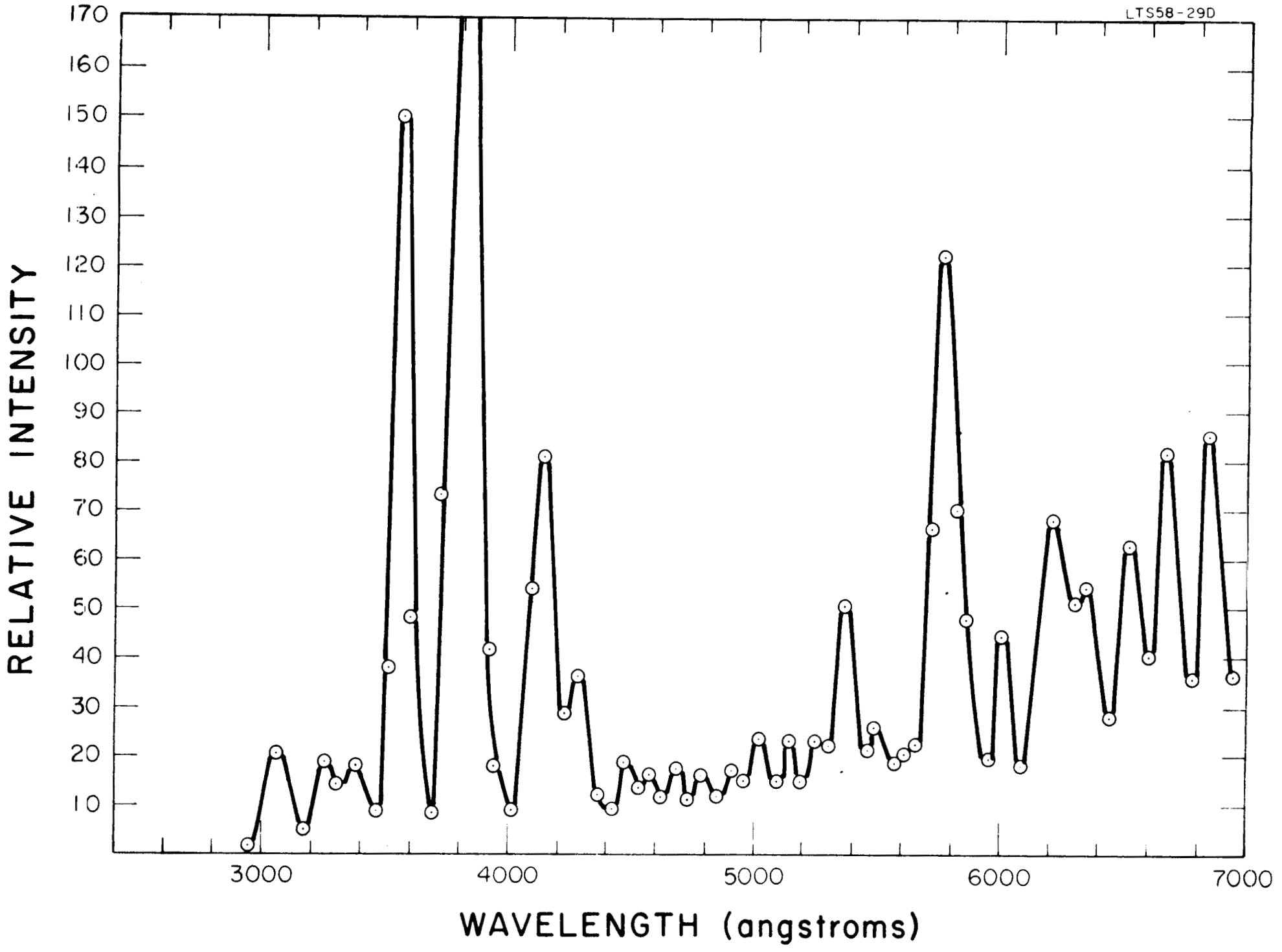

Figure 6. Spectrum of chemiluminescent reaction of atomic nitrogen with trimethyl phosphine.

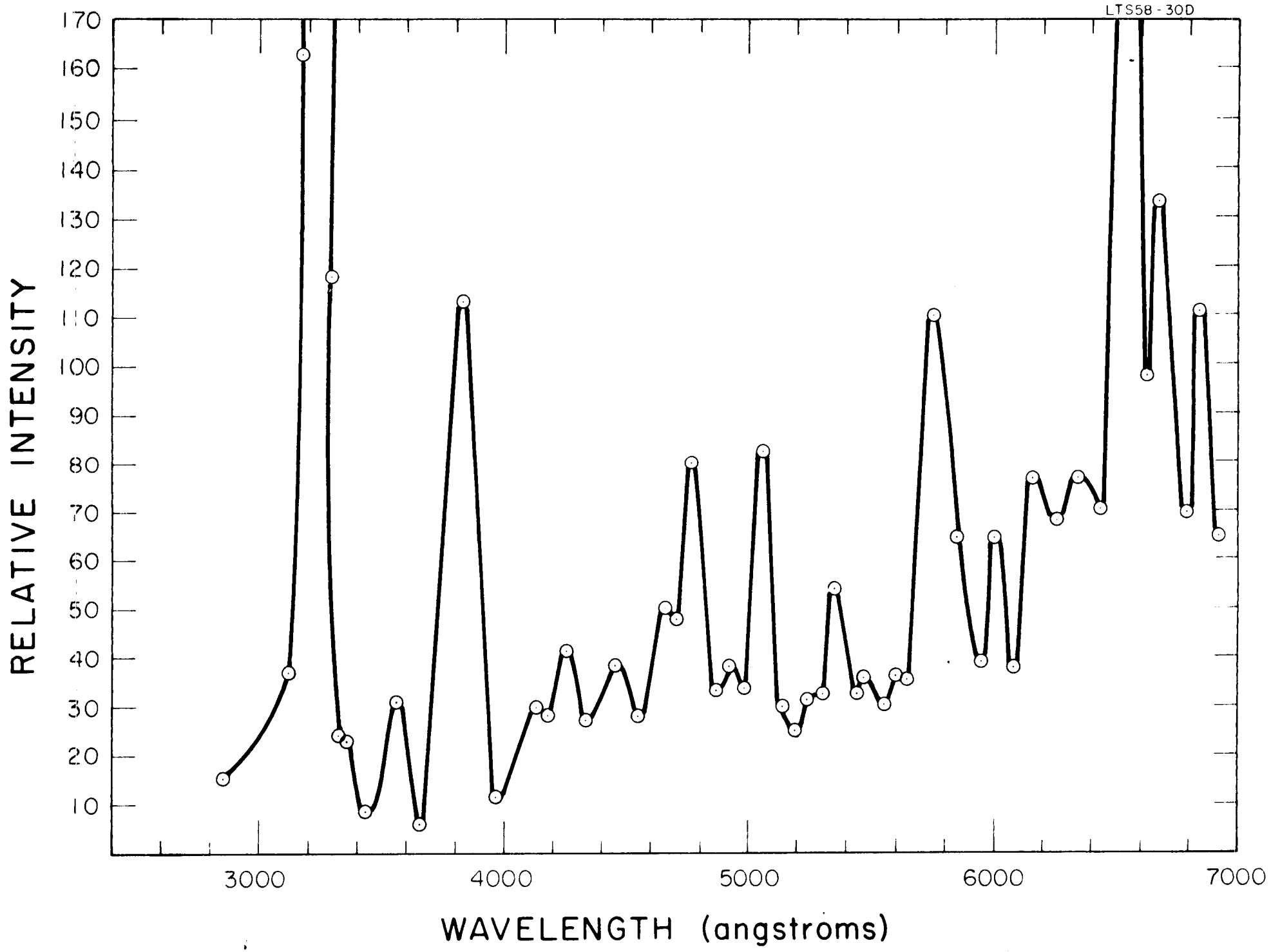

Figure 7. Spectrum of chemiluminescent reaction of atomic nitrogen with diethyl cadmium.

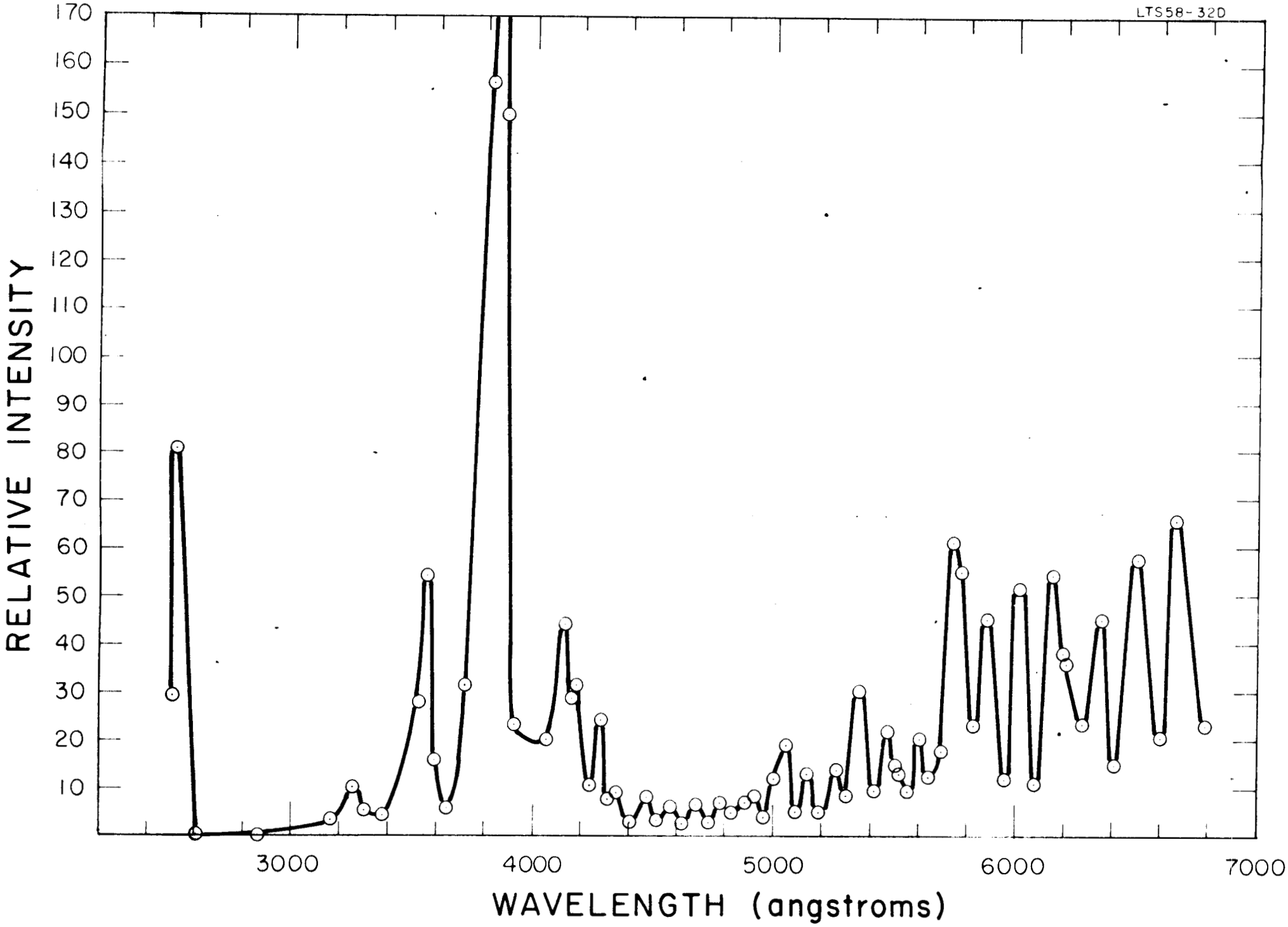

Figure 8. Spectrum of chemiluminescent reaction of atomic nitrogen with dimethyl mercury.

It is apparent from Figures 5 through 8 and from Table III that the relative intensity of CN (Red), CN (violet), CH and NH bands is different in different reactants. Moreover, the relative intensity of the bands belonging to the same system also varies. Kiess and Broida[3] have also observed a similar effect in the spectra produced by the chemiluminous reactions of several hydrocarbons with atomic nitrogen. It may be noted that among the compounds studied during the present quarter, dimethyl mercury shows the strongent chemiluminous reaction with atomic nitrogen. However, the intensity of the chemiluminous reaction between diethyl zinc with atomic nitrogen is about seven times stronger than that of dimethyl mercury.

3. Ozone

Among the compounds studied in this quarter, only diethyl cadmium did not show any visible chemiluminescence during its gas phase reaction with ozone. The spectral characteristics and the relative intensities of the chemiluminous reactions of ozone are given in Table 4. The compounds which show relatively stronger chemiluninescence during their gas phase reaction with ozone are trimethyl aluminum, triethyl boron (from the previous study) and trimethyl bismuth (studied during this quarter). The corrected spectra of the chemiluminescence produced during the reaction of trimethyl bismuth and trimethyl phosphorus with ozone are shown in Figures 9 and 10, respectively.

TABLE 4

REACTIONS WITH OZONE

Reactant	Intensity	Spectra Features	
		Bands	Continuum
Trimethyl Bismuth	8	BiO bands, OH bands and unknown bands	---------
Trimethyl Phosphorus	15	OH band (3060Å)	3800-6800Å
Dimethyl Mercury	<1	-------	---------
Diethyl Cadmium	----	-------	---------

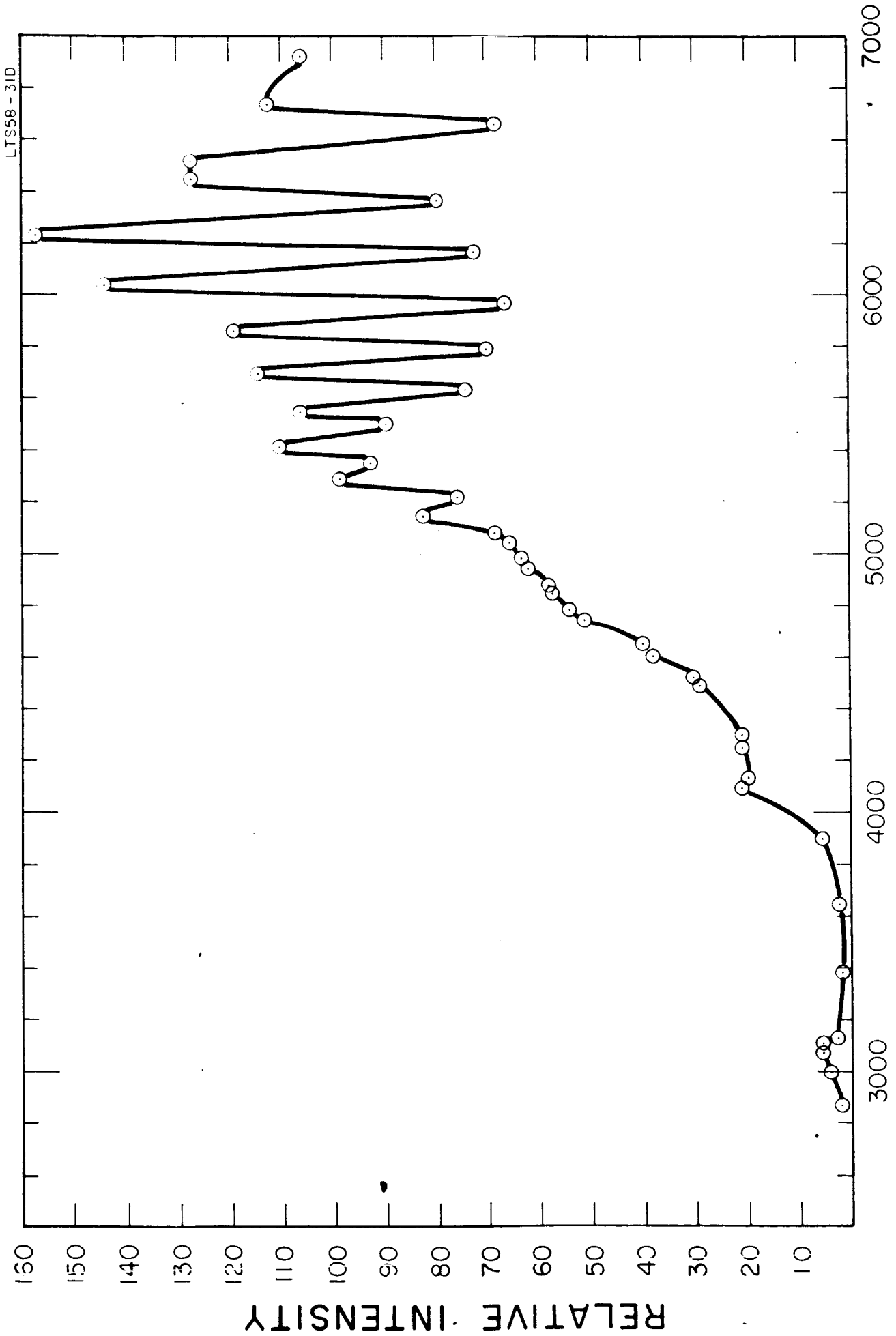

Figure 9. Spectrum of chemiluminescent reaction of ozone with trimethyl bismuth.

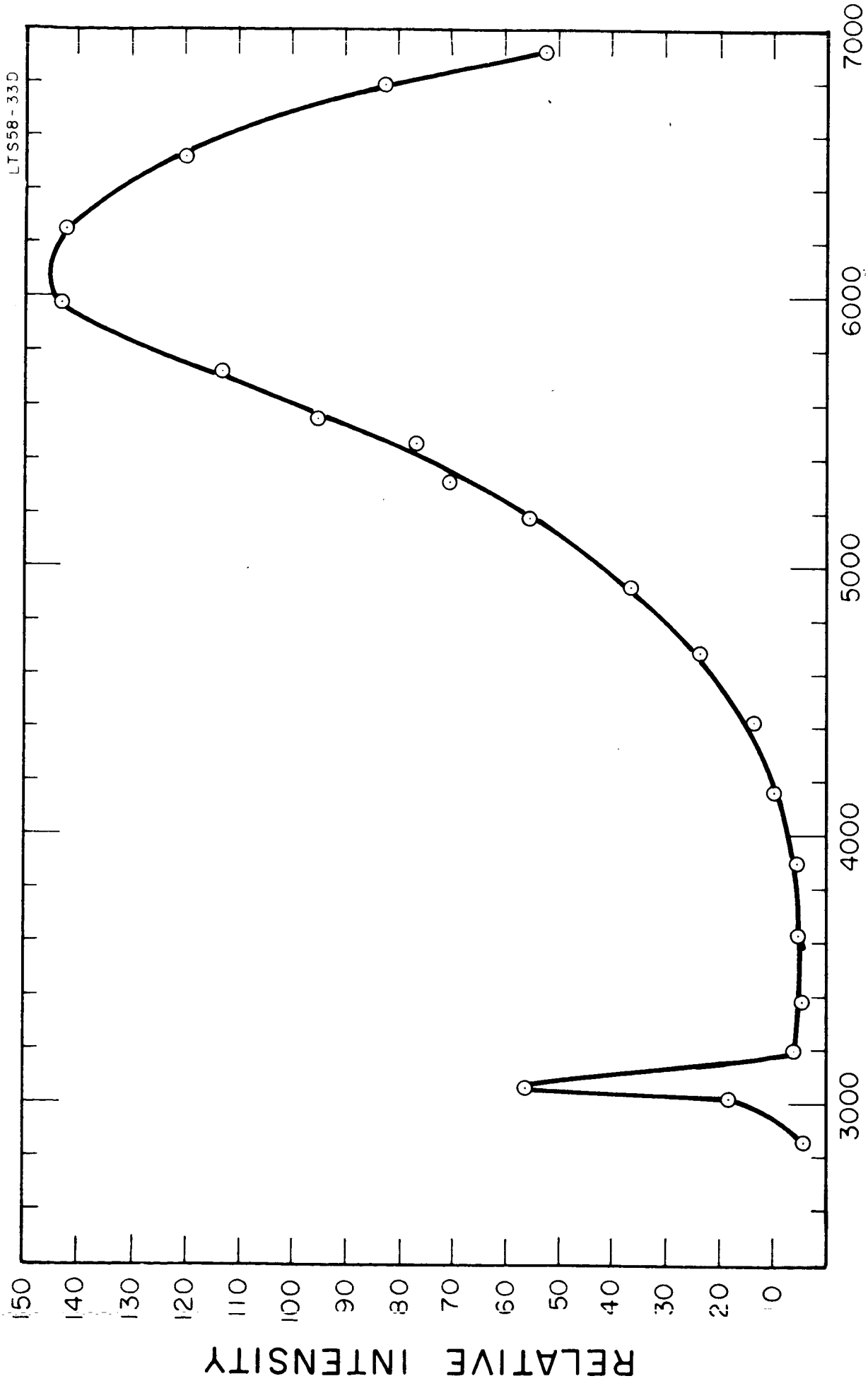

Figure 10. Spectrum of chemiluminescent reaction of ozone with trimethyl phosphine.

B. DEACTIVATION OF $O(^1D)$ BY MOLECULAR OXYGEN

This section pertains to task A5 of the work statement. Of the two subtasks required, we discuss here the problem of determining by suitable laboratory experiments the rate of deactivation of ^1D oxygen atoms by molecular oxygen. The performance of such measurements requires a suitable mode of $O(^1D)$ production as well as techniques by which the extent of ^1D deactivation can be assessed. Since a variety of processes exist and can be utilized for both aspects it is appropriate to evaluate the relative merits of the available methods.

1. Production of ^1D Oxygen Atoms

The existing techniques for the generation of ^1D oxygen atoms in the laboratory all use uv photolysis of gaseous oxides: oxygen, carbondioxide ozone, nitrous oxide and nitrogen dioxide are known to release ^1D oxygen atoms upon irradiation with light of certain wavelengths. The various photolysis mechanisms may be briefly enumerated.

a. Oxygen Dissociation

Oxygen photodissociates in the wavelength region of the Schumann continuum,

$$(1)\quad O_2 + h\nu \rightarrow O + O^* \qquad \lambda = 1350 - 1700\text{Å}$$

yielding one normal oxygen atom and one excited to the ^1D state. Subsequent reactions of O-atoms involve formation of ozone by attachment to molecular oxygen, destruction of ozone, and deactivation by O_2:

(2) $O + O_2 + M \rightarrow O_3 + M$

(3) $O + O_3 \rightarrow 2\ O_2$

(4) $O^* + O_2\ (+M) \rightarrow O_3\ (+M)$

(5) $O^* + O_3 \rightarrow 2\ O_2$

(6) $O^* + O_2 \rightarrow O + O_2$

Rate constants for reactions (2) and (3) are reasonably well known.[4] An estimate for k_5 has been given recently by Fitzsimmons and Bair.[5] It appears that reaction (5) is much faster than the corresponding reaction (3). Conversely, it is expected that $k_2 > k_4$, since reaction (4) violates the spin-rule. No information is presently available on the third body requirement of reaction (4).

The mechanism given above assumes that photodecomposition of ozone is negligible. This assumption usually is justified, because of the rapid removal of ozone by reactions (3) and (5), which keep the ozone concentration at a minimum.

b. Photolysis of Ozone

It has recently been shown by DeMore and Raper,[6] that at wavelengths around 2500Å ozone dissociates yielding O (^1D) with unity quantum yield.

(7) $O_3 + h\nu \rightarrow O_2 + O^* \qquad \lambda = 2537Å$

Subsequent reactions in the presence of oxygen are reactions (2) through (6) given above. However, complications occur due to the fact that reactions (3) and (5) both produce oxygen in excited states which can augument the rate of ozone decomposition

$$(8)\quad O_2^* + O_3 \rightarrow 2\ O_2 + O$$

Also, it is usually difficult to prevent the presence of moisture, so that the reaction

$$(9)\quad O^* + H_2O \rightarrow 2\ OH$$

and subsequent reactions involving hydroxyl radicals have to be taken into account. These difficulties have as yet prevented a complete elucidation of the entire ozone photolysis mechanism in the gas phase.

c. Carbon Dioxide Dissociation

Photodissociation of carbon dioxide via the absorption continua located in the 1200 to 1750Å wavelength region is now known to generate ^1D oxygen atoms

$$(10)\quad CO_2 + h\nu \rightarrow CO + O^* \qquad \lambda = 1200 - 1750\text{Å}$$

The mechanism has been established recently in this laboratory[7,8] and consists of two competing reactions

$$(11)\quad O^* + O^* + M \rightarrow O_2 + M$$

$$(12)\quad O^* + CO_2 \rightarrow CO_3,$$

with the CO_3 slowly decomposing. While in this work the production of CO_3 has been inferred mainly from the lack of product balance of oxygen in its various forms, the existence and production of CO_3 by photolysis of CO_2 has more recently been confirmed by the use of the matrix isolation method in conjunction with infrared analysis in experiments performed by Thompson and collaborators.[9]

The photolysis of CO_2 has the advantage that the system is initially free from any molecular oxygen. It has, however, the disadvantage that the absorption coefficients for CO_2 in the pertinent wavelength region 1200 to 1750Å are small in comparison with those for oxygen, so that the photodecomposition process (10) is replaced by photodissociation of O_2, if oxygen is added in larger amounts. The extent of oxygen admixture necessary to effect O (^1D) deactivation is dictated by the deactivation rate constant. Since it is now known from independent observations that the deactivation rate is not rapid, it is expected that the amounts of O_2 addition required for efficient deactivation may exceed the limits set by the relative values for the absorption coefficients. It appears, therefore, that the CO_2 photolysis system is less suitable for a study of deactivation due to O_2. The rate of deactivation by N_2, on the other hand, probably is very rapid so that in this case the CO_2 system has advantages. Also, the absorption of N_2 in the vacuum ultraviolet is negligible except at isolated wavelengths where N_2 absorption bands are located.

d. N_2O Photodecomposition

At wavelengths around 1850Å, the main primary process of N_2O photodecomposition is

$$(13) \quad N_2O + h\nu \rightarrow N_2 + O^* \qquad (\lambda \approx 1850\text{Å})$$

Energetically, the excited oxygen atom can be either in the ^1D or in the ^1S state, but Cvetanovic[10] has recently obtained evidence for the evolution of ^1D oxygen atoms rather than ^1S oxygen atoms. N_2O photolysis by 1849Å mercury radiation thus provides another way of generating O (^1D). Doering and Mahan[11] have shown that at this wavelength a second less important primary process is

$$(14) \quad N_2O + h\nu \rightarrow NO + N$$

comprising about 12 percent of the combined primary processes. Subsequent reactions involve mainly

$$(15) \quad O^* + N_2O \rightarrow N_2 + O_2$$

$$(16) \quad O^* + N_2O \rightarrow 2\ NO$$

$$(17) \quad N + NO \rightarrow N_2 + O$$

$$(18) \quad O \rightarrow O + M \rightarrow O_2 + M$$

The first of these is the most important as it provides the only source of nitrogen in addition to the primary process (13). The nitrogen atoms generated by reaction (14) react almost completely with NO according to reaction (17). Yamazaki and Cvetanovic[12]

have shown that the addition of scavenger gases for O (^{1}D), such as hydrogen can lower the quantum yield for N_2 evolution, so that the extent of nitrogen generated due to reaction (15) can serve as an indicator for O (^{1}D). Herein lies the value of using the photolysis of N_2O for studing reactions of ^{1}D oxygen atoms.

e. Photolysis of NO_2

The photodecomposition of NO_2 has been studied most extensively in the 3000 to 4500Å spectral region. At these wavelength, however, photodecomposition occurs via an excited NO_2 intermediate ($\lambda > 4000$Å) and by ground state oxygen atoms produced by photodissociation as the primary step, both processes being effective in varying contribution. The formation of O-atoms excited to the ^{1}D state occurs at much shorter wavelengths, namely below about 2500Å. Cvetanovic[10] has demonstrated the production of O (^{1}D) at 2288Å, by photolysing at this wavelength NO_2 in the presence of N_2O. Occurrence of reaction (15) was observed through the formation of nitrogen. It appears, however, that at present the mechanism of NO_2 photodecomposition at 2288Å is yet incompletely explored and that further work is required to make this system a useful one for O (^{1}D) reaction investigation.

2. Monitors for ^{1}D Oxygen Atoms

The determination of rate constants and deactivation coefficients is predicated upon the observation of effects specific to ^{1}D oxygen atoms. One such effect is the emission of radiation due

to the (spin-forbidden) transition $^1D - {}^3P$. Chemically, ^1D oxygen atoms can be distinguished from ground state oxygen atoms by virture of reaction (15), which excited oxygen atoms undergo easily, whereas with ground state oxygen atoms the reaction is slow. A third effect, also chemical in nature is the relative rate of ozone formation and distruction. These probabilities shall be discussed separately.

a. O (^1D) Emission

Since the $^1D - {}^3P$ transition is spin-forbidden, ^1D oxygen atoms display a long radiative lifetime. The average lifetime has a value of approximately 100 seconds. It has previously been thought that this value is too large to enable the detection of radiation due to O (^1D) in the laboratory, where the rate of chemical consumption is always much faster, but a brief calculation shows this reasoning to be faulty.

Consider, for example, the photodecomposition of CO_2 according to the mechanism given by reactions (10) through (12). In the steady state the ^1D oxygen atom concentration is calculated from

$$\frac{I}{V} = 2\, k_{11}\, [O^*]^2\, [CO_2] + k_{12}\, [O^*]\, [CO_2]$$

where the brackets signify concentrations, k_{11} and k_{12} are the rate constants associated with reactions (11) and (12) respectively, and I/V is the deposited photon flux. Solving for the oxygen atom concentration we obtain

$$(O^*) = \frac{1}{4} \frac{k_{12}}{k_{11}} \left(\sqrt{1 + \frac{8\, k_{11}\, \frac{I}{V}}{k_{12}^2\, [CO_2]}} \right) - 1$$

Previous work[8] has given $k_{11}/k_{12} = 7.8 \times 10^3$ sec. and estimates for k_{11} and k_{12} are: $k_{11} \approx 4 \times 10^{-33}$ cc^2/molecule sec and $k_{12} \approx 7 \times 10^{-19}$ cc/molecule sec. For an absorbed photonflux of 10^{15} photons/cc sec, and a CO_2 pressure of about 80 mm Hg. one calculates an atomic oxygen concentration $(O^*) = 1.8 \times 10^{14}$ atoms/cc. The radiative flux resulting from this steady state ^1D oxygen atom concentration is

$$F = \frac{1}{\tau} [O^*] = 10^{-2} \times 1.8 \times 10^{14}$$

$$\approx 10^{12} \text{ photons/cc sec.}$$

$\tau = 100$ sec is the radiative lifetime of ^1D oxygen atoms. The magnitude of the flux is sufficient for detection by means of photomultiplier filter arrangements. Even if the oxygen atom concentration were by several orders of magnitude smaller, there would still be sufficient light emission for the detection of this radiation. Since the emitted 6300Å radiation is of course the most direct and convenient mode of O (^1D) detection, it appears that this method of O (^1D) observation has particular advantages. However, other methods to be discussed below should not be ruled out.

b. The N_2O Tracing Method

To evaluate the possibility of using nitrous oxide as a chemical monitor consider again the photolysis of CO_2 by the mechanism comprised of reaction (10) through (12). Addition of a small amount of N_2O[13] to the system suppresses the recombination of oxygen atoms,[14] because reaction (15) is more rapid. Accordingly, reactions (12) and (15) are in competition with each other.

$$(12) \quad O^* + CO_2 \rightarrow CO_3$$

$$(15) \quad O^* + N_2O \rightarrow N_2 + O_2$$

The formation of NO via reaction (16) is ignored for the present purpose. It is also assumed that N_2O is present in amounts sufficiently small so that its photodecomposition is negligible in comparison with that of CO_2. If in addition the depletion of N_2O, due to the occurence of reaction (15) is neglected, the photochemical equation for nitrogen or oxygen evolution read

$$\frac{d[O_2]}{dt} = \frac{d[N_2]}{dt} = k_{15}\,[O^*]\,[N_2O]$$

$$\frac{I}{V} = k_{15}\,[O^*]\,[N_2O] + k_{12}\,[O^*]\,[CO_2]$$

leading to the expression

$$\Delta O_2 = \Delta N_2 = \frac{I\,\Delta\,t}{1 + k_{12}\,[CO_2]/k_{15}\,[N_2O]}$$

for the amount of nitrogen or oxygen evolution. If oxygen is added as a scavenger, one has to consider in addition reactions (2), (3), (4) and (6).

$$(3) \quad O^* + O_2 \rightarrow O + O_2$$

$$(4) \quad O^* + O_2(+M) \rightarrow O_3 \ (+M)$$

$$(6) \quad O^* + O_3 \rightarrow 2\ O_2$$

$$(2) \quad O + O_2 + M \rightarrow O_3 + M$$

Reaction (5) may be neglected. The amount of nitrogen evolution under these conditions is smaller, being

$$\Delta N_2 = \frac{I\ \Delta\ t}{1 + k_{12}\ [CO_2]/k_{15}\ [N_2O] + (k_3 + k_4)\ [O]_2/k_{15}[N_2O] + k_6[O]_3/k_{15}[N_2O]}$$

It can be seen that the consumption of ^1D oxygen atoms is increased not only by removal due to oxygen, but also by the subsequent fast reaction with the ozone thereby formed. If this reaction is sufficiently fast to set up steady state conditions for ozone, the rate of $O(^1D)$ removal is exactly twice that of the reaction with oxygen. It should be noted that this method cannot distinguish between reactions (3) and (4), i.e. the formation of ozone by attachment of $O(^1D)$ to oxygen, and the desired deactivation reaction because both reactions lead eventually to ozone formation.

Furthermore, it can be seen from the above equation that only ratios of rate constants can be determined. The ratio k_{12}/k_{15} is measured without oxygen addition. A preliminary value has been obtained in recent laboratory experiments from which it can be inferred on the bases $k_{12} \approx 7 \times 10^{-19}$ cc/molecule sec that $k_{15} \approx 10^{-15}$ cc/molecule sec. Accordingly, by determining the ratio $2\ (k_3 \div k_4)/k_{15}$, one can derive values for the combined rate constants $k_3 \div k_4$. If $(k_3 + k_4) \geq 10^{-15}$ cc/molecule sec, the amount of O_2 necessary to produce deactivation can be kept at less than one percent of the total gas mixture. Under these conditions, the influence of O_2 absorption upon the photolysis primary process are still tolerably small.

c. Ozone as a Tracer

The possibility of using ozone as an indicator for $O(^1D)$ atoms exists because of the different behavior of ^3P and ^1D oxygen atoms with respect to ozone and oxygen. These possibilities are best realized in the 1470Å photolysis of oxygen which will now be considered. When a flow of oxygen is irradiated at atmospheric pressure the observed ozone quantum yield is two. At these pressures, therefore, the ground state oxygen atom and the ^1D oxygen atom generated in the primary photodissociation process both attach to oxygen. The excited oxygen is most probably deactivated before being attached. The behavior at lower pressures depends on the ratio of rate constants k_2/k_5 and $(k_3 \div k_4)/k_6$ for the reactions

(2) $O + O_2 + M \rightarrow O_3 + M$

(5) $O + O_3 \rightarrow 2\ O_2$

(3) $O^* + O_2\ (+M) \rightarrow O_3\ (+M)$

(4) $O^* + O_2 \rightarrow O + O_2$

(6) $O^* + O_3 \rightarrow 2\ O_2$

Since $k_6 > k_5$ and $k_2 > k_3$ there exists a pressure range where reaction (5) can still be neglected when compared to reaction (2) while reaction (6) cannot. As a consequence, the ozone quantum yield should decrease. This is indeed in accord with observations. Previous and current expreiments in this laboratory have established that the ozone quantum yield decreases with decreasing pressure in the pressure range 25 to 760 mm Hg, keeping all other conditions (temperature, flow rate, light intensity) constant. A brief analysis of these experiments can be made in the following way.[14] Treating the reaction space next to the light source as a stirred reactor gives the equations

$$\frac{v\ \Delta O_3}{V} = \frac{I}{V} + (k_3 + k_4)(O_2)(O^*) - k_6\ (O_3)(O^*)$$

$$\frac{I}{V} = (O^*)\ \left\{ (k_3 + k_4)(O_2) + k_6\ (O_3) \right\}$$

where v is the bulk flow rate, V the reactor volume, and I the deposited light intensity. This gives an equation for ozone

$$\Delta (O_3) = \frac{I}{v} \left(1 + \frac{(k_3 + k_4)(O_2) - k_6 (O_3)}{(k_3 + k_4)(O_2) + k_6 (O_3)} \right)$$

This expression yields an ozone quantum yield $\Delta (O_3)\ v/I = 2$ for $k_6(O_3) \ll (k_3 + k_4)(O_2)$ and an ozone quantum yield of unity for $(k_3 + k_4)(O_2) = k_6 (O_3)$. The crossing point where the ozone yield is unity has been observed at room temperature to occur at pressures around 40 mm Hg of O_2, corresponding to an O_2 number density of $(O_2) = 1.2 \times 10^{18}$ molecules/cc, where light intensities of 7×10^{15} quanta/sec and flow rates around 7 cc/sec are employed. Accordingly,

$$\frac{k_3 + k_4}{k_6} = \frac{I}{v\ (O_2)} = 8 \times 10^{-4}$$

If the value $k_6 = 3 \times 10^{-12}$ cc/molecule sec given by Fitzsimmons and Bair[5] is employed our preliminary estimate for the combined rate of deactivation and ozone formation of $O\ (^1D)$ is $k_3 + k_4 = 2.5 \times 10^{-15}$ cc/molecule sec. Note that in the derivation of this value no pressure dependence was assumed to exist for reaction (3). If such a pressure dependence exists, it will be possible to separate the two rate constants k_3 and k_4.

C. CONCLUSIONS

An evaluation has been given of the various methods suitable for the determination of $O(^1D)$ deactivation by oxygen. All of these techniques generate $O(^1D)$ atoms by photolysis. One of these systems, the photolysis of oxygen has provided a preliminary estimate of the rate of $O(^1D)$ reaction with oxygen. The most profitable and convenient technique for monitoring $O(^1D)$ during reaction appears to be by detection of the 6300Å emission. Experimentation is currently underway to investigate this possibility.

III. PHASE FUNCTION OF SCATTERING FROM A HOMOGENEOUS OPTICALLY DENSE FLUORESCENT CLOUD

A. FORMULATION OF THE PHASE FUNCTION PROBLEMS

1. Motivation and Applicability

In the course of the investigation of the fluorescent behavior of released material in the upper atmosphere it became apparent that a simple treatment of the optical behavior of such clouds with regard to aspect (phase behavior) particularly during the regime of intermediate optical thickness (τ = 1-20) would be advantageous. Further it was found that such a treatment was applicable to all kinds of scattering regardless of whether the scattering was isotropic provided the optical depth was dependent in a linear fashion upon the mass. Consequently, such analysis is also applicable to atomic resonance clouds, Rayleigh scattering, and Mie scattering despite the variation of the scattering function with angle. In the Rayleigh scattering case the phase function differs from isotropicity only by a factor of two while in the Mie scattering case for $\alpha = 2\pi R/\lambda > 1$ most of the scattering is in a forward direction with lobe structure. In the Mie scattering case where scattering phase function is not uniform the geometrical shape of the scattering volume is reasonably described but the absolute brightness as a function of angle is dependent upon the phase function.

It is emphasized that the basic simple scheme analyzed is at best a first approximation to a complex phenomena really requiring the complexities of a radiation transfer calculation. Simply stated a region

is determined into which the light can penetrate. This region is further circumscribed by determining from what portion of this first region the light can escape to the observer.

The objective of this report is to depict the isophote curves in a plane image of light scattering from a homogeneous optically dense spherical cloud as they appear to an observer at an arbitrary phase angle with the sun.

2. Description of the Physical Set-up

In Figure 11 is shown a schematic of the spherical cloud of radius R being irradiated by a beam of collimated light from the sun and the image of the luminescent spherical cloud as it appears in the image plane (η, h) of an observer at an angle θ with the sun.

The immage plane (η, h) is parallel to the axis of the cloud, the Z-axis.

The line of centers, AO, which passes through the center point A of the spherical cloud and the point O, the center of the image plane, is coincident with a σ-axis of a trihedral reference system carried by the observer.

The (η, σ) plane of the observer coincides with the (x_1, y) plane of the cloud.

Since the collimated beam of sunlight is parallel to the y-axis of the cloud it is seen that the angle θ of the observer is equal to the angle between the y-axis and the σ-axis.

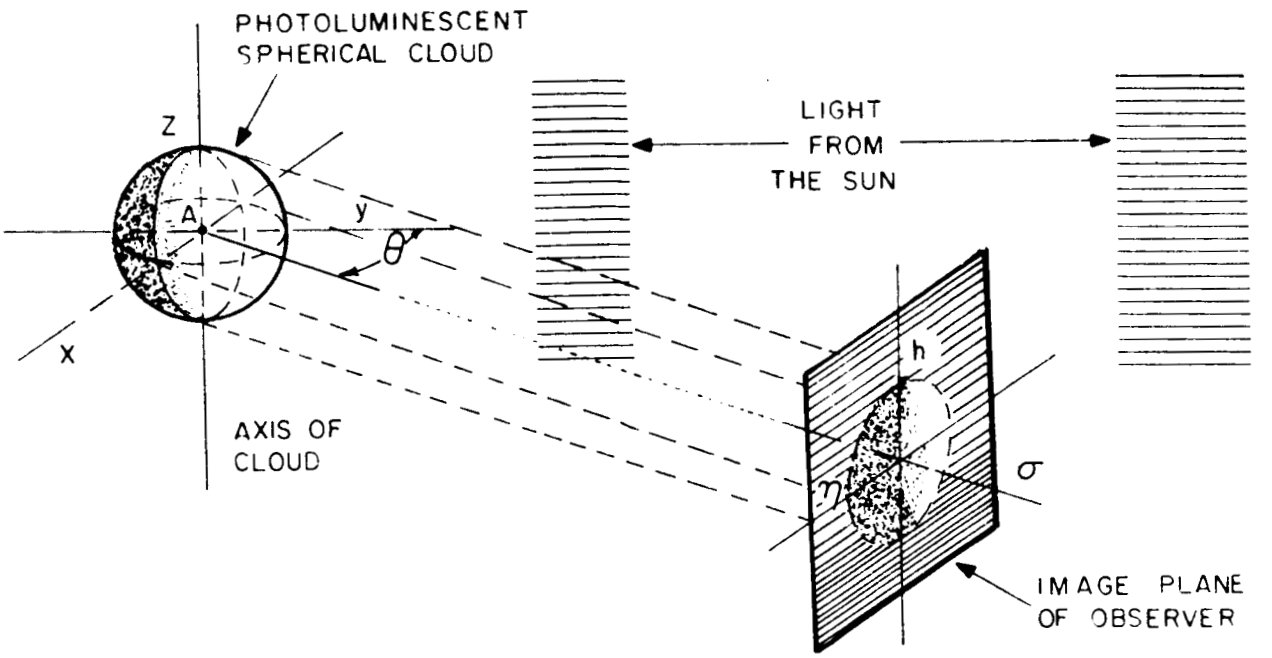

Figure 11. Schematic of photoluminescent homogeneous spherical cloud and orientation of image plane of observer at an angle θ with the sun.

2. The Photoluminescent Cloud Solid

It is assumed that the irradiated cloud is optically dense to the penetration of light for optical depths greater than unity.

Furthermore, it is assumed that the cloud is 100 percent optically then at all points penetrated by the sunlight.

It is further assumed that photons are generated homogeneously at each of these penetration points. That is to say, it is assumed that a homogeneous photoluminescent solid region is generated in the spherical cloud, as shown in Figure 12.

In Figure 12 it is seen that the parallel plane sections, h, of the spherical cloud, of radius R, shown in Figure 13, intersect the optically displaced sphere B and the spherical cloud A so as to generate a plane crescent region, defined by the intersection of two circles of radius r, wherein,

$$h^2 = R^2 - h^2 \qquad (1)$$

3. The Brightness Function $\sigma = \sigma(\eta, r, \theta)$

It is assumed that the light generated in this photoluminescent solid region can emerge from the spherical cloud only for those depths which do not exceed the unit optical length, $\sigma_e = 1$.

In other words, to the observer, only that portion of the photoluminescent cloud solid which is in front of a unit optical length displaced sphere, will emerge from the cloud and appear in the image plane

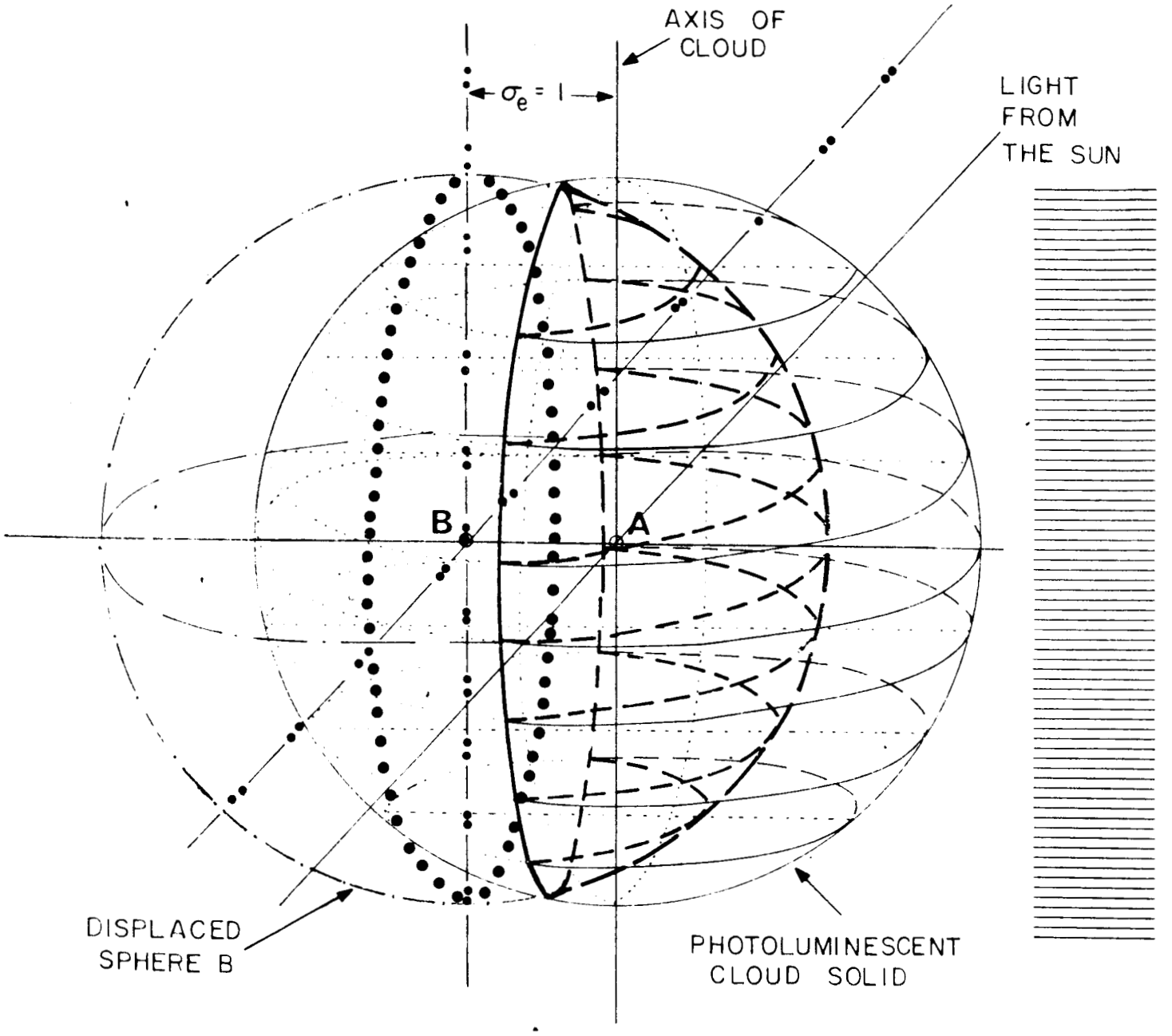

Figure 12. Schematic of photoluminescent cloud solid formed from initial spherical cloud by intersection with displaced sphere B, showing displacement distance equal to optical depth $\sigma_e = |AB| = 1$, and plane sections h.

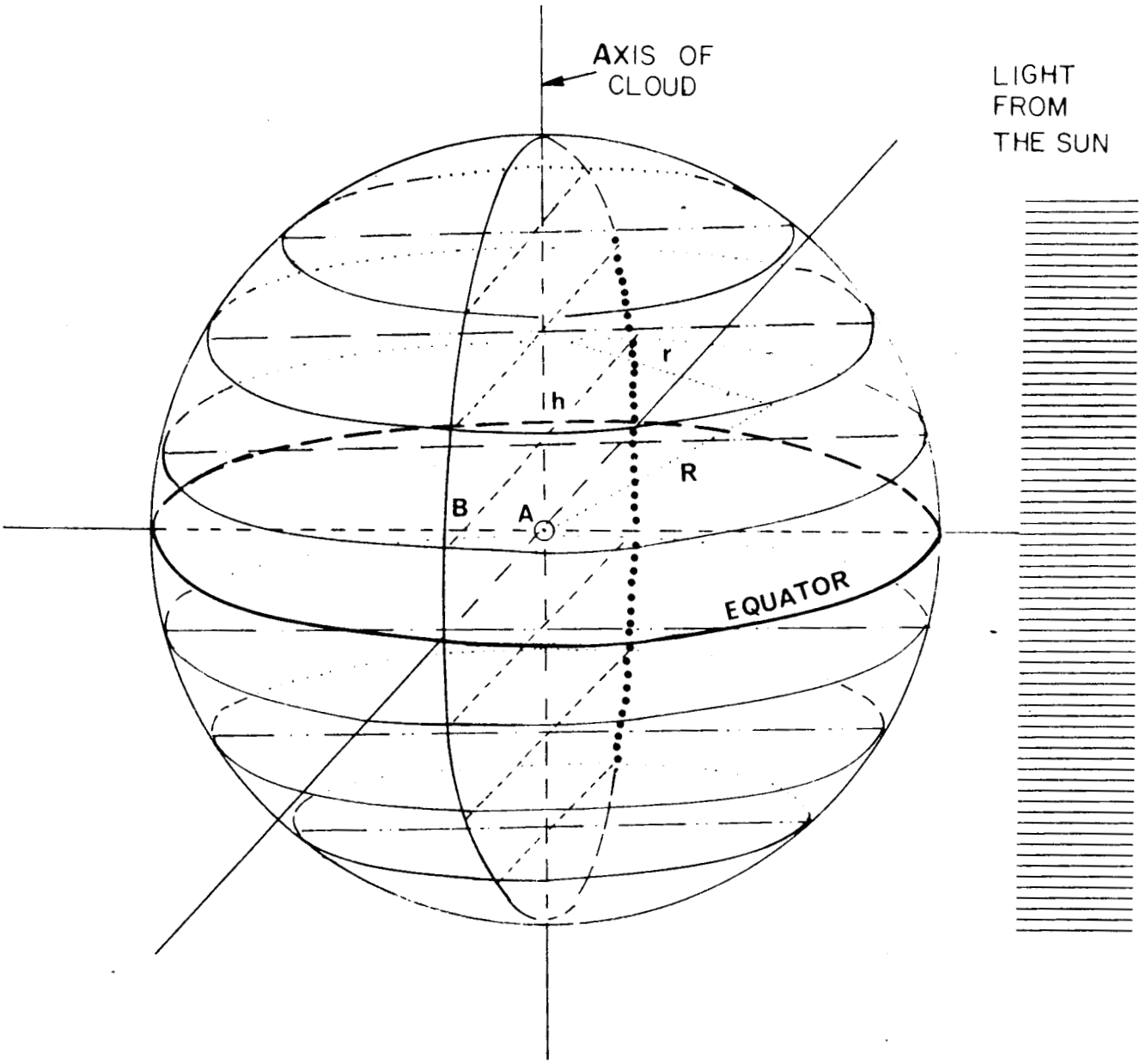

Figure 13. Schematic of spherical cloud, of radius R, showing reference plane sections h, parallel to the equator, with section radii r, $h^2 = R^2 - r^2$.

of his camera (or photosensitive device). This truncated solid is shown in Figure 14.

It is further assumed that this emerging light, in passing through the spherical cloud to the observer, does so without diminution in intensity.

The amount of light, σ_1 which reaches the image plane at the point (η, h) is defined by the formula

$$\sigma = \sigma(\eta, r, \theta) \tag{2}$$

where $\sigma = \sigma(\eta, r, \theta)$ is the length of the segment of the line, defined by the intersection of the two planes

$$\eta = \text{constant}, -R \leq \eta \leq R \tag{3a}$$

and

$$h = \pm \sqrt{R^2 - r^2}, \ 0 \leq r \leq R \tag{3b}$$

wherein η and h are defined relative to the trihedral frame (η, h, σ) of the observer, at an angle θ with the sun, cut off by the truncated photoluminescent cloud solid. The line segment $\sigma = \sigma(\eta, r, \theta)$ is illustrated in Figure 14.

For a fixed value of the angle of observation θ and for a fixed value of thesection redius r (that is, with h fixed in $h^2 = R^2 - r^2$), for a given size spherical cloud of radius R, the σ equation, (2) can be

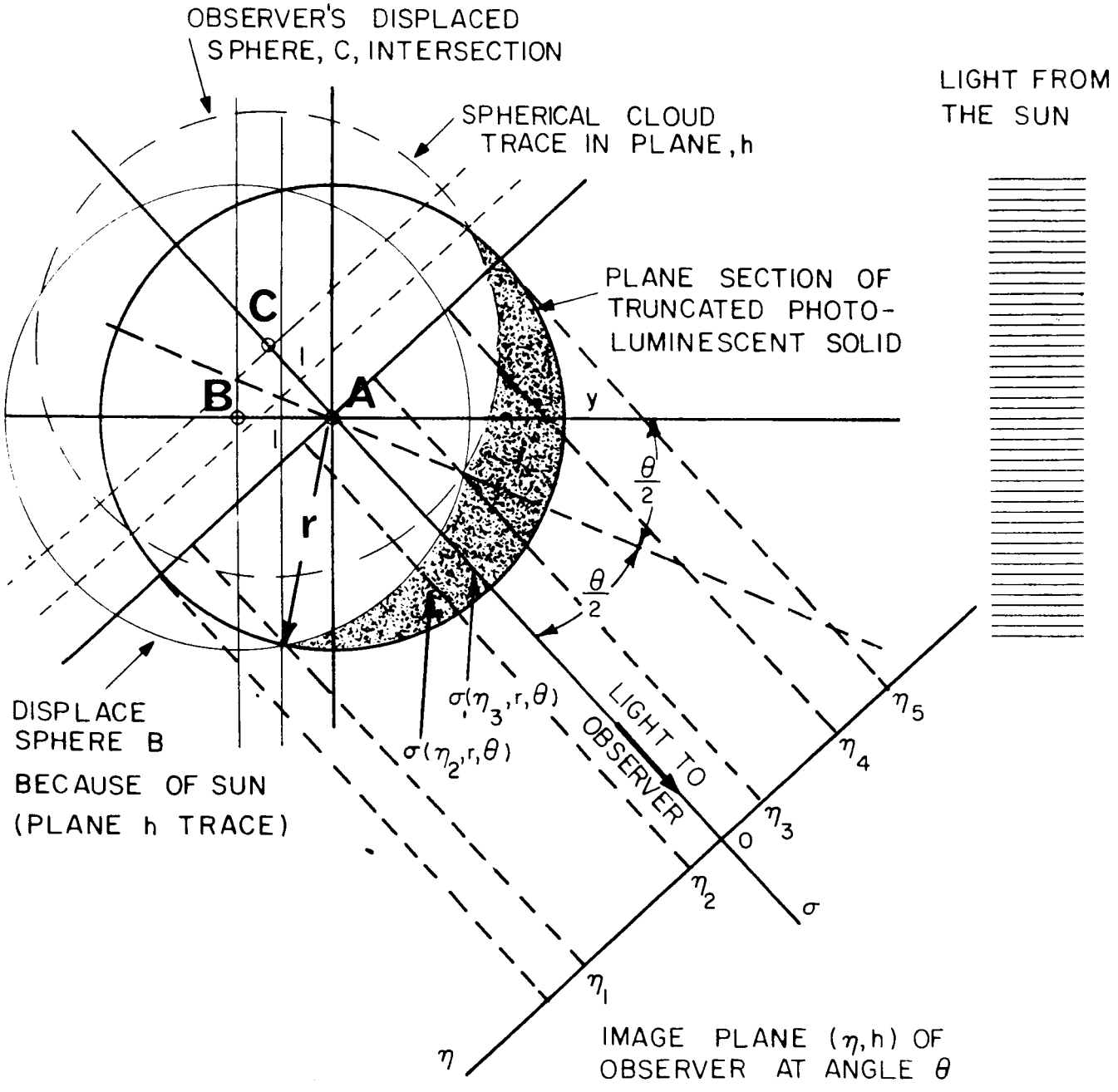

Figure 14. Schematic of plane section, h equal a constant, of truncated photoluminescent cloud solid, showing line segment $\sigma=\sigma(\eta,r,\theta)$, $h^2=R^2-r^2$, and intersection of image plane (η,h) of observer at the angle θ with the sun.

solved for the horizontal component η of the plane image point (η, h):

$$\eta = \eta(\sigma, r, \theta) \tag{4}$$

The pair of equations

$$\eta = n(\sigma, r, \theta) \text{ and } h = \pm\sqrt{R^2 - r^2} \tag{5}$$

determine the locus of the isophote

$$\sigma = \sigma(\eta_o, r_o, \theta) = \text{constant} \tag{5'}$$

in the image plane (η, h) for a given orientation angle θ of the observer.

The isophote curves, σ = constant, for the photoluminescent spherical cloud of radius R, in the image plane θ = constant, are found by plotting the points (η, h) which satisfy the equations in (5) for the specified values of R and θ, $0 \leq \theta \leq 180$ degrees, and for arbitrary values of σ in the range $0 \leq \sigma \leq 1$.

4. The Circular Arc Region of Definition of σ

This descriptive statement about the isophote curves σ = constant not only provides a statement of the phase function problem but it also specifies its solution: The operations required to define the isophote curves $\sigma = \sigma(\eta, r, \theta)$ = constant, for each phase angle θ, can be interpreted as operations to be followed graphically or analytically which lead to a representation of the isophote curves.

The operational instructions required to construct the curves $\sigma = \sigma(\eta, r, \theta)$ are embodied in the description of the plane sections of the truncated photoluminescent solid depicted in Figure 14.

The region of definition of $\sigma = \sigma(\eta, r, \theta)$ is a circular are region in a plane section, h = constant, $-R \leqq h \leqq R$, of the truncated photoluminescent cloud solid defined as that portion of the spherical cloud A which is exterior to both displaced spheres B and C, of equal radius R, illustrated in Figure 14.

In the plane h = constant, $-R \leqq h \leqq R$, the traces are circles of radius r, with $r^2 = R^2 - h^2$.

These circles have centers A, B, and C, corresponding to the axes of the homogeneous spherical cloud A, the displaced sphere B because of the sun and the observer's displaced sphere C, respectively. These center points A, B, and C, in the plane h = constant, form an isosceles triangle with sides

$$|A\,B| = 1,\ |A\,C| = 1, \text{ and } |B\,C| = 2 \sin 1/2\,\theta \tag{6}$$

In the plane h = constant, the region of $\sigma = \sigma(\eta, r, \theta)$ is the portion of circle A which is exterior to both circles B and C.

In particular, $\sigma(\eta, r, \theta)$ is defined as the length of a chord of the boundary of this circular arc region, which shord is in the direction of the σ-axis (see Figure 14).

The geometric shape of this circular arc region of definition of $\sigma = \sigma(\eta, r, \theta)$ is a function of r and θ; typical shapes are illustrated in Figure 15.

Note in Figure 15 (and in Figure 14) that the line segment $\sigma(\eta, r, \theta)$ is parallel with the direction of the line segment A C, that is, the direction defined by the angle θ, while the position of σ, relative to the circular arc region, is a function of η.

A simple excercise in constructing circular arc shape regions like those in Figure 15 points out the fact that a systematic description of the line segment $\sigma(\eta, r, \theta)$ is not a simple matter. Sketches (a), (b), and (c), of Figure 15 are usually guessed at beforehand, when $r > 1$; but sketches (d), (e), and (f) are only realized when r is in the range $1/2 < r < 1$ and θ is nearly 180 degrees.

Because of the apparent labor in a systematic, analytic tabulation and description of the possible length and orientation of the chord which defines $\sigma(\eta, r, \theta)$ for these circular arc regions, and because of the questionable, severe physical assumptions that the cloud can be both optically dense and thin, it was deemed advisable to concentrate on a graphical approach to the problem. This approach is taken up in paragraph B of this section.

In order, however, to gain an insight into the systematic complications which arise when the phase function problem is tackled from an analytic approach, paragraph C of this section takes up an analytic

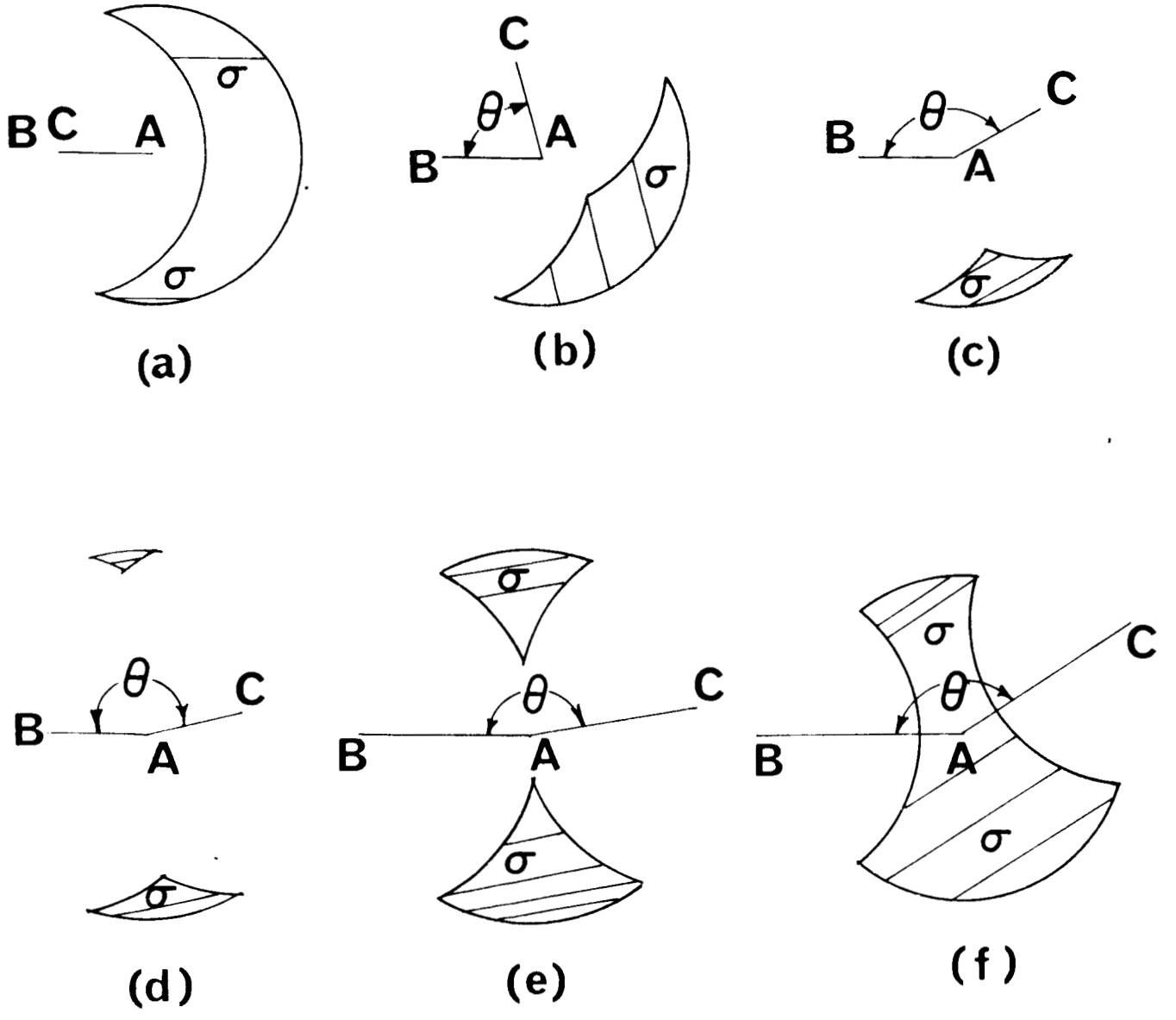

Figure 15. Sketches of typical shapes of the circular arc region of definition of $\sigma = \sigma(\eta, r, \theta)$.

description of the regions of definition of $\sigma(\eta\ \ r,\ \theta)$ in a manner which leads to specific fomulas for $\sigma(\eta,\ r,\ \theta) = \sigma$ which can be handled numerically.

B. GRAPHICAL APPROACH TO THE PROBLEM

1. The Isophote Curves in the Image Plane for Different Size Clouds

The function $\sigma = \sigma(\eta,\ r,\ \theta)$ represents the brightness at the point (η, h) of the image plane, θ = constant, of an observer who is viewing the homogeneous optically dense spherical cloud, of radius R, along lines of sight which make an angle θ with the sun (see Figures 11 and 14), wherein, $h^2 = R^2 - r^2$.

The plane h = constant, in the $\eta,\ h,\ \sigma$ trihedral frame associated with the image plane of the observer, is coincident with the plane Z = h in the (x, y, z) coordinate axes frame associated with the spherical cloud.

The circle of radius r, $r = \sqrt{R^2 - h^2}$, is the plane trace circle with the sphere R = constant.

It is evident that both r and $|h|$ have the range from 0 to R, the length of the radius of the spheres A, B, and C, and that the choice of either r or h within this range is independent of R.

The point is that the parameter r, in the definition of the brightness function $\phi = \sigma(\eta, r, \theta)$, can be shoxen in the range $0 \leq r \leq R$ for any value of R, but that once R is fixed in value, then h is determined by the simple formula $h = \pm\sqrt{R^2 - r^2}$, for the given choices of r and R.

This means two things: first, that the value of the brightness function $\sigma = (\eta, r, \theta)$ is fixed with the choice of η, r, and θ; and, second, that the brightness at the point (η, h) of the image plane, $\mathcal{Q}$, say (orientated by the choice of the parameter θ) is σ for all choices of h which satisfy the equation $h = \pm\sqrt{R^2 - r^2}$, for all choices of R such that $0 \leqq r \leqq R$.

In other words, suppose that the trace circle r is fixed at $r = 5$ (optical lengths, say) in the formula $\sigma(\eta, r, \theta)$. Then, on one hand, if the spherical cloud has a radius $R = 5$, then the value τ of the brightness function $\sigma(\eta, r, \theta)$ is $\sigma = (\eta_1, 5, \theta_1) \equiv \sigma_1$ at the point $\eta = \eta_1$, $h = 0$ in the image plane $\theta = \theta_1$, since $h = \pm\sqrt{r^2 - r^2} = \pm\sqrt{25 - 25} = 0$; while on the other hand, if the spherical cloud has the enlarged radius $R = 10$, then $\sigma = \sigma_1$ at the point $\eta = \eta_1$, $h = \pm\ 5\sqrt{3}$ of the image plane $\theta = \theta_1$, since $h = \pm\sqrt{R^2 - r^2} = \pm\sqrt{100 - 25} = \pm\sqrt{75} = \pm\ 5\sqrt{3}$, in this case. The value of the brightness σ remains at $\sigma = \sigma_1$, but σ has shifted from the point $\eta = \eta_1$, $h = 0$ to the points $\eta = \eta_1$, $h = \pm\ 5\sqrt{3}$ when the spherical cloud enlarged from $R = 5$ to $R = 10$.

Alternately, this means that if the brightness function $\sigma = \sigma(\eta, r, \theta)$ has the value $\sigma = \sigma_1$ for given values of η_1 and h_1 in the image plane $\mathcal{Q}_1$, associated with the spherical cloud $\mathcal{C}_1$, of radius $R = R_1$, say, then in the image plane $\mathcal{Q}_2$ associated with the spherical cloud $\mathcal{C}_2$, of radius $R = R_2 > R_1$, the brightness σ_2 at the point $\eta = \eta_2$, $h = h_2$ has the former value σ_1, that is, $\sigma_2 \equiv \sigma_1$, provided $\eta_2 = \eta_1$ and $r_2 = r_1$, that is,

$$R_2^2 - h_2^2 = R_1^2 - h_1^2 \tag{7}$$

This leads to the important

Lemma

The two image planes $\mathcal{Q}_1$: (η_1, h_1) and $\mathcal{Q}_2$: (η_2, h_2), at the same orientation angle θ, have isophote curves $\sigma = \sigma(\eta, r, \theta)$ = constant which map into each other under the transformations

$$\eta_2 = \eta_1,\ h_2^2 = R_2^2 - R_1^2 + h_1^3 \geq 0,\ R_2 > R_1 \tag{8}$$

The physical significance of this conclusion is that knowledge of the brightness function $\sigma(\eta, r, \theta)$ is transferable from one size cloud to another, provided both clouds are of the same species.

2. Specification of the Cloud Examined Graphically

Consider now a graphical approach to the determination of the brightness function $\sigma = \sigma(\eta, r, \theta)$ for a particular cloud $\mathcal{P}$.

If the unit optical length is chosen equal to 1 7/16 inches then a scale

$$1 : 1.4375 \tag{9a}$$

is fixed for all drawings corresponding to

$$1 \text{ optical length} \equiv 1.4375 \text{ inches} \tag{9b}$$

However, from a practical point of view an engineer scale in (9a) can be used, so that in the drawings

$$1 \text{ optical length} \equiv 1 \text{ unit} \tag{9c}$$

A cloud with radius R equal to four optical lengths (depth of penetration, that is) was used:

$$R = 4 \text{ optical depths} \equiv 5.75 \text{ inches} = 4 \text{ units} \qquad (10)$$

The following selection of trace circles r was made:

TABLE 5

TABULATION OF TRACE CIRCLES r

Designation	Optical Length	Units
No.2	0.75	0.75
No.3	1.00	1.00
No.4	1.25	1.25
No.5	1.55	1.55
No.6	2.05	2.05
No.7	2.55	2.55
No.8	3.00	3.00
No.9	3.55	3.55
No.10	4.00	4.00

3. Description of a Simple Analog Device

In order to facilitate the graphical constructions a simple analog device was designed.

This device consists of four items:

(1) a bristol board 15 inches by 20 inches

(2) a sheet of acetate of circular form with a 13-inch diameter, nearly

(3) a sheet of acetate of 10 inches by 14 inches retangular form

(4) a strip of acetate about 1 inch by 8 inches.

On the bristol board two systems of the concentric trace circles r (see Table 5) were drawn with centers A and B, displaced one optical length (depth) apart, that is one unit (= 1.4375 inches), along a y-axis, corresponding to the direction of the light from the sun (see Figures 11 and 14).

Those circles with center at A, origin of an x, y system, correspond to the plane traces of the spherical cloud $\wp$, and those circles with center at B correspond to the plane traces of the displaced sphere B because of the sun (see Figures 12, 13, and 14).

A unit circle with center at A, passing through the point B, was drawn to designate the locus of the point C, the axis of the observer's displaced sphere.

On the circular form acetate sheet the tabulated system of concentric trace circles r was inscribed, with a stylus, with a center point designated as C, as well as two perpendicular lines through the point C, to correspond to the pair of η, σ corrdinate axes.

The inscribed circles and pair of lines were rubbed over with a piece of red crayon and the acetate sheet wiped off, leaving a grid of red circles and the η, σ axes.

The point A was designated on the σ-axis, a unit distance (one optical depth) from the point C.

This circular acetate sheet was then placed on top of the bristol board with the points A matching and the overlay was then attached with a pin through the bristol board at the point A.

With the point C of the overlay turned to coincide with the point B of the bristol board, the positive η-axis was chosen to fall along the positive x-axis with the σ-axis along the y-axis, the direction of light from the sun.

By rotating (clockwise) the circular acetate overlay sheet about the fixed pin at A, the system of concentric circles, with centers at C, moves with the point C (as it (C) traces the unit (optical depth) circle on the bristol board) and a system of circular arc regions is established for each orientation θ of the sheet. These circular arc regions correspond to the plane sections of the truncated photoluminescent cloud solid (see Figures 12 and 14).

In order to easily read off the values of the segments $\sigma = \sigma(\eta, r, \theta)$, the chord length across the boundary of the circular arc region, in the σ-direction, the rectangular sheet of acetate is used.

On this 10-inch by 14-inch rectangular sheet a fine system of parallel lines was inscribed to correspond to the η = constant lines, as well as a coarse system of parallel lines to correspond to σ = constant lines.

This (η, σ) grid of inscribed lines was rubbed with a green crayon and wiped off, leaving a grid of green lines.

The principal axes $\eta = 0$ and $\sigma = 0$ were clearly marked off and the origin designated as the point C. The η lines were designated by positive and negative numbers running the range of the trace circles r (with the necessary intermediate values).

This rectangular acetate sheet was then laid over the circular acetate sheet (pinned to the bristol board at the point A) so that the two points C on the two acetate sheets were superimposed, the positive η axes of both sheets coinciding.

The system of constant η lines (of the rectangular grid) fall across the system of circular arc regions corresponding to the set of trace curves r = constant, and the intercepted chord lengths define the value σ of $\sigma(\eta, r, \theta)$.

The numerical value of σ, wherein $0 \leqq \sigma \leqq 1$ unit, is read off the line η = constant by means of the 1-inch by 8-inch strip of acetate film. This strip of acetate is scribed off in unit length which are then divided up into tenths, which are then halved. This gives a fineness of 1/20 = 0.05 units in reading off the value of σ.

4. The Circular Arc Regions for θ Equal a Constant

In applying this analog device to the phase function problems at hand it is found best to take the operations in smaller steps. That is it was found best to perform the graphical steps one at a time rather than use the completely assembled device.

For a given orientation θ (selected at 10-degree intervals) of the observer the system of circular arc regions was constructed by placing a piece of tracing paper over the bristol board (with the circular form acetate sheet removed) and using the operational scheme indicated on the bristol board as a reference background. In order to avoid confusion and

too much superposition, the trace circles r were taken in two groups according to the evenness or address of the designation number (see Table 5). That is to say the circular arc regions were drawn in on one sheet (for a given value of θ) for the trace circles No.2, No.4 No.6, No.8, No.10, while the trace circles No.3, No.5, No.7, No.9 were drawn in on another sheet (for the same value of θ).

In each case the η, σ reference lines were clearly marked on each drawing.

In Figures 16, 17, and 18 are shown representative reproductions of such drawings for $\theta = 70$, 120, and 160 degrees, respectively, for even numbered designated trace circles r.

After the circular arc regions are drawn in the value of the brightness $\sigma = \sigma(\eta, r, \theta)$ is found by means of the rectangular acetate grid. This grid is laid on top of the drawing with the η, σ axes of the drawing and sheet coinciding, and the length of chord σ across each circular arc region read off, by peering through the transparent acetate sheet, for each value of η = constant. Reading off the chord length $\sigma(\eta, r, \theta)$ is a simple matter by use of the scale on the acetate sheet.

5. The Evaluation of $\sigma = \sigma(\eta, r, \theta)$ and $\eta = \eta(\sigma, r, \theta)$

The values of $\sigma = \sigma(\eta, r, \theta)$ were read off the drawings for θ equal to multiples of 10 degrees: $\theta = 0, 10, \ldots, 170, 180$ degrees and for values of η varying by steps of 1/10 of a unit as well as the extreme values of r and apparent critical points of abrupt changes in the boundary of the circular arc regions.

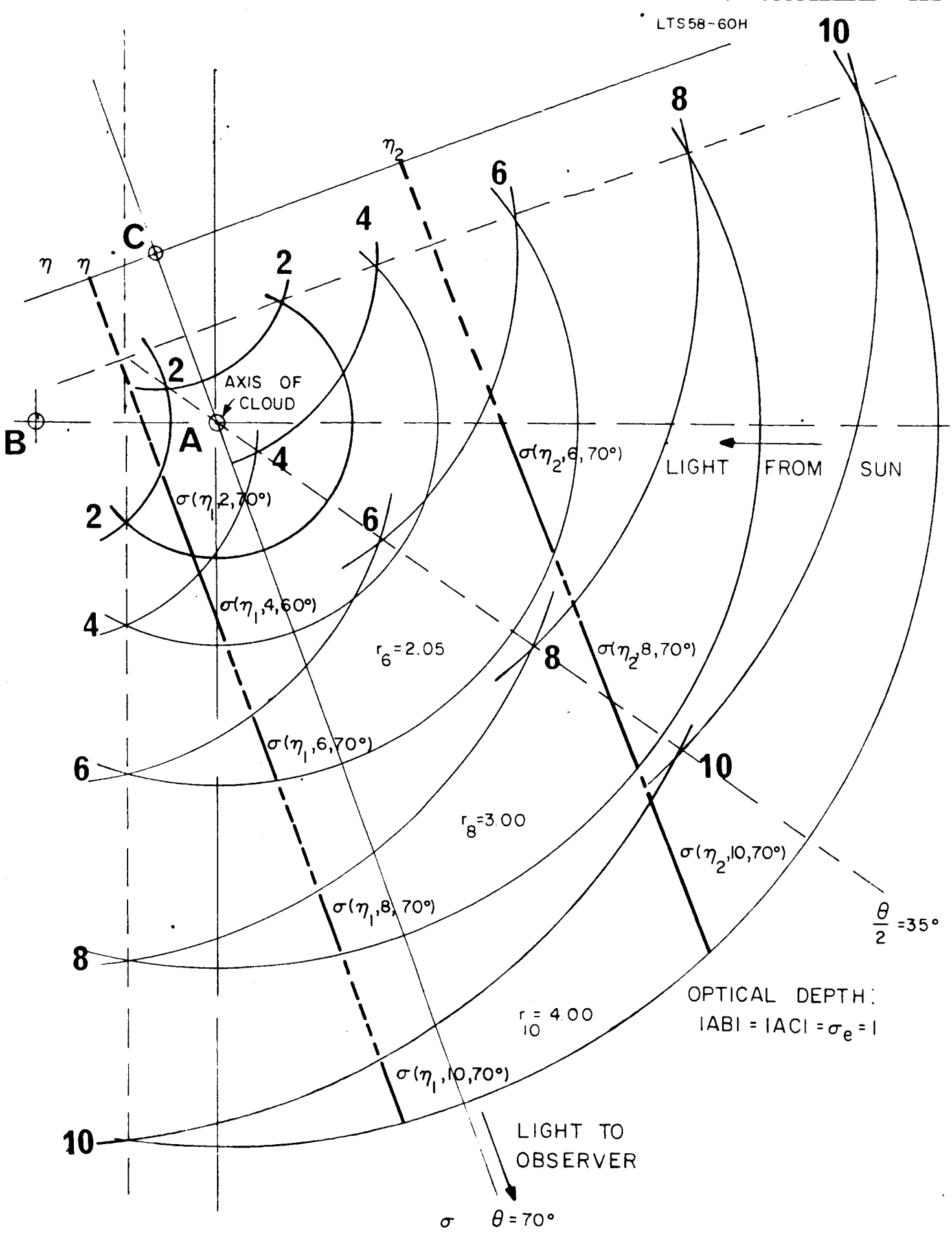

Figure 16. Plane sections of photoluminescent cloud; $\theta = 70^{\circ}$

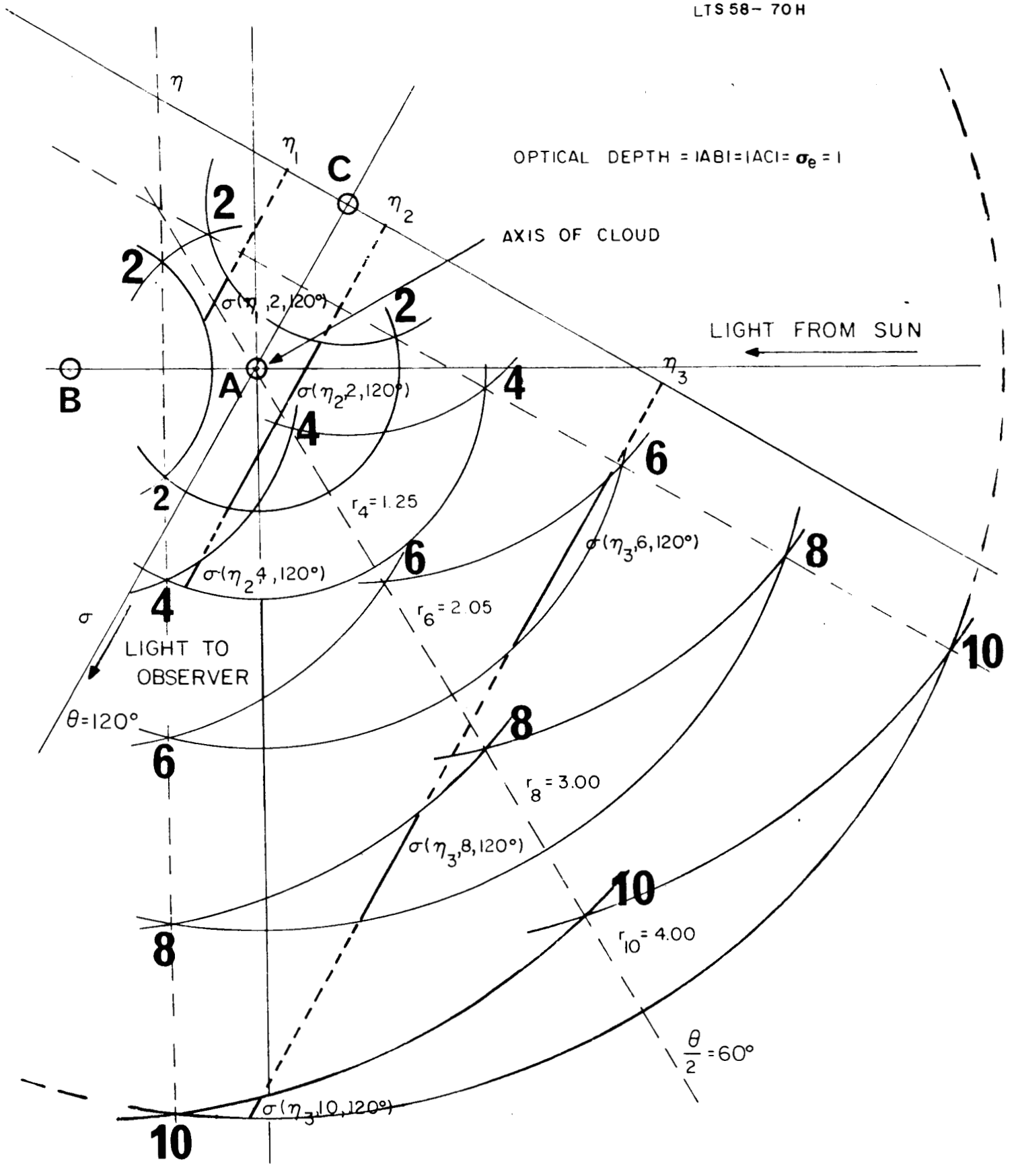

Figure 17. Plane sections of photoluminescent cloud; $\theta = 120^{\circ}$.

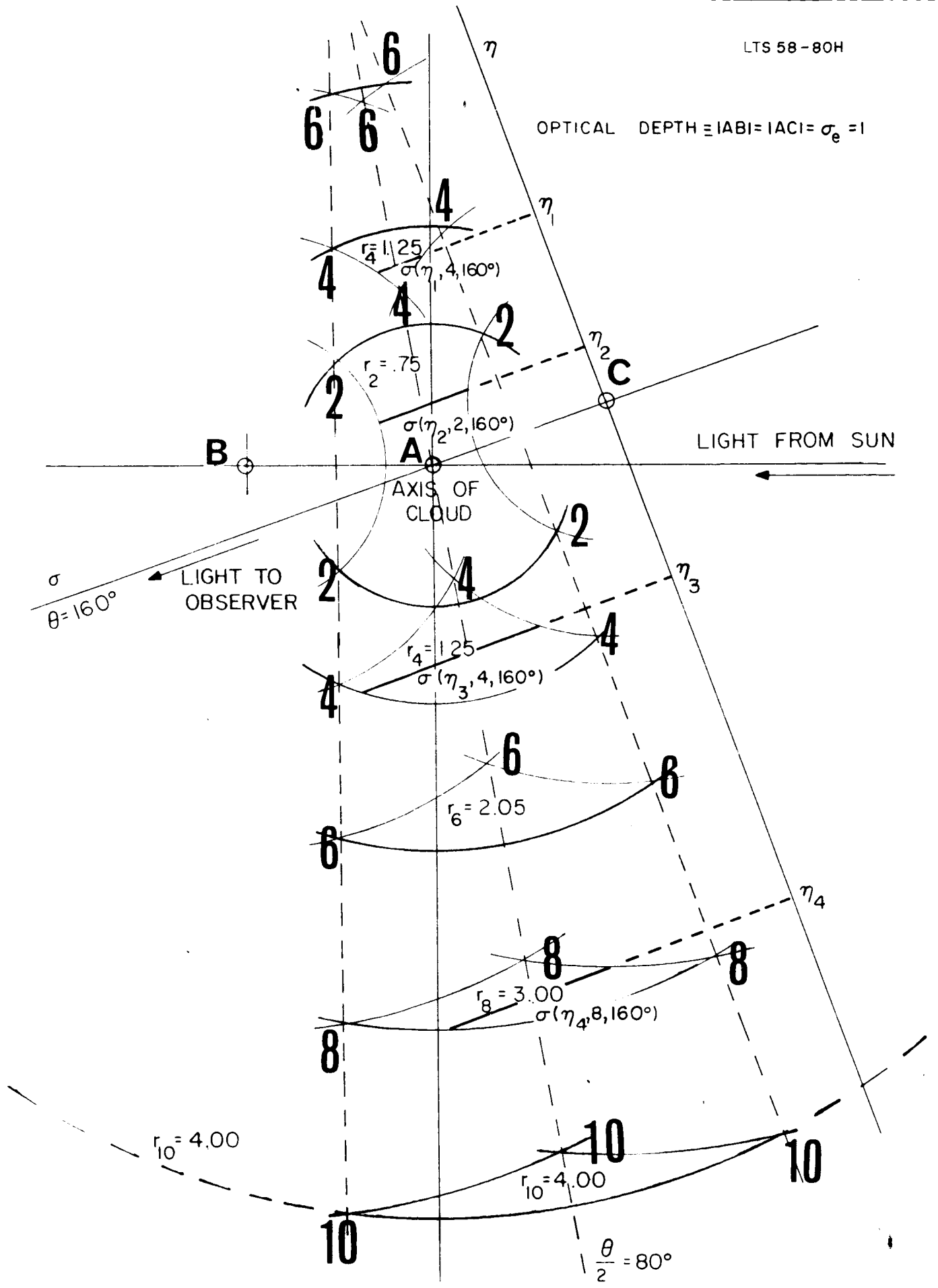

Figure 18. Plane sections of photoluminescent cloud; θ = 160°.

The data sheets for the values of $\sigma(\eta, r, \theta)$, for each orientation angle θ, were filled out by direct reading of the chord lengths on the drawings. A sample data sheet is shown in Table 6 corresponding to $\theta = 70$ degrees. In Figures 16, 17, and 18 note the constructed $\sigma(\eta, r, \theta)$ chord segments.

For a given orientation angle θ, the table of values of $\sigma = \sigma(\eta, r, \theta)$ shows how the image of the apparent brightness (of the photoluminescent cloud) varies in the image plane η, h, where $h^2 = R^2 - r^2$ and R = 4 optical depths = 4 units.

In such an image plane, for a given value of h, (that is, r) the value of σ varies from the value zero at one boundary (of the spherical cloud) to a possible maximum value $\sigma = 1$ and then other back to a zero value again at the other boundary of the cloud.

The horizontal component γ of the image point (η, h) of the isophote σ = constant, $0 \leqq \sigma \leqq 1$, is designated by formula (4) and is defined by the pair of equations

$$\sigma = \sigma(\eta, r, \theta) \tag{11a}$$

and

$$\sigma = \text{constant} = \frac{1}{10}s, \; s = 0,1,\ldots,9,10, \text{ say} \tag{11b}$$

For a given orientation angle θ and trace circle r, the horizontal components η corresponding to $\sigma = 1/10s$, for a fixed value of s, s=0,1,2,...,9,10, are found graphically by plotting the values of the

TABLE 6

VARIATION OF BRIGHTNESS $\sigma = \sigma(\eta, r, \theta)$ OF IMAGE POINT (η, h) WITH SECTION RADIUS r, $h^2 = R^2 - r^2$, AND HORIZONTAL DISPLACEMENT η FROM PLANE THROUGH AXIS OF PHOTOLUMINESCENT CLOUD OF RADIUS R, WHEN OBSERVER IS AT ANGLE $\theta = 70^\circ$

$\sigma(\eta, r, \theta)$ $\theta = 70^\circ$

	2		3		4		5		6		7		8		9		10	
	r = .75		r = 1.00		r = 1.25		r = 1.55		r = 2.05		r = 2.55		r = 3.00		r = 3.55		r = 4.00	
η	$+\eta$	$-\eta$	$+\eta$	$-\eta$	$+\eta$	$-\eta$	$+\eta$	$-\eta$	$+\eta$	$-\eta$	$+\eta$	$-\eta$	$+\eta$	$-\eta$	$+\eta$	$-\eta$	$+\eta$	$-\eta$
0	1.0	1.0	.96	.96	.77	.77	.67	.67	.58	.58	.53	.53	.50	.50	.45	.45	.45	.45
.1	1.0	1.0	.76	1.0	.66	.92	.60	.76	.54	.63	.50	.56	.46	.53	.44	.50	.43	.47
.2	1.0	1.0	.65	1.0	.58	1.0	.54	.85	.50	.69	.45	.61	.44	.56	.42	.53	.40	.50
.3	.65	1.0	.53	1.0	.50	1.0	.47	.95	.44	.76	.43	.65	.40	.60	.37	.55	.38	.54
.4	.47	1.0	.43	1.0	.40	1.0	.40	1.0	.38	.85	.37	.70	.36	.64	.36	.60	.36	.55
.5	.30	1.0	.33	1.0	.33	1.0	.35	1.0	.34	.90	.34	.76	.34	.67	.34	.62	.33	.58
.6	.22	.85	.21	1.0	.24	1.0	.27	1.0	.30	.98	.30	.80	.31	.70	.31	.65	.32	.61
.7	0	.45	.11	1.0	.15	1.0	.20	1.0	.23	1.0	.26	.85	.26	.75	.28	.67	.30	.64
.75	0	0	.07	1.0	.07	1.0	.17	1.0	.21	1.0	.24	.90	.25	.76	.27	.69	.28	.65
.8	0	0	0	1.0	.06	1.0	.13	1.0	.18	1.0	.22	.91	.26	.80	.25	.71	.27	.67
.9	0	0	0	.95	0	1.0	.07	1.0	.15	1.0	.18	.98	.20	.83	.23	.74	.23	.68
1.0	0	0	0	0	0	1.0	0	1.0	.09	1.0	.15	1.0	.17	.88	.20	.78	.21	.72
1.1	0	0	0	0	0	1.0	0	1.0	.04	1.0	.10	1.0	.15	.94	.18	.82	.19	.75
1.2					0	.60	0	1.0	0	1.0	.06	1.0	.11	.97	.15	.87	.17	.78
1.25					0	0	0	1.0	0	1.0	.02	1.0	.09	1.0	.13	.88	.15	.80
1.3							0	1.0	0	1.0	0	1.0	.07	1.0	.10	.90	.15	.81
1.4							0	1.0	0	1.0	0	1.0	.05	1.0	.09	.94	.12	.85
1.5							0	.67	0	1.0	0	1.0	0	1.0	.06	1.0	.10	.88
1.6									0	1.0	0	1.0	0	1.0	.03	1.0	.07	.93
1.7									0	1.0	0	1.0	0	1.0	0	1.0	.05	.96
1.8									0	1.0	0	1.0	0	1.0	0	1.0	.02	1.0
1.9									0	1.0	0	1.0	0	1.0	0	1.0	0	1.0
2.0									0	.60	0	1.0	0	1.0	0	1.0	0	1.0
2.1											0	1.0	0	1.0	0	1.0	00	1.0
2.2											0	1.0	0	1.0	0	1.0	0	1.0
2.3											0	1.0	0	1.0	0	1.0	0	1.0
2.4											0	1.0	0	1.0	0	1.0	0	1.0
2.5											0	.77	0	1.0	0	1.0	0	1.0

TABLE 6 (Continued)

VARIATION OF BRIGHTNESS $\sigma = \sigma(\eta, r, \theta)$ OF IMAGE POINT (η, h) WITH SECTION RADIUS r, $h^2 = R^2 - r^2$, AND HORIZONTAL DISPLACEMENT η FROM PLANE THROUGH AXIS OF PHOTOLUMINESCENT CLOUD OF RADIUS R, WHEN OBSERVER IS AT ANGLE $\theta = 70^\circ$

$\sigma(\eta, r, \theta)$ $\theta = 70^\circ$

	2		3		4		5		6		7		8		9		10	
	r = .75		r = 1.00		r = 1.25		r = 1.55		r = 2.05		r = 2.55		r = 3.00		r = 3.55		r = 4.00	
η	$+\eta$	$-\eta$	$+\eta$	$-\eta$	$+\eta$	$-\eta$	$+\eta$	$-\eta$	$+\eta$	$-\eta$	$+\eta$	$-\eta$	$+\eta$	$-\eta$	$+\eta$	$-\eta$	$+\eta$	$-\eta$
2.6													0	1.0	0	1.0	0	1.0
2.7													0	1.0	0	1.0	0	1.0
2.8													0	1.0	0	1.0	0	1.0
2.9													0	1.0	0	1.0	0	1.0
3.0													0	0	0	1.0	0	1.0
3.1															0	1.0	0	1.0
3.2															0	1.0	0	1.0
3.3															0	1.0	0	1.0
3.4															0	1.0	0	1.0
3.5															0	0	0	1.0
3.6																	0	1.0
3.7																	0	1.0
3.8																	0	1.0
3.9																	0	1.0
4.0																	0	0

brightness function $\sigma = \sigma(\eta, r, \theta)$, as given by the table of values of $\sigma(\eta, r, \theta)$, σ versus η, and then intersecting this brightness curve with the horizontal line $\sigma = 1/10s$, s fixed.

In order to smooth out the values of $\sigma(\eta, r, \theta)$ (as read off the drawings) at was deemed advisable to make a blown up plot of the brightness function curve, σ versus η, that is, $\sigma = \sigma(\eta, r, \theta)$, for r = constant and θ equal a constant, and sketching* in the σ versus η curve.

The values of $\eta = \eta(\sigma, r, \theta)$, $\sigma = 1/10s$, for s = 0,1,2,..., 9,10 were read off the σ versus η curves for the following thirteen values of θ: 0,10,20,30,40,50,70,90,110,130,150,170, and 180 degrees and are presented in the series of tables designated as Tables 7 through 19, respectively.

The set of isophote curves $\sigma = 1/10s$, s in the range zero to ten, in the image planes (η, h) corresponding to these same thirteen values of θ, are presented in the series of figures designated as Figures 19 through 31, respectively (the reader is also referred to the Frontispiece for a pictorial representation of Figure 19).

---

* It was not evident how much liberty could be taken in this smoothing out operation, to distinguish between reading fluctuations and functional variations. The final isophote plots indicated, however, that minor individual point fluctuations still persist in the values of $\eta = \eta(\sigma_1, r_1, \theta)$ which could be reduced to some further extent.

TABLE 7

VARIATION OF HORIZONTAL COMPONENT $\eta = \eta(\sigma, r, \theta)$ OF PLANE IMAGE POINT (η, h), $h = \pm\sqrt{R^2 - r^2}$, WITH SECTION RADIUS r AND ISOPHOTE VALUE σ, WHEN $\theta = 0^\circ$; OPTICAL DEPTH $\sigma_e = 1$

				$\eta = \eta(\sigma, r, \theta)$ $\theta = 0^\circ$					
σ	r = .75	r = 1.00	r = 1.25	r = 1.55	r = 2.05	r = 2.55	r = 3.00	r = 3.55	r = 4.00
0	.75 -.75	1.00 -1.00	1.25 -1.25	1.55 -1.55	2.05 -2.05	2.55 -2.55	3.00 -3.00	3.55 -3.55	4.00 -4.00
.1	.745 -.745	.99 -.99	1.245 -1.245	1.545 -1.545	2.045 -2.045	2.55 -2.55	3.00 -3.00	3.55 -3.55	4.00 -4.00
.2	.74 -.74	.985 -.985	1.240 -1.240	1.54 -1.54	2.04 -2.04	2.55 -2.55	3.00 -3.00	3.55 -3.55	4.00 -4.00
.3	.73 -.73	.98 -.98	1.235 -1.235	1.535 -1.535	2.035 -2.035	2.548 -2.548	3.00 -3.00	3.548 -3.548	4.00 -4.00
.4	.72 -.72	.975 -.975	1.230 -1.230	1.530 -1.530	2.030 -2.030	2.546 -2.546	2.99 -2.99	3.546 -3.546	4.00 -4.00
.5	.71 -.71	.97 -.97	1.225 -1.25	1.52 -1.52	2.025 -2.025	2.544 -2.544	2.987 -2.987	3.544 -3.544	3.998 -3.998
.6	.69 -.69	.96 -.96	1.22 -1.22	1.51 -1.51	2.02 -2.02	2.543 -2.542	2.984 -2.984	3.542 -3.542	3.996 -3.996
.7	.67 -.67	.95 -.95	1.21 -1.21	1.50 -1.50	2.01 -2.01	2.541 -2.541	2.98 -2.98	3.5411 -3.5411	3.994 -3.994
.8	.66 -.66	.94 -.94	1.18 -1.18	1.48 -1.48	2.00 -2.00	2.540 -2.540	2.96 -2.96	3.540 -3.540	3.992 -3.992
.9	.59 -.59	.93 -.93	1.16 -1.16	1.46 -1.46	1.97 -1.97	2.535 -2.535	2.955 -2.955	3.535 -3.535	3.99 -3.99
1.0	.50 -.50	.80 -.80	1.10 -1.10	1.40 -1.40	1.90 -1.90	2.50 -2.50	2.95 -2.95	3.53 -3.53	3.98 -3.98

TABLE 8

VARIATION OF HORIZONTAL COMPONENT $\eta = \eta(\sigma, r, \theta)$ OF PLANE IMAGE POINT (η, h), $h = \pm\sqrt{R^2 - r^2}$, WITH SECTION RADIUS r AND ISOPHOTE VALUE σ, WHEN $\theta = 10^\circ$; OPTICAL DEPTH $\sigma_e = 1$

				$\eta = \eta(\sigma, r, \theta)$			$\theta = 10^\circ$		
σ	r = .75	r = 1.00	r = 1.25	r = 1.55	r = 2.05	r = 2.55	r = 3.00	r = 3.55	r = 4.00
0	.75 -.75	1.00 -1.00	1.250 -1.250	1.550 -1.550	2.050 -2.050	2.550 -2.550	3.000 -3.000	3.550 -3.550	4.000 -4.000
.1	.745 -.741	.99 -1.00	1.240 -1.245	1.550 -1.550	2.04 -2.05	2.545 -2.550	2.995 -3.000	3.550 -3.550	3.995 -4.000
.2	.74 .735	.98 -.995	1.231 -1.230	1.545 -1.545	2.03 -2.05	2.53 -2.545	2.99 -3.000	3.54 -3.550	3.98 -4.000
.3	.73 -.715	.975 -.99	1.230 -1.22	1.540 -1.535	2.025 -2.045	2.520 -2.54	2.980 -2.995	3.52 -3.55	3.97 -4.00
.4	.72 -.70	.97 -.98	1.22 -1.21	1.532 -1.52	2.005 -2.035	2.50 -2.52	2.970 -2.99	3.48 -3.55	3.95 -4.00
.5	.71 -.69	.96 -.96	1.215 -1.20	1.52 -1.51	1.98 -2.015	2.46 -2.505	2.95 -2.98	3.44 -3.55	3.90 -4.00
.6	.69 -.67	.95 -.94	1.185 -1.19	1.492 -1.495	1.93 -2.00	2.40 -2.495	2.87 -2.975	3.27 -3.549	3.78 -3.995
.7	.67 -.65	.93 -.92	1.10 -1.18	1.42 -1.485	1.80 -1.985	2.26 -2.48	2.73 -2.97	3.09 -3.548	3.61 -3.99
.8	.60 -.62	.78 -.91	.89 -1.16	1.20 -1.47	1.55 -1.97	1.95 -2.47	2.40 -2.96	2.70 -3.547	3.00 -3.985
.9	.38 -.57	.50 -.88	.56 -1.14	.78 -1.45	.9 -1.95	1.20 -2.45	1.5 -2.95	2.0 -3.545	2.95 -3.97
1.0	0 -.5	0 -.8	0 -1.1	0 -1.4	.1 -1.9	.2 -2.4	.2 -2.9	-.2 -3.54	-.3 -3.95

TABLE 9

VARIATION OF HORIZONTAL COMPONENT $\eta = \eta(\sigma,r,\theta)$ OF PLANE IMAGE POINT (η,h), $h^2 = R^2 - r^2$, WITH SECTION RADIUS r AND ISOPHOTE VALUE σ, WHEN $\theta = 20^\circ$; OPTICAL DEPTH $\sigma_e = 1$

	$\eta = \eta(\sigma,r,\theta)$						$\theta = 20^\circ$		
σ	r = .75	r = 1.00	r = 1.25	r = 1.55	r = 2.05	r = 2.55	r = 3.00	r = 3.55	r = 4.00
0	.75 -.75	1.00 -1.00	1.25 -1.25	1.55 -1.55	2.05 -2.05	2.55 -2.55	3.00 -3.00	3.50 -3.55	3.92 -4.00
.1	.745 -.74	.99 -1.00	1.24 -1.245	1.549 -1.54	2.00 -2.05	2.49 -2.55	2.95 -2.995	3.40 -3.55	3.88 -4.00
.2	.74 -.735	.98 -.995	1.23 -1.24	1.53 -1.53	1.98 -2.045	2.47 -2.545	2.90 -2.99	3.33 -3.54	3.81 -3.995
.3	.735 -.73	.970 -.99	1.215 -1.235	1.50 -1.52	1.97 -2.04	2.38 -2.54	2.83 -2.988	3.25 -3.535	3.72 -3.992
.4	.73 -.72	.96 -.98	1.19 -1.22	1.43 -1.51	1.89 -2.03	2.29 -2.53	2.73 -2.985	3.115 -3.534	3.585 -3.99
.5	.695 -.70	.94 -.97	1.135 -1.215	1.35 -1.50	1.78 -2.02	2.135 -2.515	2.615 -2.983	2.92 -3.533	3.33 -3.987
.6	.66 -.68	.855 -.96	1.04 -1.20	1.23 -1.49	1.60 -2.01	1.92 -2.50	2.30 -2.981	2.61 -3.532	2.965 -3.985
.7	.56 -.66	.73 -.95	.885 -1.195	1.04 -1.48	1.38 -2.00	1.59 -2.495	1.87 -2.98	2.18 -3.531	2.50 -3.983
.8	.42 -.62	.555 -.93	.63 -1.17	.77 -1.47	.93 -1.995	1.035 -2.47	1.36 -2.97	1.38 -3.53	1.70 -3.98
.9	.225 -.585	.32 -.89	.33 -1.15	.34 -1.465	.35 -1.97	.38 -2.43	.625 -.295	.65 -3.525	.68 -3.97
1.0	0 -.50	0 -.80	0 -1.0	-1.0 -1.4	-.20 -1.9	-.30 -2.4	-.40 -2.9	-.45 -3.5	-.50 -3.95

TABLE 10

VARIATION OF HORIZONTAL COMPONENT $\eta = \eta(\sigma, r, \theta)$ OF PLANE IMAGE POINT (η, h), $h^2 = R^2 - r^2$, WITH SECTION RADIUS r AND ISOPHOTE VALUE σ, WHEN $\theta = 30^\circ$; OPTICAL DEPTH $\sigma_e = 1$

	$\eta = \eta(\sigma, r, \theta)$						$\theta = 30^\circ$		
σ	r = .75	r = 1.00	r = 1.25	r = 1.55	r = 2.05	r = 2.55	r = 3.00	r = 3.55	r = 4.00
0	.75 -.75	1.00 -1.00	1.25 -1.25	1.52 -1.25	1.95 -2.05	2.35 -2.55	2.83 -3.00	3.23 -3.55	3.715 -4.00
.1	.735 -.747	.99 -.995	1.23 -1.245	1.48 -1.545	1.92 -2.045	2.31 -2.546	2.76 -2.996	3.165 -3.55	3.585 -4.00
.2	.72 -.74	.98 -.993	1.20 -1.24	1.44 -1.54	1.85 -2.04	2.225 -2.54	2.67 -2.995	3.05 -3.55	3.42 -4.00
.3	.71 -.735	.95 -.99	1.17 -1.234	1.36 -1.535	1.75 -2.03	2.135 -2.536	2.53 -2.993	2.90 -3.548	3.23 -3.998
.4	.69 -.73	.92 -.985	1.125 -1.23	1.26 -1.53	1.63 -2.03	1.98 -2.534	2.32 -2.992	2.675 -3.546	3.00 -3.996
.5	.635 -.71	.82 -.98	1.00 -1.225	1.13 -1.52	1.42 -2.02	1.76 -2.532	2.065 -2.99	2.38 -3.543	2.70 -3.994
.6	.55 -.685	.70 --.975	.82 -1.215	.95 -1.505	1.17 -2.01	1.45 -2.528	1.68 -2.986	1.92 -3.541	2.24 -3.992
.7	.465 -.66	.57 -.97	.70 -1.20	.715 -1.485	.92 -2.00	1.099 -2.52	1.22 -2.984	1.40 -3.538	1.67 -3.98
.8	.33 -.63	.40 -.96	.465 -1.185	.44 -1.475	.50 -1.985	.60 -2.50	.665 -2.98	.76 -3.535	.86 -3.975
.9	.215 -.59	.25 -.94	.27 -1.17	.145 -1.445	.13 -1.975	.10 -2.475	.099 -2.965	.042 -3.53	.045 -3.96
1.0	-.10 -.50	-.10 -.90	-.10 -1.1	-.20 -1.4	-.30 -1.9	-.40 -2.4	-.50 -2.9	-.67 -3.5	-.75 -3.92

TABLE 11

VARIATION OF HORIZONTAL COMPONENT $\eta = \eta(\sigma,r,\theta)$ OF PLANE IMAGE POINT (η,h), $h^2 = R^2 - r^2$, WITH SECTION RADIUS r AND ISOPHOTE VALUE σ, WHEN $\theta = 40^\circ$; OPTICAL DEPTH $\sigma_e = 1$

	$\eta = \eta(\sigma,r,\theta)$						$\theta = 40^\circ$		
	r = .75	r = 1.00	r = 1.25	r = 1.55	r = 2.05	r = 2.55	r = 3.00	r = 3.55	r = 4.00
0	.75 -.75	1.00 -1.00	1.25 -1.25	1.50 -1.55	1.86 -2.05	2.22 -2.55	2.62 -3.00	2.935 -3.55	3.34 -4.00
.1	.735 .74	.97 .99	1.20 1.246	1.44 1.55	1.78 2.05	2.12 2.55	2.50 3.00	2.82 3.55	3.20 4.00
.2	.72 -.735	.925 -.985	1.12 -1.244	1.345 -1.546	1.68 -2.046	2.00 -2.549	2.31 -3.00	2.635 -3.55	3.00 -4.00
.3	.695 -.72	.87 -.98	1.04 -1.24 η	1.21 -1.54	1.55 -2.04	1.815 -2.547	2.115 -2.998	2.38 -3.55	2.68 -4.00
.4	.63 -.705	.793 -.975	.94 -1.22	1.04 -1.535	1.35 -2.03	1.61 -2.545	1.88 -2.996	2.08 -3.547	2.27 -3.997
.5	.57 -.69	.70 -.97	.825 -1.215	.88 -1.53	1.12 -2.02	1.33 -2.53	1.535 -2.994	1.70 -3.543	1.815 -3.994
.6	.50 -.66	.54 -.96	.665 -1.20	.67 -1.52	.87 -2.01	.925 -2.525	1.14 -2.99	1.30 -3.54	1.25 -3.99
.7	.40 -.63	.40 -.945	.520 -1.19	.465 -1.50	.55 -2.00	.555 -2.515	.67 -2.985	.775 -3.53	.675 -3.985
.8	.30 -.60	.235 -.93	.30 -1.18	.27 -1.49	.26 -1.995	.20 -2.50	.18 -2.975	.20 -3.50	.13 -3.975
.9	.199 -.565	.10 -.90	.10 -1.165	.025 -1.47	-.03 -1.975	-.17 -2.475	-.275 -2.96	-.345 -3.485	-.525 -3.96
1.0	.05 -.50	-.03 -.80	-.14 -1.1	-.27 -1.4	-.38 -1.9	-.59 -2.4	-.715 -2.9	-.875 -3.4	-1.14 -3.9

TABLE 12

VARIATION OF HORIZONTAL COMPONENT $\eta = \eta(\sigma, r, \theta)$ OF PLANE IMAGE POINT (η, h), $h^2 = R^2 - r^2$, WITH SECTION RADIUS r AND ISOPHOTE VALUE σ, WHEN $\theta = 50^\circ$; OPTICAL DEPTH $\sigma_e = 1$

	$\eta = \eta(\sigma, r, \theta)$					$\theta = 50^\circ$			
σ	r = .75	r = 1.00	r = 1.25	r = 1.55	r = 2.05	r = 2.55	r = 3.00	r = 3.55	r = 4.00
0	.75 -.75	.915 -1.00	1.10 -1.25	1.31 -1.55	1.63 -2.05	1.93 -2.55	2.225 -3.00	2.59 -3.55	2.90 -4.00
.1	.70 -.749	.88 -.998	1.03 -1.25	1.225 -1.55	1.535 -2.05	1.815 -2.55	2.11 -3.00	2.40 -3.55	2.64 -4.00
.2	.675 -.747	.815 -.996	.925 -1.248	1.125 -1.55	1.38 -2.05	1.64 -2.55	1.87 -3.00	2.10 -3.55	2.36 -4.00
.3	.615 -.745	.725 -.994	.83 -1.246	1.01 -1.545	1.20 -2.05	1.43 -2.549	1.625 -3.00	1.80 -3.55	2.00 -4.00
.4	.56 -.74	.63 -.992	.717 -1.244	.855 -1.54	1.00 -2.045	1.14 -2.547	1.305 -2.995	1.43 -3.545	1.55 -4.00
.5	.50 -.73	.535 -.99	.60 -.24	.70 -.535	.76 -.04	.84 -.544	.94 -2.993	1.06 -3.54	1.115 -3.998
.6	.42 -.70	.435 -.985	.442 -1.22	.50 -1.527	.50 -2.035	.55 -2.54	.525 -2.99	.50 -3.53	.57 -3.996
.7	.325 -.665	.325 -.98	.30 -1.20	.30 -1.50	.25 -2.03	.201 -2.53	.145 -2.98	.10 -3.52	0 -3.993
.8	.25 -.62	.22 -.955	.155 -1.175	.10 -1.48	0 -2.02	-.10 -2.525	-.20 -2.97	-.34 -3.505	-.46 -3.99
.9	.165 -.575	.11 -.91	.01 -1.145	-.01 -1.445	-.21 -1.99	-.40 -2.495	-.57 -2.955	-.725 -3.49	-.935 -3.97
1.0	-.04 -.43	-.075 -.79	-.17 -1.04	-.36 -1.37	-.48 -1.90	-.75 -2.39	-1.025 2.87	-1.175 -3.38	-1.46 -3.88

TABLE 13

VARIATION OF HORIZONTAL COMPONENT $\eta = \eta(\sigma, r, \theta)$ OF PLANE IMAGE POINT (η, h), $h^2 = R^2 - r^2$, WITH SECTION RADIUS r AND ISOPHOTE VALUE σ, WHEN $\theta = 70^\circ$; OPTICAL DEPTH $\sigma_e = 1$

	$\eta = \eta(\sigma, r, \theta)$					$\theta = 70^\circ$			
σ	r = .75	r = 1.00	r = 1.25	r = 1.55	r = 2.05	r = 2.55	r = 3.00	r = 3.55	r = 4.00
0	.66 -.75	.77 -1.00	.80 -1.25	.93 -1.55	1.115 -2.05	1.25 -2.55	1.45 -3.00	1.615 -3.55	1.815 -4.00
.1	.64 -.745	.70 -1.00	.715 -1.25	.84 -1.55	.96 -2.05	1.06 -2.55	1.21 -3.00	1.33 -3.55	1.465 -4.00
.2	.58 -.74	.61 -.999	.615 -1.245	.70 -1.547	.78 -2.05	.80 -2.547	.90 -3.00	.975 -3.55	1.05 -4.00
.3	.515 -.73	.52 -.997	.525 -1.24	.555 -1.545	.60 -2.045	.60 -2.545	.60 -2.999	.645 -3.547	.70 -4.00
.4	.445 -.72	.425 -.994	.40 -1.23	.43 -2.04	.375 -2.54	.30 -2.998	.30 -2.998	.25 -3.54	.22 -3.996
.5	.38 -.68	.33 -.99	.30 -1.215	.265 -1.53	.20 -2.03	.06 -2.53	0 -2.997	-.08 -3.53	-.165 -3.994
.6	.325 -.67	.245 -.98	.17 -1.2	.125 -1.515	0 -2.02	-.16 -2.52	-.30 -2.995	-.43 -3.52	-.58 -3.992
.7	.285 -.645	.15 -.965	.065 -1.18	-.005 -1.49	-.20 -1.98	-.355 -2.515	-.598 -2.993	-.75 -3.50	-.93 -3.99
.8	.255 -.61	.08 -.95	-.03 -1.16	-.14 -1.46	-.36 -1.97	-.570 -2.485	-.81 -2.99	-1.06 -3.485	-1.23 -3.98
.9	.22 -.57	.02 -.91	-.10 -1.14	-.25 -1.437	-.50 -1.93	-.75 -2.46	-.93 -2.97	-1.3 -3.47	-1.53 -3.97
1.0	.10 -.465	-.12 -.78	-.25 -1.08	-.445 -1.28	-.70 -1.88	-1.06 -2.37	-1.325 -2.88	-1.60 -3.38	-1.84 -3.88

TABLE 14

VARIATION OF HORIZONTAL COMPONENT $\eta = \eta(\sigma, r, \theta)$ OF PLANE IMAGE POINT (η, h), $h^2 = R^2 - r^2$, WITH SECTION RADIUS r AND ISOPHOTE VALUE σ, WHEN $\theta = 90^\circ$; OPTICAL DEPTH $\sigma_e = 1$

	$\eta = \eta(\sigma, r, \theta)$					$\theta = 90^\circ$			
σ	r = .75	r = 1.00	r = 1.25	r = 1.55	r = 2.05	r = 2.55	r = 3.00	r = 3.55	r = 4.00
0	.515 -.75	.515 -1.00	.515 -1.25	.515 -1.55	.515 -2.05	.515 -2.55	.515 -3.00	.515 -3.55	.515 -4.00
.1	.45 -.745	.42 -1.00	.37 -1.25	.37 -1.55	.32 -2.05	.325 -2.55	.20 -3.00	.10 -3.55	.13 -4.00
.2	.41 -.74	.34 -.99	.26 -1.245	.23 -1.547	.125 -2.045	0 -2.545	-.085 -3.00	-.20 -3.55	-.225 -4.00
.3	.375 -.73	.27 -.985	.17 -1.24	.10 -1.543	-.05 -2.04	-.20 -2.543	-.32 -2.998	-.475 -3.545	-.575 -4.00
.4	.345 -.72	.20 -.975	.10 -1.23	-.02 -1.54	-.203 -2.03	-.40 -2.54	-.60 -2.996	-.785 -3.54	-.90 -3.998
.5	.315 -.70	.155 -.965	.025 -1.22	-.12 -1.53	-.36 -2.02	-.58 -2.53	-.835 -2.994	-1.055 -3.535	-1.20 -3.996
.6	.299 -.675	.10 -.955	-.035 -1.20	-.22 -1.52	-.50 -2.01	-.725 -2.52	-1.00 -2.992	-1.28 -3.525	-1.50 -3.992
.7	.26 -.65	.075 -.94	-.10 -1.175	-.30 -1.50	-.60 -2.00	-.885 -2.50	-1.20 -2.99	-1.45 -3.505	-1.765 -3.99
.8	.235 -.62	.05 -.905	-.14 -1.15	-.36 -1.475	-.70 -1.98	-1.00 -2.485	-1.34 -2.98	-1.625 -3.485	-1.96 -3.975
.9	.210 -.57	.033 -.88	-.17 -1.12	-.425 -1.43	-.765 -1.96	-1.10 -2.46	-1.45 -2.97	-1.785 -3.47	-2.10 -3.96
1.0	.165 -.47	-.04 -.785	-.24 -1.088	-.535 -1.36	-.890 -1.87	-1.225 -2.38	-1.625 -2.88	-1.96 -3.38	-2.32 -3.88

TABLE 15

VARIATION OF HORIZONTAL COMPONENT $\eta = \eta(\sigma, r, \theta)$ OF PHASE IMAGE POINT (η, h), $h^2 = R^2 - r^2$, WITH SECTION RADIUS r AND ISOPHOTE VALUE σ, WHEN $\theta = 110^\circ$; OPTICAL DEPTH $\sigma_e = 1$

	$\eta = \eta(\sigma, r, \theta)$								$\theta = 110^\circ$
σ	r = .75	r = 1.00	r = 1.25	r = 1.55	r = 2.05	r = 2.55	r = 3.00	r = 3.55	r = 3.00
0	.665 -.75	.26 -1.00	.065 -1.25	-.04 -1.55	-.16 -2.05	-.37 -2.55	-.56 -3.00	-.76 -3.55	-.88 -4.00
.1	.60 -.735	.15 -1.00	-.06 -1.25	-.15 -1.49	-.38 -2.05	-.59 -2.55	-.80 -3.00	-1.0 -3.55	-1.22 -4.00
.2	.44 -.72	.06 -.995	-.125 -1.245	-.26 -1.48	-.50 -2.045	-.78 -2.545	-1.00 -3.00	-1.25 -3.545	-1.50 -4.00
.3	.34 -.70	0 -.99	-.18 -1.24	-.35 -1.47	-.64 -3.04	-.94 -2.543	-1.18 -2.995	-1.48 -3.54	-1.77 -3.998
.4	.30 -.685	-.04 -.98	-.23 -1.235	-.42 -1.46	-.725 -2.03	-1.05 -2.54	-1.365 -2.994	-1.665 -3.53	-2.015 -3.996
.5	.27 -.665	-.06 -.975	-.265 -1.22	-.50 -1.45	-.81 -2.02	-1.16 -2.535	-1.50 -2.992	-1.86 -3.52	-2.22 -3.995
.6	.255 -.64	-.07 -.96	-.30 -1.20	-.545 -1.44	-.90 -2.01	-1.25 -2.525	-1.63 -2.99	-2.00 -3.51	-2.37 -3.993
.7	.23 -.61	-.075 -.95	-.34 -1.19	-.56 -1.43	-.945 -2.00	-1.32 -2.50	-1.72 -2.975	-2.10 -3.50	-2.47 -3.99
.8	.22 -.585	-.08 -.93	-.365 -1.17	-.57 -1.42	-1.00 -1.99	-1.37 -2.485	-1.80 -2.965	-2.16 -3.49	-2.54 -3.975
.9	.20 -.545	-.09 -.89	-.375 -1.15	-.585 -1.41	-1.045 -1.96	-1.42 -2.46	-1.87 -2.95	-2.22 -3.46	-2.60 -3.955
1.0	.199 -.46	-.17 -.78	-.445 -1.08	-.65 -1.38	-1.15 -1.88	-1.50 -2.38	-1.97 -2.88	-2.30 -3.38	-2.755 -3.86

TABLE 16

VARIATION OF HORIZONTAL COMPONENT $\eta = \eta(\sigma, r, \theta)$ OF PLANE IMAGE POINT (η, h), $h^2 = R^2 - r^2$, WITH SECTION RADIUS r AND ISOPHOTE VALUE σ, WHEN $\theta = 130^\circ$; OPTICAL DEPTH $\sigma_e = 1$

	$\eta = \eta(\sigma, r, \theta)$					$\theta = 130^\circ$			
σ	r = .75	r = 1.00	r = 1.25	r = 1.55	r = 2.05	r = 2.55	r = 3.00	r = 3.55	r = 4.00
0	.75 -.75	-.025 -1.00	-.395 -1.25	-.55 -1.50	-.95 -2.05	-1.18 -2.50	-1.575 -3.00	-1.83 -3.50	-2.20 -4.00
.1	.72 -.745	-.07 -.998	-.405 -1.247	-.600 -1.499	-1.015 -2.05	-1.30 -2.498	-1.70 -3.00	-2.00 -3.50	-2.40 -4.00
.2	.70 -.74	-.10 -.995	-.415 -1.242	-.635 -1.497	-1.06 -2.048	-1.38 -2.497	-1.83 -3.00	-2.16 -3.50	-2.55 -4.00
.3	.67 -.735	-.13 -.99	-.42 -1.235	-.66 -1.495	-1.115 -2.046	-1.46 -2.495	-1.92 -2.995	-2.28 -3.497	-2.675 -3.997
.4	.60,.50,.265 -.725	-.165 -.98	-.43 -1.23	-.68 -1.49	-1.16 -2.042	-1.53 -2.49	-2.00 -2.993	-2.37 -3.495	-2.80 -3.995
.5	.175 -.70	-.20 -.975	-.44 -1.225	-.69 -1.485	-1.18 -2.035	-1.60 -2.485	-2.07 -2.99	-2.45 -3.493	-2.89 -3.99
.6	.115 -.67	-.225 -.96	-.455 -1.21	-.70 -1.48	-1.21 -2.02	-1.64 -2.48	-2.13 -2.98	-2.50 -3.49	-2.965 -3.985
.7	.075 -.645	-.245 -.94	-.460 -1.185	-.71 -1.47	-1.225 -2.00	-1.675 -2.47	-2.17 -2.97	-2.55 -3.48	-3.03 -3.975
.8	.055 -.60	-.26 -.925	-.475 -1.17	-.72 -1.46	-1.23 -1.98	-1.70 -2.465	-2.20 -2.96	-2.595 -3.47	-3.10 -3.965
.9	.025 -.565	-.285 -.875	-.49 -1.15	-.73 -1.435	-1.24 -1.95	-1.735 -2.45	-2.22 -2.94	-2.63 -3.455	-3.15 -3.95
1.0	-.045 -.48	-.35 -.78	-.525 -1.085	-.77 -1.385	-1.26 -1.90	-1.775 -2.40	-2.27 -2.88	-2.67 -3.40	-3.20 -3.885

TABLE 17

VARIATION OF HORIZONTAL COMPONENT $\eta = \eta(\sigma,r,\theta)$ OF PLANE IMAGE POINT (η,h), $h^2 = R^2 - r^2$, WITH SECTION RADIUS r AND ISOPHOTE VALUE σ, WHEN $\theta = 150^\circ$; OPTICAL DEPTH $\sigma_e = 1$

	$\eta = \eta(\sigma,r,\theta)$					$\theta = 150^\circ$			
σ	r = .75	r = 1.00	r = 1.25	r = 1.55	r = 2.05	r = 2.55	r = 3.00	r = 3.55	r = 4.00
0	.75	1.00,.57, .02	1.25,.05, -.47	-.885	-1.45	-1.95	-2.35	-2.78	-3.20
	-.75	-1.00	-1.25	-1.50	-2.05	-2.55	-3.00	-3.55	-4.00
.1	.74	.99,-.12, .665	1.215,1.09, -.57	-.925	-1.47	-1.97	-2.40	-2.85	-3.26
	-.74	-.995	-1.245	-1.50	-2.05	-2.547	-2.997	-3.55	-4.00
.2	.73	.97,-.23 .75	-.61	-.95	-1.49	-1.99	-2.44	-2.885	-3.32
	-.73	-.99	-1.243	-1.498	-2.045	-2.545	-2.995	-3.548	-3.999
.3	.72	.95,-.33 .80	-.64	-.97	-1.51	-2.00	-2.47	-2.93	-3.37
	-.72	-.985	-1.24	-1.496	-2.04	-2.54	-2.99	-3.547	-3.997
.4	.71	-.385	-.66	-1.00	-1.525	-2.035	-2.51	-2.96	-3.40
	-.70	-.98	-1.23	-1.494	-2.03	-2.53	-2.985	-3.545	-3.995
.5	.68,.43 .20	-.42	-.69	-1.015	-1.535	-2.035	-2.535	-2.985	-3.425
	-.68	-.975	-1.215	-1.492	-2.02	-2.525	-2.98	-3.54	-3.99
.6	.615,.52 -.03	-.45	-.71	-1.03	-1.54	-2.055	-2.545	-3.02	-3.45
	-.65	-.97	-1.20	-1.49	-2.00	-2.52	-2.975	-3.53	-3.98
.7	-.115	-.48	-.72	-1.05	-1.555	-2.065	-2.565	-3.04	-3.46
	-.617	-.96	-1.18	-1.48	-1.99	-2.515	-2.965	-3.52	-3.97

TABLE 17 (Continued)

VARIATION OF HORIZONTAL COMPONENT $\eta = \eta(\sigma, r, \theta)$ OF PLANE IMAGE POINT (η, h), $h^2 = R^2 - r^2$, WITH SECTION RADIUS r AND ISOPHOTE VALUE σ, WHEN $\theta = 150^\circ$; OPTICAL DEPTH $\sigma_e = 1$

				$\eta = \eta(\sigma, r, \theta)$		$\theta = 150^\circ$			
σ	r = .75	r = 1.00	r = 1.25	r = 1.55	r = 2.05	r = 2.55	r = 3.00	r = 3.55	r = 4.00
.8	-.175	-.50	-.73	-1.07	-1.565	-2.07	-2.58	-3.055	-3.475
	-.595	-.945	-1.16	-1.47	-1.98	-2.495	-2.95	-3.50	-3.95
.9	-.20	-.53	-.74	-1.08	-1.575	-2.08	-2.60	-3.07	-3.49
	-.565	-.935	-1.14	-1.45	-1.96	-2.47	-2.935	-3.46	-3.93
1.0	-.27	-.57	-.75	-1.095	-1.59	-2.09	-2.615	-3.08	-3.5
	-.48	-.90	-1.09	-1.38	-1.90	-2.42	-2.88	-3.40	-3.88

TABLE 18

VARIATION OF HORIZONTAL COMPONENT $\eta = \eta(\sigma, r, \theta)$ OF PLANE IMAGE POINT (η, h), $h^2 = R^2 - r^2$, WITH SECTION RADIUS r AND ISOPHOTE VALUE σ, WHEN $\theta = 170^\circ$; OPTICAL DEPTH $\sigma_e = 1$

				$\eta = \eta(\sigma, r, \theta)$		$\theta = 170^\circ$			
σ	r = .75	r = 1.00	r = 1.25	r = 1.55	r = 2.05	r = 2.55	r = 3.00	r = 3.55	r = 4.00
0	.75	1.00,.285	1.25,.86	1.55,1.23	2.05,1.86	2.55,2.44	3.00,2.90	3.55,3.44	4.00,3.925
		0	-.57	-1.03	-1.58	-2.20	-2.74	-3.26	-3.78
	-.75	-1.00	-1.25	-1.55	-2.05	-2.55	-3.00	-3.55	-4.00
.1	.745	.995,.42	1.25,.94	1.545,1.28	2.03,1.90	2.545,2.455	3.00,2.92	3.545,3.46	3.97,3.935
		-.22	-.725	-1.115	-1.68	-2.25	-2.77	-3.28	-3.80
	-.735	-.997	-1.245	-1.55	-2.045	-2.547	-3.00	-3.55	-3.995
.2	.74	.99,.54	1.245,1.00	1.54,1.32	2.00,1.92	2.542,2.465	2.99,2.93	3.54,2.475	3.97,3.945
		-.36	-.795	-1.165	-1.71	-2.28	-2.78	-3.3	-3.82
	-.72	-.995	-1.24	-1.545	-2.04	-2.545	-2.998	-3.547	-3.993
.3	.73	.98,.62	1.242,1.045	1.525,1.35	1.99,1.925	2.54,2.48	2.98,2.94	3.53,3.49	-3.84
		-.45	-.84	-1.20	-1.73	-2.29	-2.80	-3.315	
	-.70	-.99	-1.235	-1.54	-2.03	-2.54	-2.996	-3.545	-3.99
.4	.70	.97,.68	1.235,.08	1.51,1.39	1.925,1.935	2.535,2.49	2.97,2.95	-3.33	-3.85
		-.50	-.88	-1.22	-1.76	-2.30	-2.815		
	-.69	-.985	-1.225	-1.53	-2.02	-2.53	-2.994	-3.54	-3.985
.5	.71,.10	.95,.75	1.23,1.12	1.49,1.42	1.98,1.945	2.52,2.51	-2.825	-3.34	-3.86
	-.10	-.565	-.925	-1.24	-1.78	-2.32			
	-.675	-.975	-1.215	-1.52	-2.01	-2.525	-2.99	-3.53	-3.98
.6	.70,.33	.93,.80	1.225,1.145	-1.255	-1.805	-2.34	-2.845	-3.355	-3.87
	-.16	-.61	-.95						
	-.66	-.96	-1.20	-1.50	-2.00	-2.50	-2.98	-3.525	-3.97

TABLE 18 (Continued)

VARIATION OF HORIZONTAL COMPONENT $\eta = \eta(\sigma,r,\theta)$ OF PLANE IMAGE POINT (η,h), $h^2 = R^2 - r^2$, WITH SECTION RADIUS r AND ISOPHOTE VALUE σ, WHEN $\theta = 170^\circ$; OPTICAL DEPTH $\sigma_e = 1$

	$\eta = \eta(\sigma,h,\theta)$					$\theta = 170^\circ$			
σ	r = .75	r = 1.00	r = 1.25	r = 1.55	r = 2.05	r = 2.55	r = 3.00	r = 3.55	r = 4.00
.7	.67,.45 -.28 -.64	.90,.835 -.66 -.945	1.20,1.20 -.985 -1.19	-1.285 -1.49	-1.835 -1.99	-2.35 -2.49	-2.86 -2.97	-3.36 -3.515	-3.88 -3.96
.8	.60,.60 -.35 -.60	-.70 -.92	-1.01 -1.185	-1.31 -1.485	-1.855 -1.98	-2.365 -2.47	-2.87 -2.96	-3.365 -3.50	-3.885 -3.94
.9	-.40 -.585	-.72 -.88	-1.045 -1.175	-1.33 -1.465	-1.88 -1.97	-2.38 -2.45	-2.89 -2.945	-3.37 -3.48	-3.89 -3.93
1.0	-.45 -.545	-.75 -.825	-1.06 -1.13	-1.345 -1.42	-1.90 -1.95	-2.39 -2.42	-2.90 -2.91	-3.38 -3.43	-3.90 -3.92

TABLE 19

VARIATION OF HORIZONTAL COMPONENT $\eta = \eta(\sigma,r,\theta)$ OF PLANE IMAGE POINT (η,h), $h^2 = R^2 - r^2$, WITH SECTION RADIUS r AND ISOPHOTE VALUE σ, WHEN $\theta = 180^\circ$; OPTICAL DEPTH $\sigma_e = 1$

				$\eta = \eta(\sigma,r,\theta)$		$\theta = 180^\circ$			
σ	r = .75	r = 1.00	r = 1.25	r = 1.55	r = 2.05	r = 2.55	r = 3.00	r = 3.55	r = 4.00
0	±.75	±1.00 ±.08	±1.25 ±.72	±1.55 ±1.13	±2.05 ±1.735	±2.55 ±2.33	±3.00 ±2.875	±3.55 ±3.44	±4.00 ±3.90
.1	±.74	±.99 ±.32	±1.245 ±.815	±1.543 ±1.18	±2.05 ±1.79	±2.545 ±2.35	±3.00 ±2.90	±3.549 ±3.39	±3.999 ±3.91
.2	±.735	±.98 ±.445	±1.24 ±.87	±1.54 ±1.235	±2.045 ±1.82	±2.535 ±2.37	±2.999 ±2.915	±3.548 ±3.42	±3.998 ±3.92
.3	±.725	±.97 ±.525	±1.23 ±.93	±1.53 ±1.265	±2.04 ±1.85	±2.532 ±2.40	±2.998 ±2.925	±3.547 ±3.44	±3.997 ±3.93
.4	±.71	±.96 ±.60	±1.225 ±.965	±1.52 ±1.30	±2.03 ±1.87	±2.53 ±2.42	±2.997 ±2.935	±3.546 ±3.46	±3.996 ±3.94
.5	±.70	±.95 ±.66	±1.215 ±1.00	±1.51 ±1.335	±2.02 ±1.90	±2.525 ±2.44	±2.996 ±2.94	±3.545 ±3.47	±3.995 ±3.95
.6	±.67 ±.26	±.94 ±.70	±1.210 ±1.045	±1.50 ±1.36	±2.01 ±1.915	±2.52 ±2.445	±2.995 ±2.95	±3.544 ±3.48	±3.994 ±3.95
.7	±.645 ±.36	±.93 ±.76	±1.20 ±1.07	±1.495 ±1.39	±2.00 ±1.945	±2.51 ±2.45	±2.993 ±2.955	±3.543 ±3.49	±3.993 ±3.955
.8	±.62 ±.445	±.915 ±.80	±1.18 ±1.10	±1.49 ±1.42	±1.995 ±1.955	±2.50 ±2.46	±2.99 ±2.96	±3.542 ±3.50	±3.992 ±3.96
.9	±.58 ±.50	±.90 ±.84	±1.16 ±1.125	±1.48 ±1.45	±1.99 ±1.965	±2.49 ±2.47	±2.985 ±2.965	±3.54 ±3.51	±3.99 ±3.97
1.0	±.54	±.88	±1.15	±1.47	±1.98	±2.48	±2.98	±3.53	±3.98

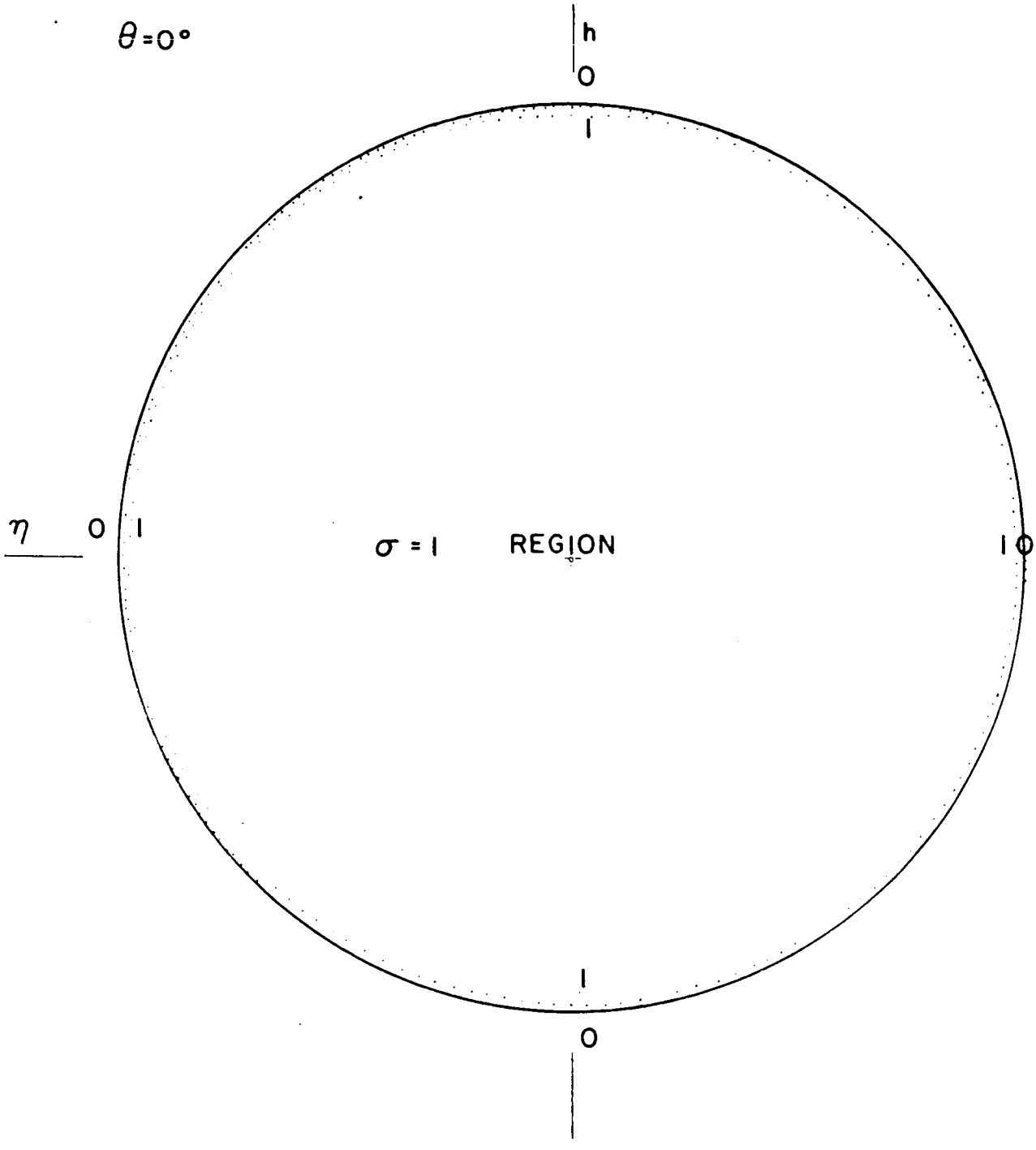

Figure 19. Plane image of photoluminescent homogeneous spherical cloud as seen by an observer at an angle $\theta = 0^{o}$ with the sun, showing isophote curves $\sigma(\eta,h,\theta)$ = constant; optical depth $\sigma_e = 1$, radius of sphere R = 4.

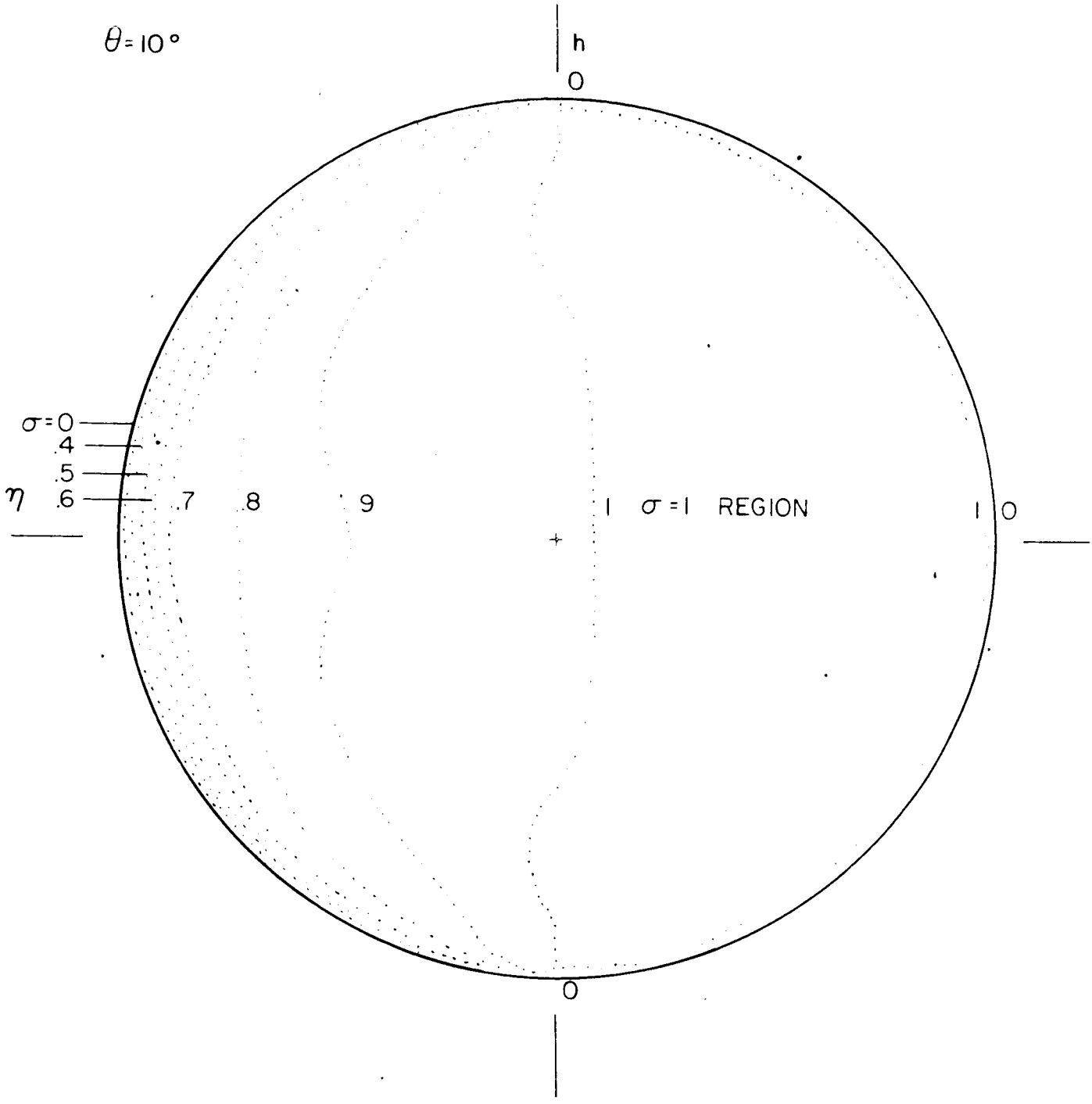

Figure 20. Plane image of photoluminescent homogeneous spherical cloud as seen by an observer at an angle $\vartheta = 10^{\circ}$ with the sun, showing isophote curves $v(\tau, h, \vartheta)$ = constant; optical depth $\sigma_e = 1$, radius of sphere R = 4.

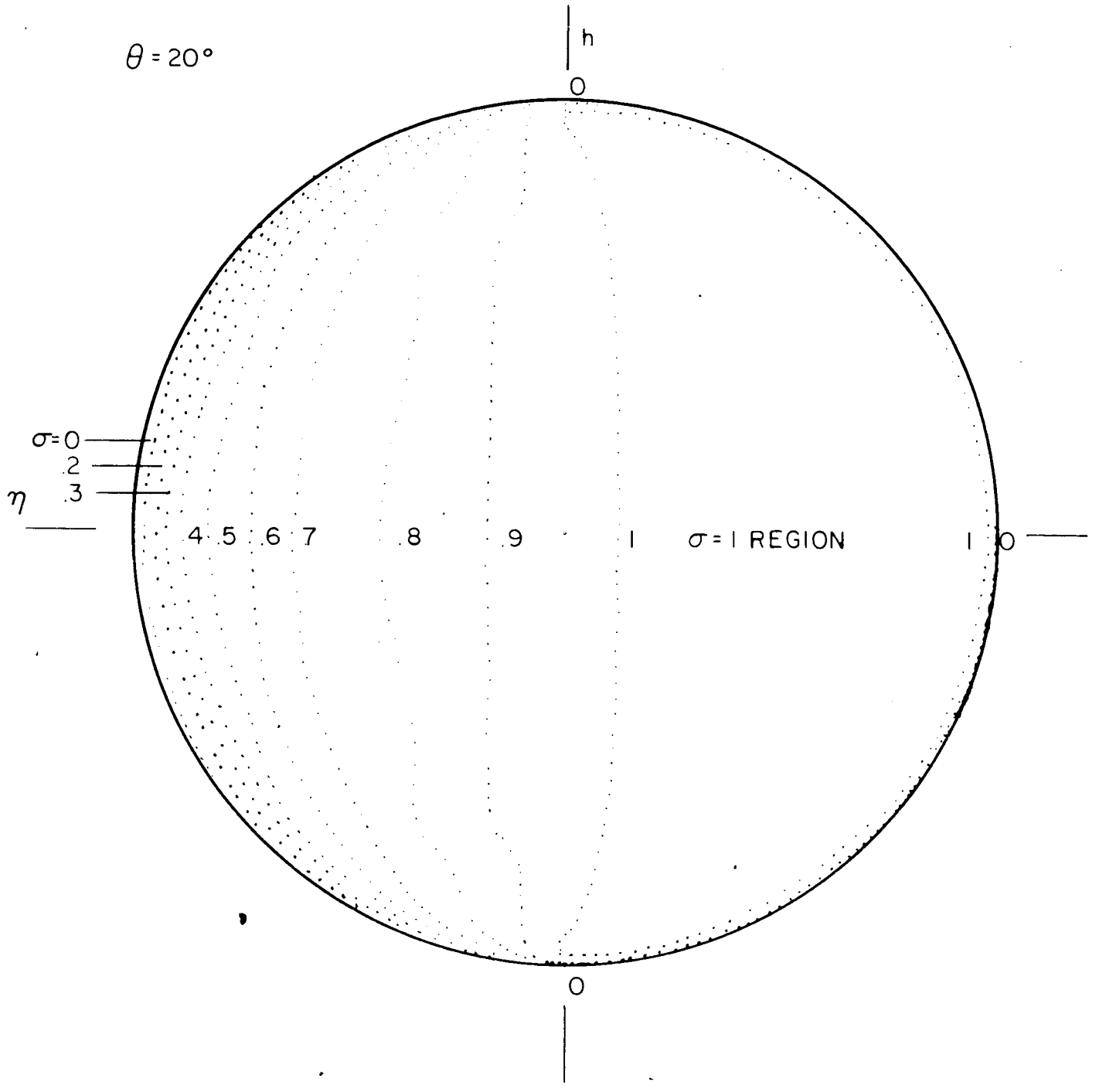

Figure 21. Plane image of photoluminescent homogeneous spherical cloud as seen by an observer at an angle $\vartheta = 20^{\circ}$ with the sun, showing isophote curves $\sigma(\tau,h,\theta)$ = constant; optical depth $\sigma_e = 1$, radius of sphere R = 4.

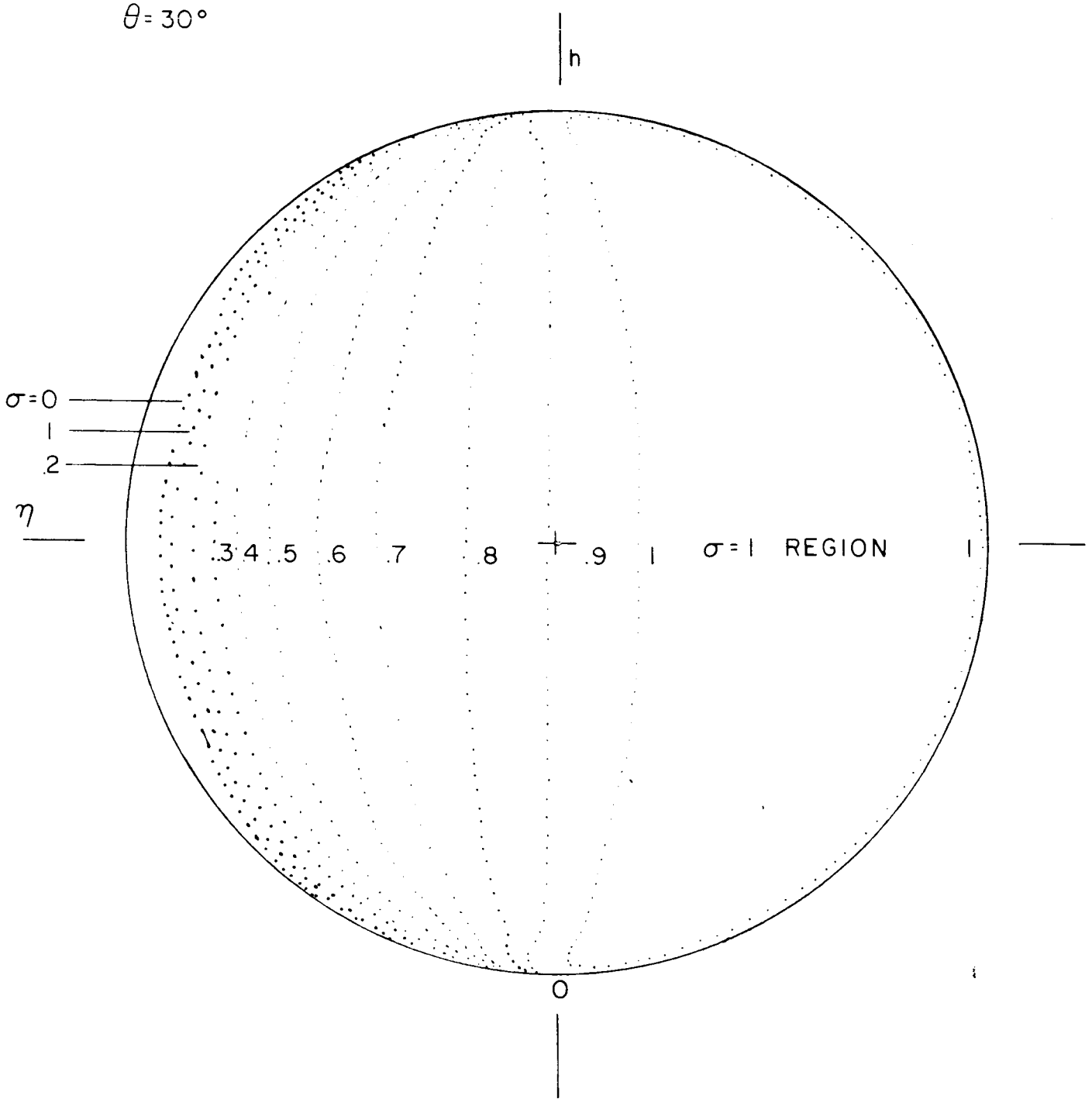

Figure 22. Plane image of photoluminescent homogeneous spherical cloud as seen by an observer at an angle $\theta = 30^{\circ}$ with the sun, showing isophote curves $\sigma(\eta,h,\theta)$ = constant; optical depth $\sigma_e = 1$, radius of sphere R = 4.

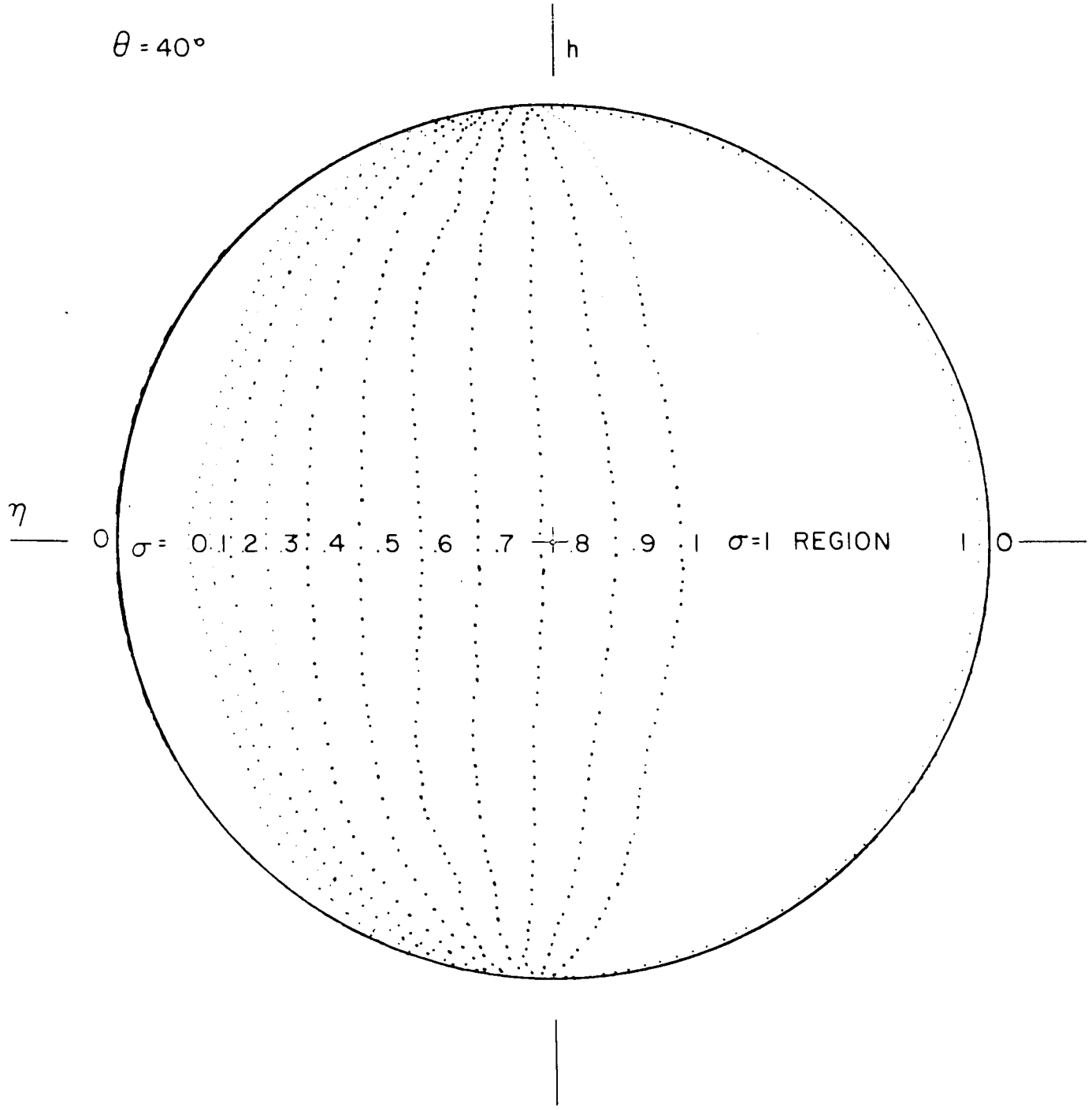

Figure 23. Plane image of photoluminescent homogeneous spherical cloud as seen by an observer at an angle $\theta = 40^{\circ}$ with the sun, showing isophote curves $J(\eta,h,\vartheta)$ = constant; optical depth $\sigma_e = 1$, radius of sphere R = 4.

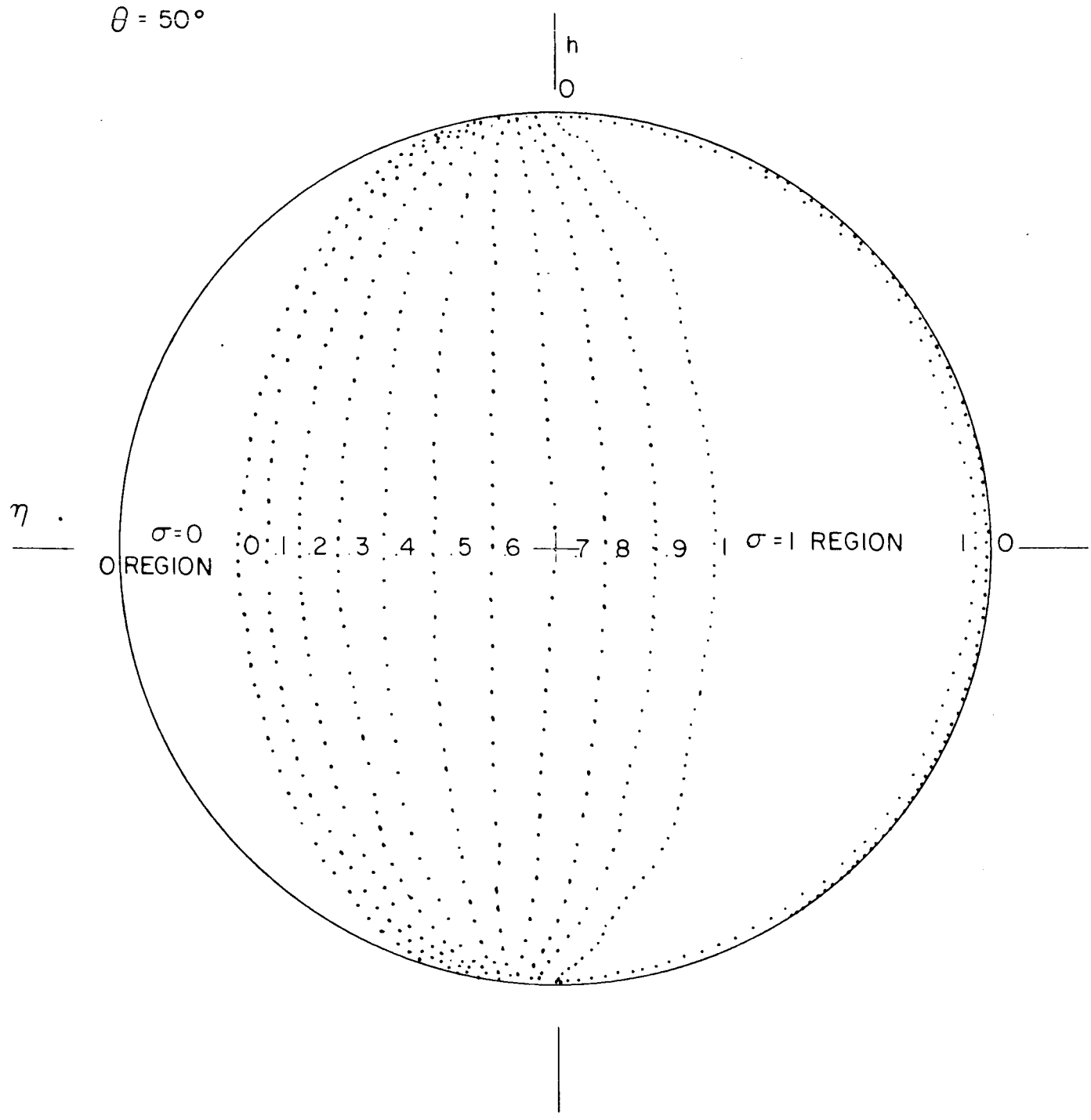

Figure 24. Plane image of photoluminescent homogeneous spherical cloud as seen by an observer at an angle $\vartheta = 50^{\circ}$ with the sun, showing isophote curves $J(\tau,h,\vartheta)$ = constant; optical depth $\sigma_e = 1$, radius of sphere R = 4.

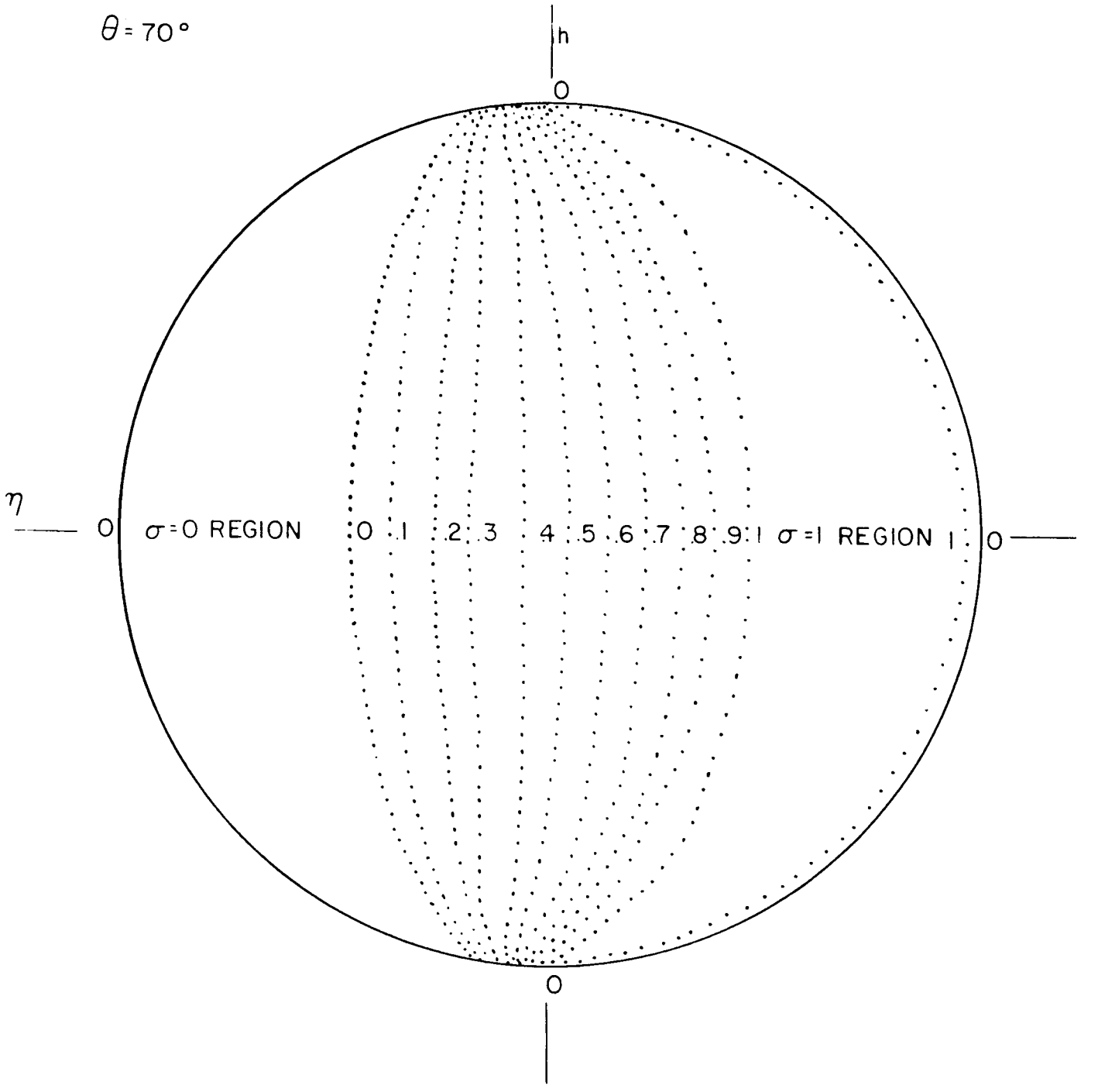

Figure 25. Plane image of photoluminescent homogeneous spherical cloud as seen by an observer at an angle $\theta = 70^{\circ}$ with the sun, showing isophote curves $\sigma(\eta,h,\theta)$ = constant; optical depth $\sigma_e = 1$, radius of sphere R = 4.

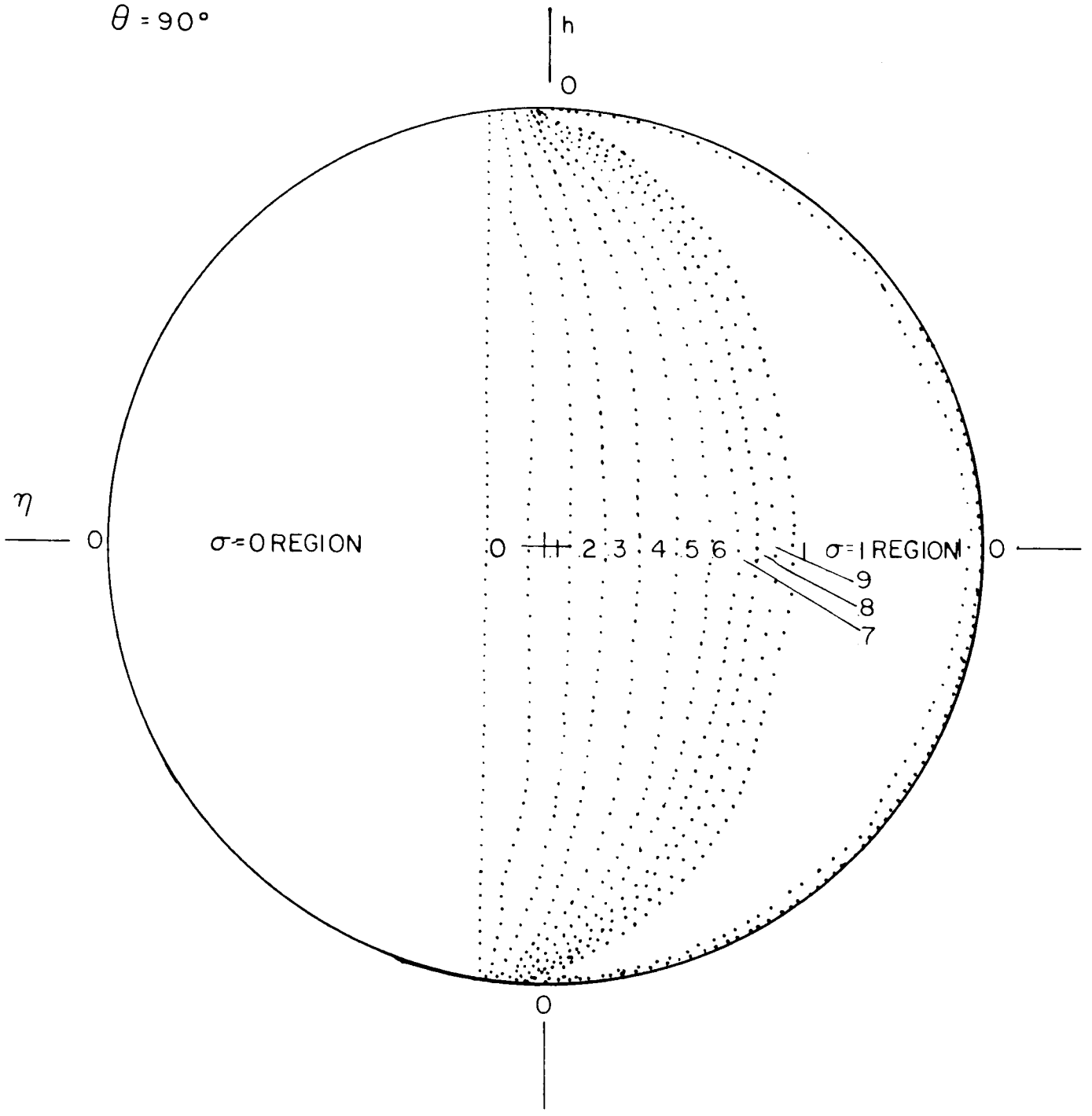

Figure 26. Plane image of photoluminescent homogeneous spherical cloud as seen by an observer at an angle $\theta = 90^{\circ}$ with the sun, showing isophote curves $\sigma(\eta,h,\theta)$ = constant; optical depth $\sigma_e = 1$, radius of sphere R = 4.

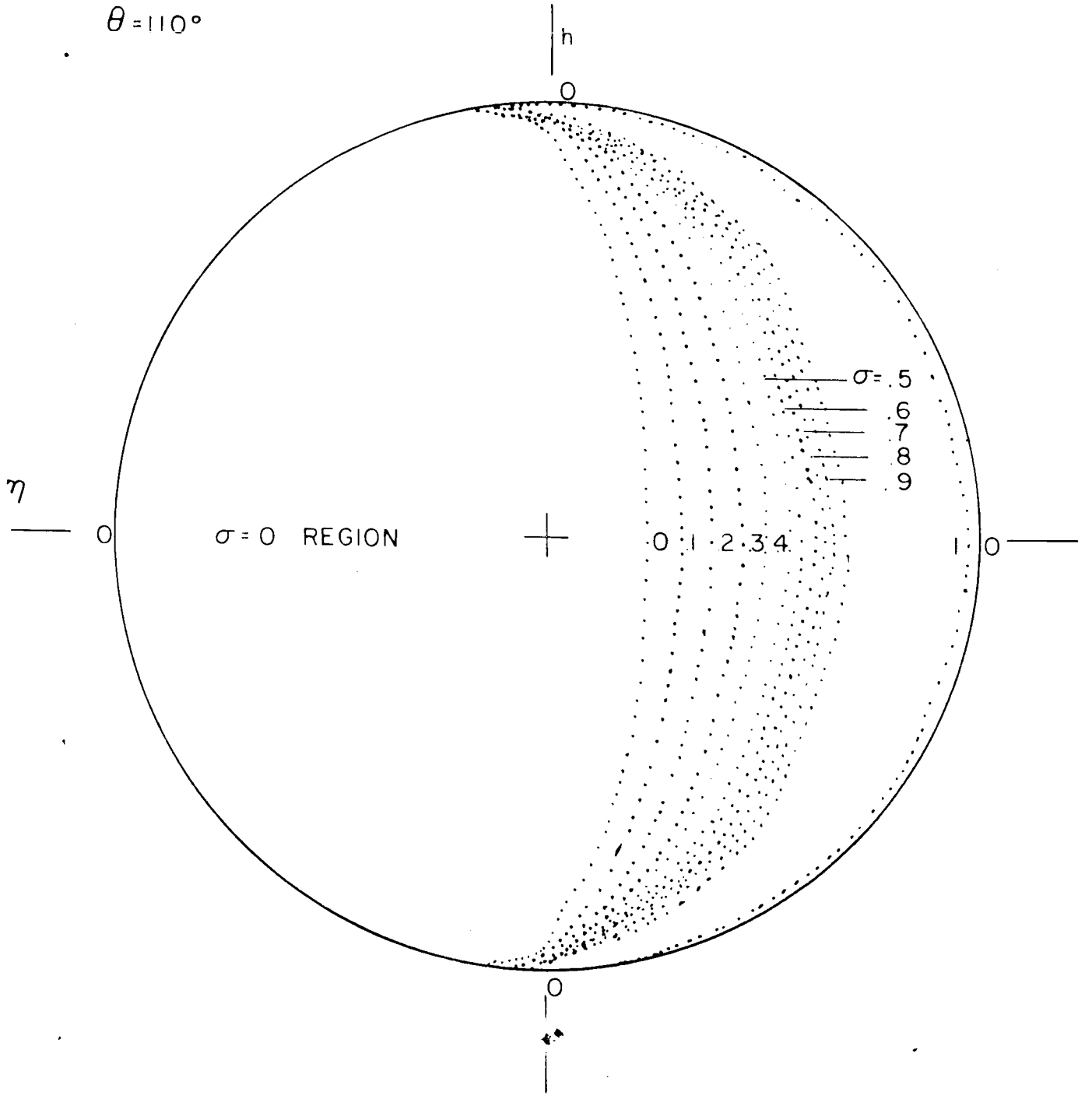

Figure 27. Plane image of photoluminescent homogeneous spherical cloud as seen by an observer at an angle $\theta = 110^{\circ}$ with the sun, showing isophote curves $\sigma(\eta,h,\theta)$ = constant; optical depth $\sigma_e = 1$, radius of sphere R = 4.

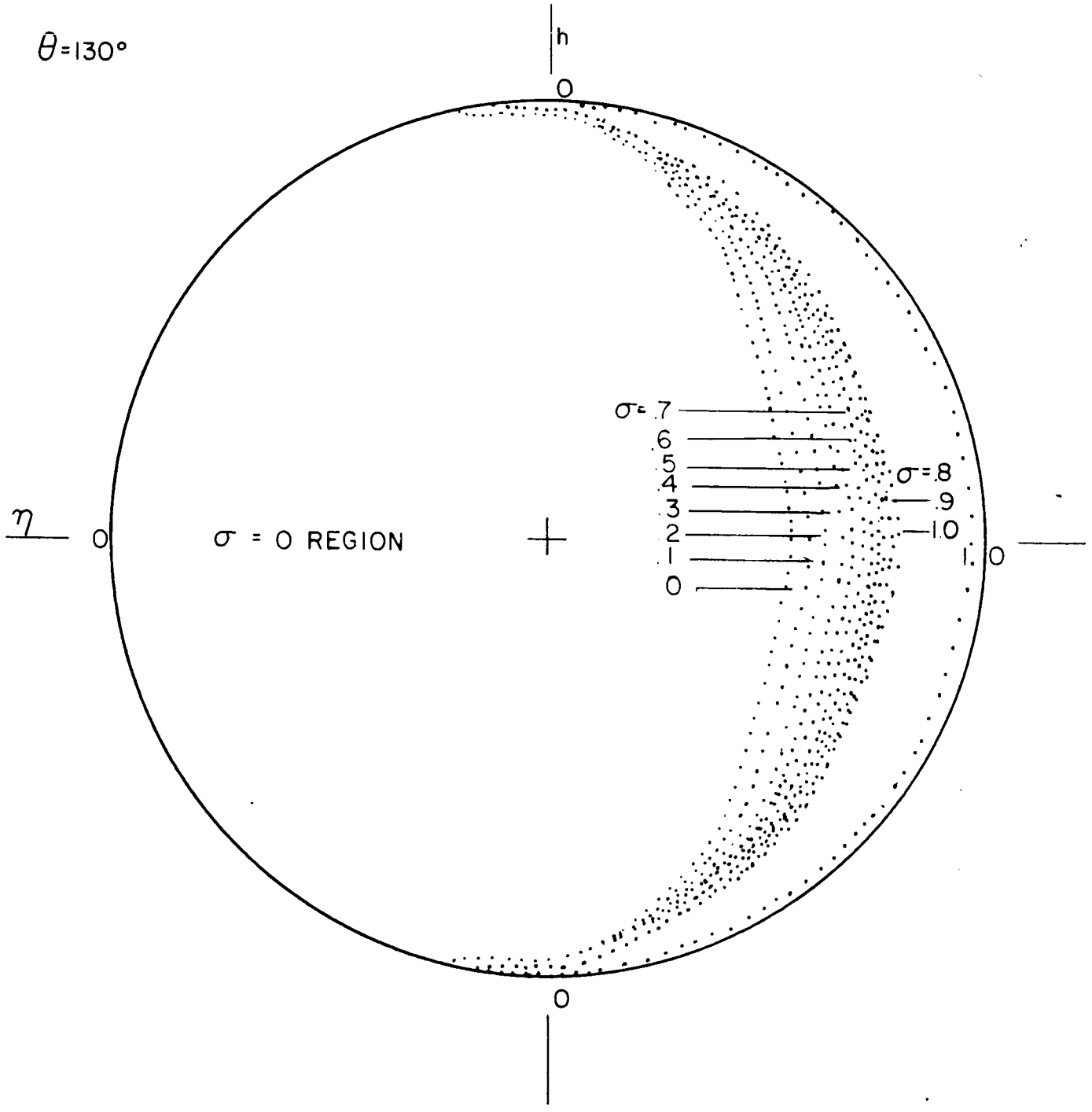

Figure 28. Plane image of photoluminescent homogeneous spherical cloud as seen by an observer at an angle $\theta = 130^{\circ}$ with the sun, showing isophote curves $\sigma(\eta,h,\theta)$ = constant; optical depth $\sigma_e = 1$, radius of sphere R ≒4.

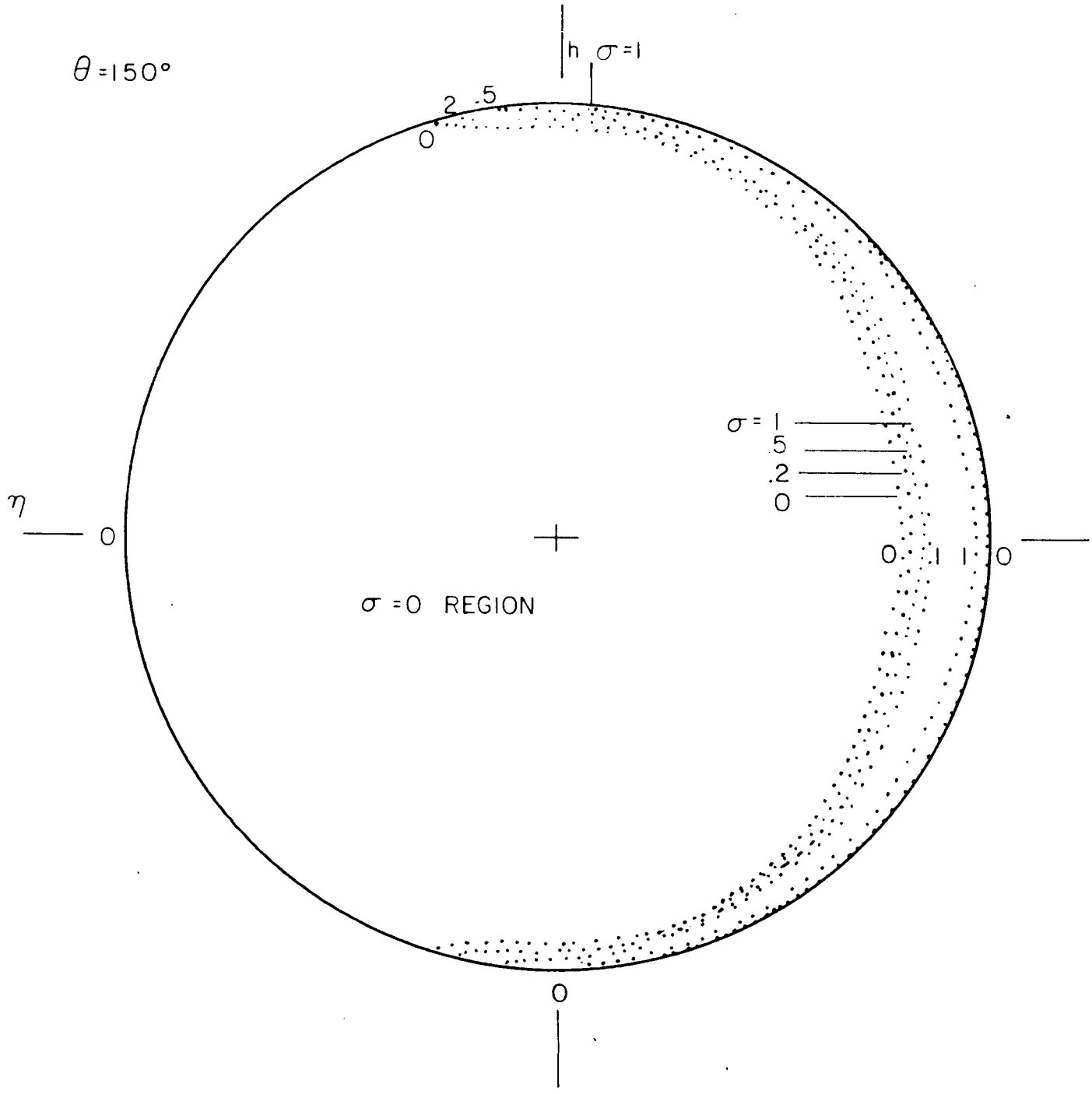

Figure 29. Plane image of photoluminescent homogeneous spherical cloud as seen by an observer at an angle $\theta = 150^{\circ}$ with the sun, showing isophote curves $\sigma(\tau_1, h, \theta)$ = constant; optical depth $\sigma = 1$, radius of sphere R = 4.

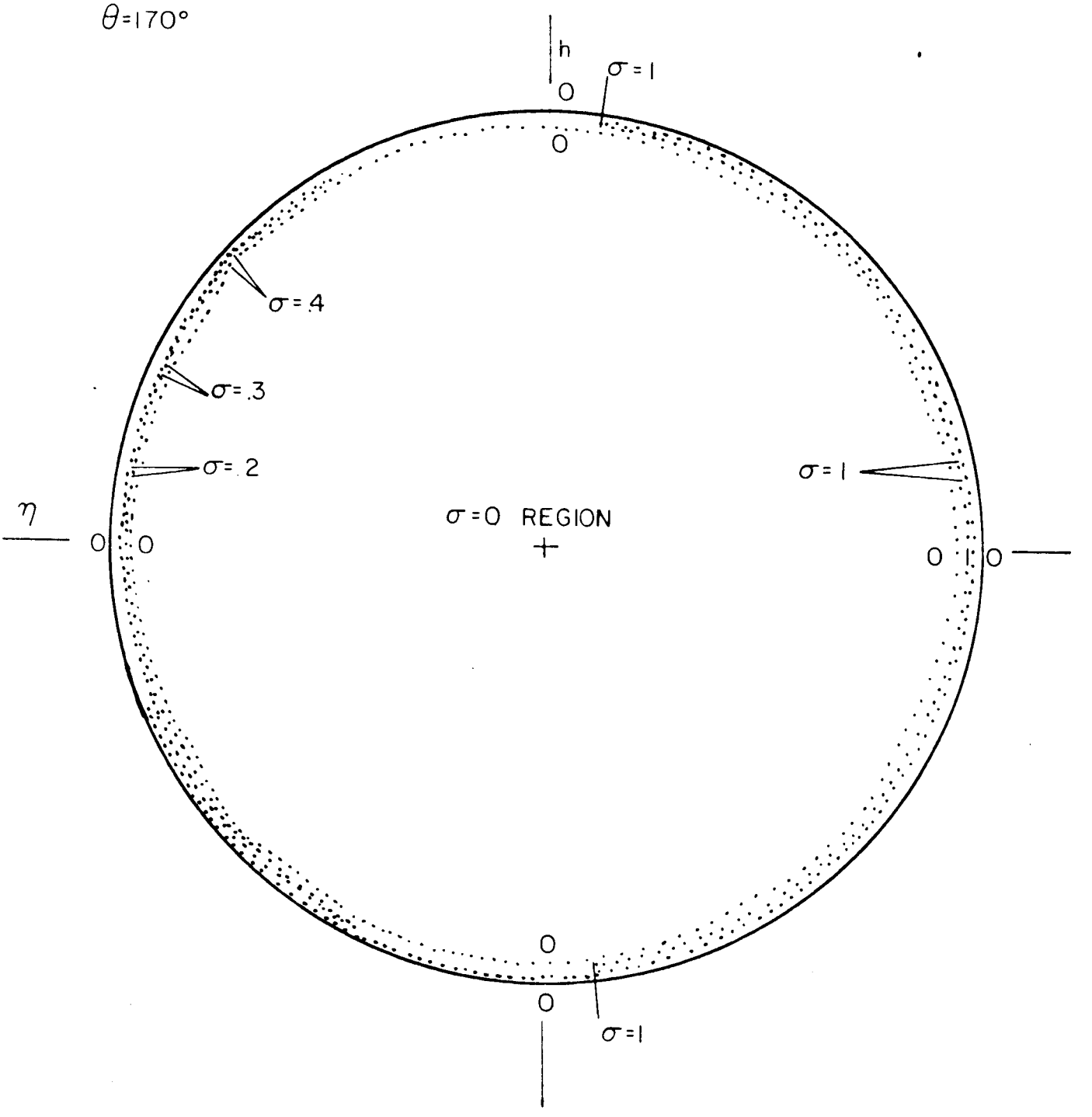

Figure 30. Plane image of photoluminescent homogeneous spherical cloud as seen by an observer at an angle $\theta = 170^{\circ}$ with the sun, showing isophote curves $\sigma(\eta,h,\theta)$ = constant; optical depth $\sigma_e = 1$, radius of sphere R = 4.

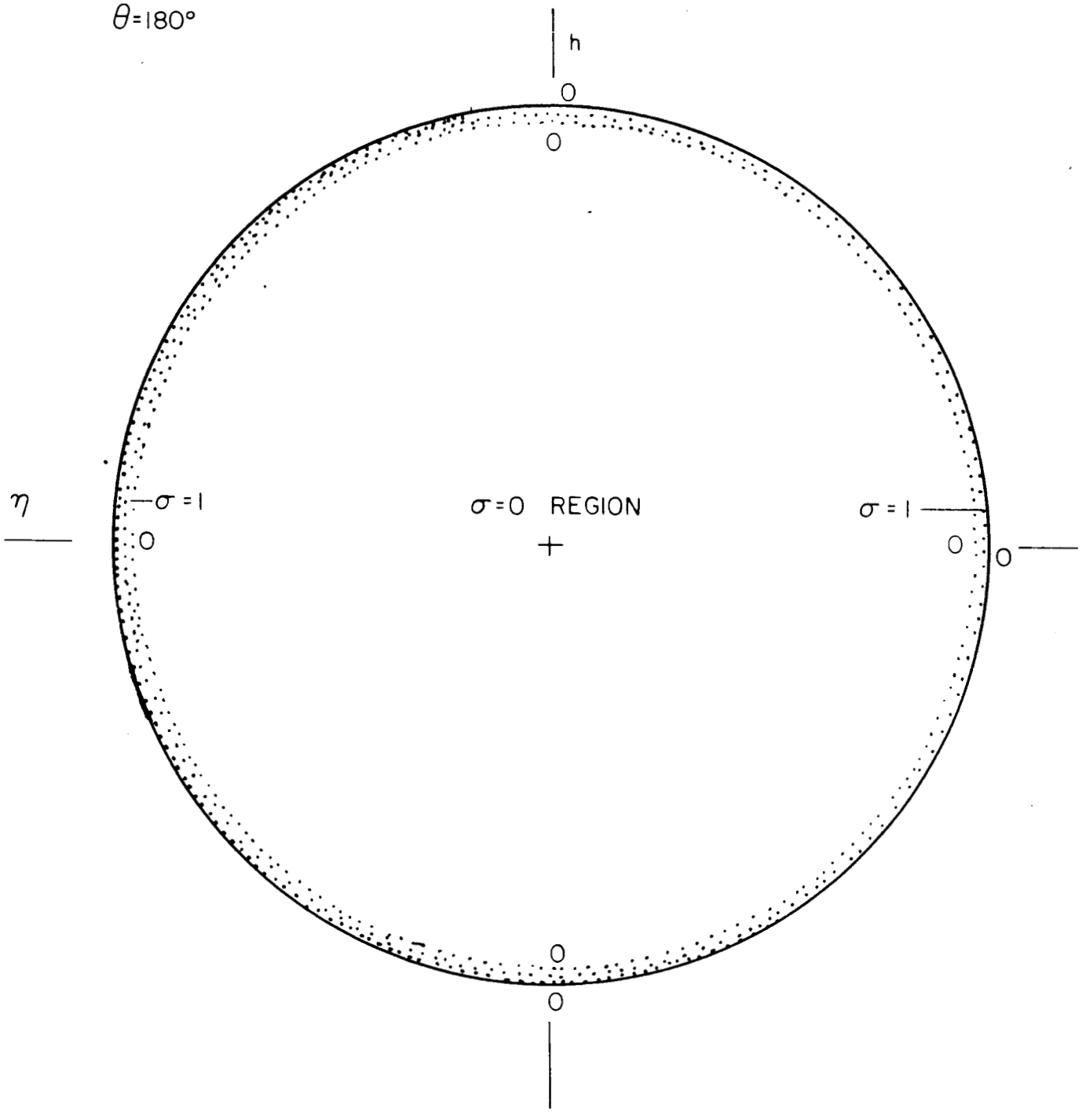

Figure 31. Plane image of photoluminescent homogeneous spherical cloud as seen by an observer at an angle $\theta = 180^{\circ}$ with the sun, showing isophote curves $\sigma(\eta,h,\theta)$ = constant; optical depth $\sigma_e = 1$, radius of sphere R = 4.

This concludes the discussion of the graphical approach to the construction of the isophote curves in the image plane (η, h) for a given orientation θ of the observer relative to the sun.

The reader should refer to the remarks in paragraph B.1 relative to the application of the tabular values of the brightness function to larger size spherical clouds (that is, R greater than four optical lengths).

In paragraph C of this section an excursion into an analytic approach to the phase function problem is made. The evident ease, with which the analog (graphical) approach circumvented the need for a detailed description of the circular arc regions, is made all the more evident by contrast with the minute analysis necessitated by an analytic approach. Though the level of mathematics involved is elementary, it is soon found that a handling of the problem (of defining the function $\sigma = \sigma(\eta, r, \theta)$ by simple-valued analytic representations) is not a simple task.

C. ANALYTIC APPROACH TO THE PROBLEM

1. Case 1: $0 \leq \theta \leq 90^\circ + \alpha$, $\alpha = \arcsin(1/2\ e/r)$

In Figure 32 let the circles with centers at A, B, and C be designated either as A, B, and C or as 1, 2, and 3, respectively. Each has a radius r.

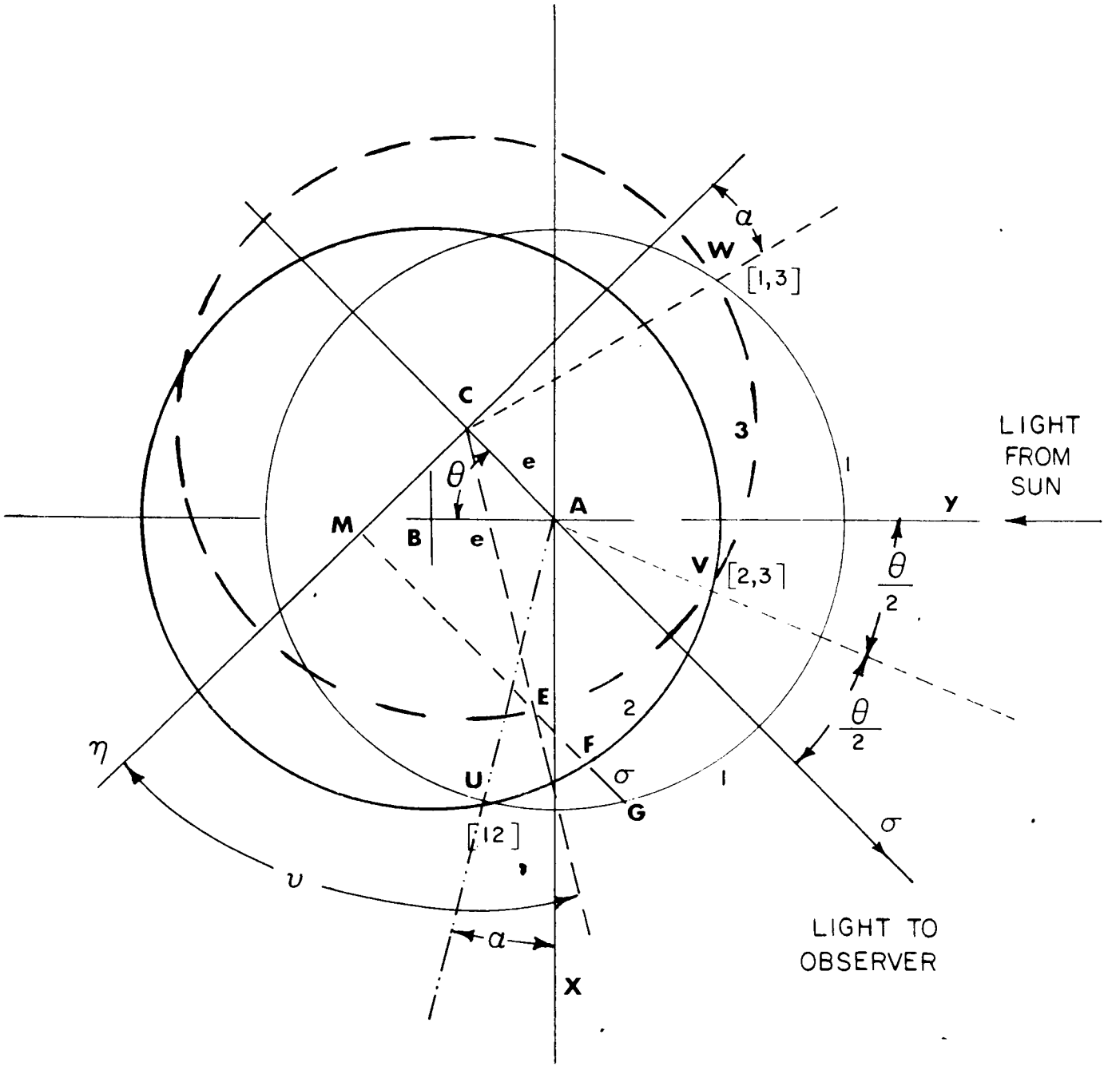

Figure 32. Schematic of plane section of truncated photoluminescent cloud solid, $0 \leq \theta \leq 90^{o} + \alpha$.

The optical length (depth) is designated as e, so that

$$|A\ B| = |A\ C| = e \tag{12}$$

The point E on the C circle is defined by the (parametric) angle υ so that

$$\overset{X}{1}\ MCE \equiv \upsilon \tag{13}$$

where M is a point on the η-axis and C is the origin, $\eta = 0$, $\sigma = 0$, of the η, σ coordinate system associated with circle C.

Let $\sigma(1)$, $\sigma(2)$, and $\sigma(3)$ designate the distance from the $\eta\sigma$axis, $\sigma = 0$, to the circles 1, 2, and 3, respectively, measured along an $\eta \equiv$ constant line.

The brightness function $\sigma(\eta, r, \theta)$ is defined as the (chord) length of the intersection of the line η = constant across the circular arc region U-V-W defined by the three circles A, B, and C.

For υ in the range $0 \leq \upsilon \leq$ MCW $= 180^{\circ} - \alpha$, it is seen from an inspectionof Figure 32 that

$$\sigma(1) = e + r \sin \upsilon \tag{14a}$$

$$\sigma(2) = e - e \cos \theta + \sqrt{r^2 - (r \cos \upsilon - e \sin \theta)^2} \tag{14b}$$

$$\sigma(3) = r \sin \upsilon \tag{14c}$$

and for υ in range $180^\circ - \alpha \leqq \upsilon \leqq 180^\circ$

$$\sigma(1+) = e + r \sin \upsilon \qquad (14a_1')$$

$$\sigma(1-) = e - r \sin \upsilon \qquad (14a_2')$$

and

$$\sigma(3) = r \sin \upsilon \qquad (14c')$$

where

$$\sin \alpha = 1/2\ e/r\ ,\ \alpha = \arcsin\ (1/2\ e/r) \qquad (15)$$

Let the intersection of circle 1 with 2 be designated by (1, 2), circle 1 with 3 as (1, 3), and circle 2 with 3 as (2, 3); these points of intersection are labeled U, W, and V, respectively in Figure 32. (The diametrically opposite points of intersection are not needed in this case.)

To find the value of υ corresponding to the point U: (1, 2), one requires that

$$\sigma(1) = \sigma(2) \qquad (16)$$

This means that

$$e + r \sin \upsilon = e - e \cos \theta + [r^2 - (r \cos \upsilon - e \sin \theta)^2]^{1/2} \qquad (16a)$$

according to the formulas in (14).

Eliminating the term e and moving the term e cos θ to the left hand side and squaring and simplifying, it is seen that at U: (1, 2)

$$e = 2r \sin(\theta - \upsilon) \equiv 2r \sin[180^{\circ} - (\theta - \upsilon)] \qquad (16b)$$

according to (15)

$$e = 2r \sin \alpha \qquad (15)$$

so that one has by comparison of (15) and (16b) that either

$$\theta - \upsilon = \alpha \quad \text{or} \quad 180^{\circ} - (\theta - \upsilon) = \alpha \qquad (16c)$$

To resolve this branch question, it is necessary to consider the point F on the circle 2 when it is at U: (1, 2). The diagram in Figure 33 is useful in this resolution.

An inspection of Figure 33 discloses that

$$\upsilon + \alpha = \theta \qquad (16d)$$

so that

$$\upsilon = \theta - \alpha \quad \text{at} \quad U : (1, 2) \qquad (16d')$$

The necessity of selecting between multiple choices of the values of the variables involved is a continuing task inherent in this analytic approach.

The value of υ associated with the intersection point (2, 3) at V is determined by the equation

$$\sigma(2) = \sigma(3) \qquad (17)$$

This means that

$$e - e \cos\theta + [r^2 - (r \cos\upsilon - e \sin\theta)^2]^{1/2} = r \sin\upsilon \qquad (17a)$$

according to the formulas in (14).

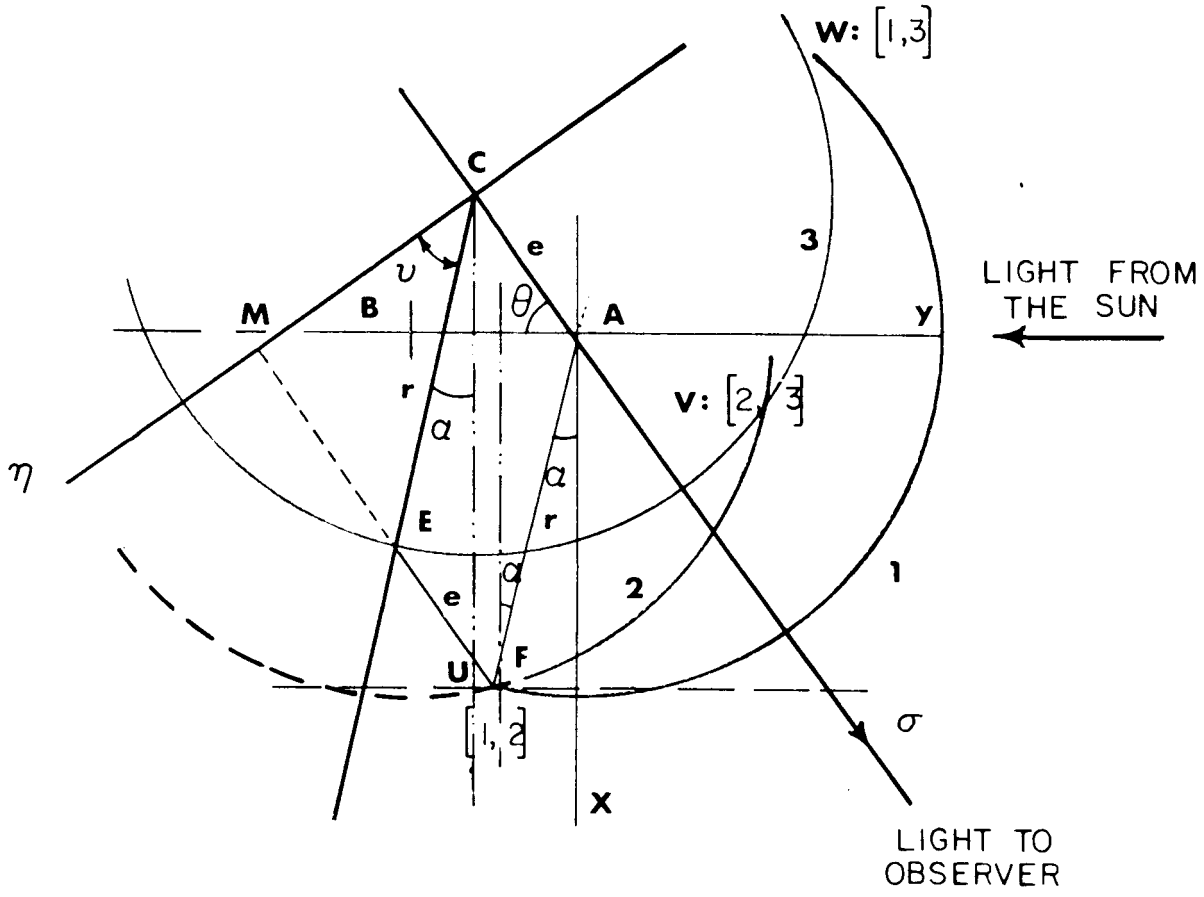

Figure 33. Diagram to determine υ at U : (1,2).

Rearranging terms and squaring, one has

$$(r \sin \upsilon + e \cos \theta - e)^2 = r^2 - (r \cos \upsilon - e \sin \theta)^2 \qquad (17b)$$

which reduces to the equation

$$e\,(1 - \cos \theta) = r\,[\sin \upsilon + \sin\,(\theta - \upsilon)] \qquad (17c)$$

for the angle υ at the point V : (2, 3).

It is convenient at this time to introduce the rectangular coordinates η, σ associated with the η, σ reference system associated with the circle C:

$$\eta = r \cos \upsilon \quad \text{and} \quad \sigma = r \sin \upsilon \qquad (17d)$$

Using these definitions of r cos υ and r sin υ in the expanded form of equation (17c) it is found that the η, σ relationship at the point V : (2, 3) is

$$e \sin 1/2\,\theta = \sigma \sin 1/2\,\theta + \eta \cos 1/2\,\theta \qquad (17e)$$

In terms of the coordinate η.

$$\eta = (e - \sigma) \tan 1/2\,\theta \qquad (17f)$$

Equation (17f) is a single equation in the two unknows η and σ at the point V : (2, 3) of the circle C. A second equation relating η and σ is

$$r^2 = \eta^2 + \sigma^2 \qquad (17g)$$

the equation of the circle C in the η, σ frame. Combining (17g) and (17f) results in the equation

$$r^2 = (e - \sigma)^2 \tan^2 1/2\,\theta + \sigma^2 \qquad (17h)$$

which is quadratic in σ. The canonical form of this quadratic equation is

$$(\sigma - e \sin^2 1/2\,\theta)^2 = (r^2 - e^2 \sin^2 1/2\,\theta) \cos^2 1/2\,\theta \qquad (17i)$$

Extracting the square root it is seen that σ at V : (2, 3) is determined by the branch point equations

$$\sigma = e \sin^2 1/2\,\theta + \sqrt{r^2 - e^2 \sin^2 1/2\,\theta} \cos 1/2\,\theta \qquad (17j')$$

and

$$\sigma = e \sin^2 1/2\,\theta - \sqrt{r^2 - e^2 \sin^2 1/2\,\theta} \cos 1/2\,\theta \qquad (17j'')$$

The resolution of the branch question in this case, as to which of these two equations to use to define $\sigma = r \sin \upsilon$ at V : (2, 3), consider Figure 32 as $\theta \to 0$: when $\theta \to 0$, point C $\to$ point B and the point V : (2, 3) then falls on the y-axis as the σ-axis $\to$ y-axis; meanwhile the equations (17j′) and (17j″) take on the forms $\sigma = r$ and $\sigma = -r$, respectively. Sence $\sigma \cong r$ when $\theta \cong 0$, according to Figure 32, the choice of σ is resolved:

$$\sigma = e \sin^2 1/2\,\theta + [r^2 - e^2 \sin^2 1/2\,\theta]^{1/2} \cos 1/2\,[\text{ at V : (2, 3)} \qquad (17k)$$

which requires that

$$\upsilon \equiv \upsilon(V) \tilde{\equiv} \arcsin \left[\frac{e}{r} \sin^2 1/2\,\theta + \sqrt{1 - \frac{e^2}{r^2} \sin^2 1/2\,\theta}\, \cos 1/2\,\theta\right] \text{ at } V : (2,3) \tag{17ℓ}$$

since $\sigma = r \sin \upsilon$, according to equation (17d).

To find the value of υ corresponding to the point W : (1, 3), one requires that

$$\sigma(1-) = \sigma(3) \quad \text{at} \quad W : (1, 3) \tag{18}$$

This means that

$$e - r \sin \upsilon = r \sin \upsilon \tag{18a}$$

according to equation ($14a_2'$) and Figure 32, with υ in the range $180^\circ \geqq \alpha \leqq \upsilon \leqq 180^\circ$.

Evidently, from (18a), the angle υ is determined by the relationship

$$2r \sin \upsilon = e \quad \text{at} \quad W : (1, 3) \tag{18b}$$

But

$$e = 2r \sin \alpha = 2r \sin (180^\circ - \alpha)$$

so that

$$\upsilon = 180^\circ - x \quad \text{at} \quad W: (1, 3) \tag{18c}$$

since the choice $\upsilon = \alpha$ is excluded by Figure 32.

This concludes the determination of the end points U, V, and W of the circular arc region U, V, W, so that the range of the parameter υ is known as $\eta = r \cos \upsilon$ sweeps through the range of definition of the brightness function $\sigma(\eta, r, \theta)$.

According the shape and orientation of the circluar arc region U, V, W in Figure 32, the function $\sigma(\eta, r, \theta)$ has the following definitions:

for υ in the range U : (1, 2) $\leftrightarrow$ V : (2,3),

$$\sigma(\eta, r, \theta) \equiv \sigma(1) - \sigma(2) \tag{19a}$$

so that

$$\sigma(\eta, r, \theta) = r \sin \upsilon + \cos \theta - [r^2 - (r \cos \upsilon - e \sin \theta)^2]^{1/2} \tag{19a'}$$

for υ in the range $\theta - \alpha \leqq \upsilon \leqq \upsilon(V)$, where $\upsilon(V)$ is defined by equation (17ℓ); for υ in the range V : (2, 3) $\leftrightarrow$ W : (1, 3)

$$\sigma(\eta, r, \theta) \equiv \sigma(1+) - \sigma(3) \tag{19b}$$

so that

$$\sigma(\eta, r, \theta) = e \tag{19b'}$$

for υ in the range $\upsilon(V) \leqq \upsilon \leqq 180^\circ - \alpha$, where $\alpha = \arcsin (1/2\ e/r)$;

and, finally, for υ in the range $180^\circ - \alpha \leqq \upsilon \leqq 180^\circ$

$$\sigma(\eta, r, \theta) \equiv \sigma(1+) - \sigma(1-) \equiv 2r \sin \upsilon \tag{19c}$$

2. Case 2: $90^\circ + \alpha \leqq \theta \leqq 180^\circ - 2\alpha$, $\alpha = \arcsin(1/2\ e/r)$

Reference is made to Figure 34 and to the notation used in Case 1.

An examination of Figure 34 reveals that

$$\sigma(1) = e + r \sin \upsilon \quad \text{for} \quad 0 \leqq \upsilon \leqq 180^\circ - \alpha \tag{20a}$$

while

$$\left.\begin{aligned} \sigma(1+) &= e + r \sin \upsilon \\ \sigma(1-) &= e - r \sin \upsilon \end{aligned}\right\} \quad \text{for } 180^\circ - \alpha \leqq \upsilon \leqq 180^\circ \tag{20a'}$$

Further, for υ in the range U : (1, 2) $\leftrightarrow$ V : (2, 3),

$$\sigma(2+) = e - e \cos \theta + [r^2 - (r \cos \upsilon - e \sin \theta)^2]^{1/2} \tag{20b$'_1$}$$

for υ satisfying the inequality

$$r \sin \upsilon > e - c \cos \theta \tag{20b$''_1$}$$

while

$$\sigma(2-) = e - e \cos \theta - [r^2 - (r \cos \upsilon - e \sin \theta)^2]^{1/2} \tag{20b$'_2$}$$

for υ satisfying the unequality

$$r \sin \upsilon < e - e \cos \theta \tag{20b$''_2$}$$

Furthermore

$$\sigma(3) = r \sin \upsilon \quad \text{for} \quad 0 \leqq \upsilon \leqq 180^\circ \tag{20c}$$

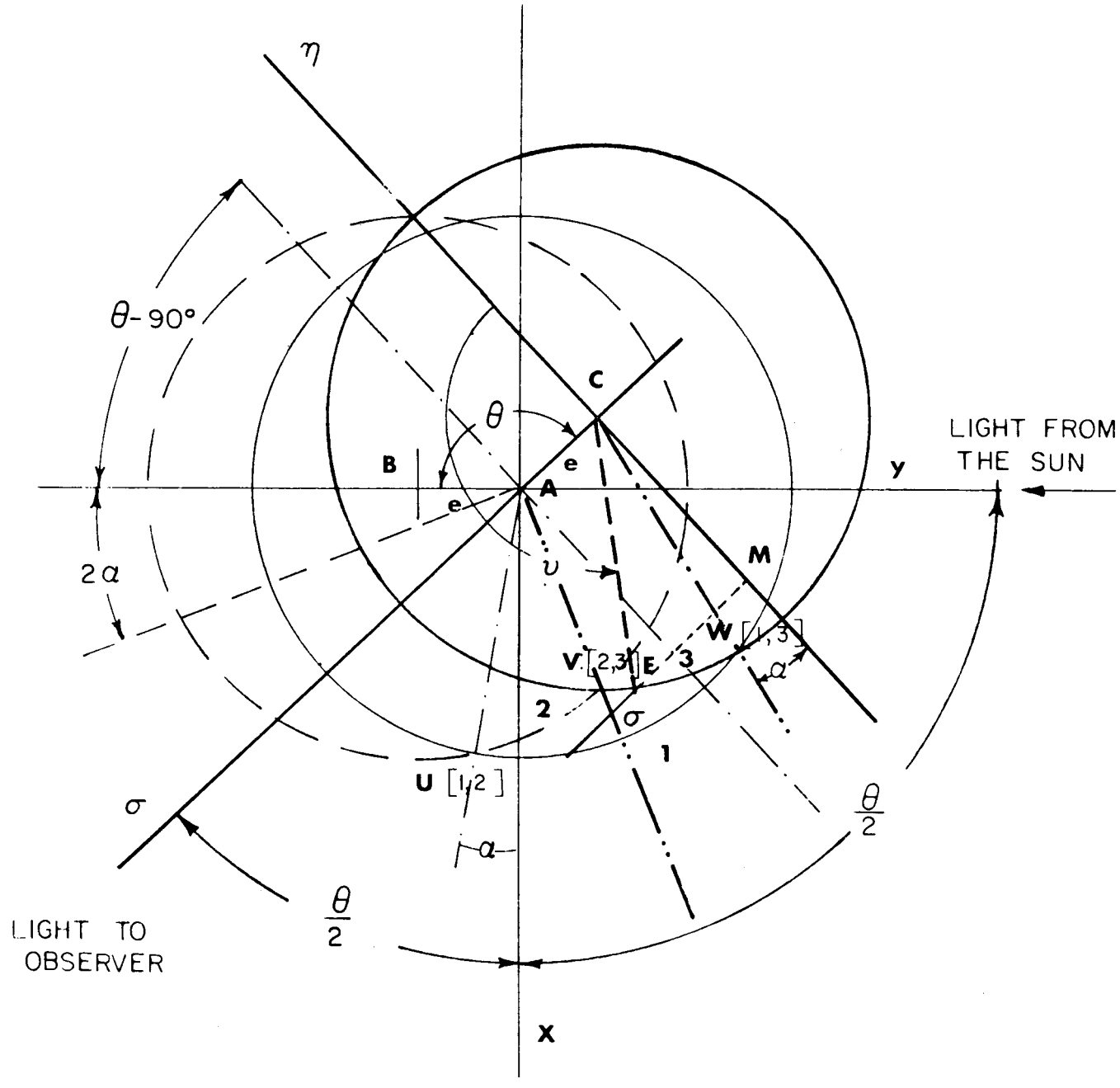

Figure 34. Schematic of plane section of truncated photoluminescent cloud solid, $90^{\circ} + \alpha \leq \theta = 180^{\circ} - 2\alpha$.

A comparison of the formulas for $\sigma(1)$, $\sigma(2+)$, and $\sigma(3)$ for the two cases, Case 1 and Case 2, shows that the formulas are identical in these two cases. This means that the end-point intersections U : (1, 2), V : (2, 3), and W : (1, 3) are determined by conditions on υ for Case 2 which are identical with those required in Case 1. That is to say, the values of the angle υ at the end-points are determined by the following conditions:

$$U : (1, 2) \rightarrow e = 2r \sin (\theta - \upsilon) \tag{21a}$$

$$V : (2, 3) \rightarrow \sigma = e \sin^2 1/2\,\theta \pm [r^2 - e^2 \sin^2 1/2\,\theta]^{1/2} \cos 1/2\,\theta \tag{21b}$$

and

$$W : (1, 3) \rightarrow e = 2r \sin \upsilon \tag{21c}$$

according to equations (16b), (17j′), (17j′), (17j″), and (18b), respectively.

A compatible root of equation (21a) is

$$\upsilon = \theta - \alpha \quad \text{for} \quad U : (1, 2) \tag{21a′}$$

In regard to equation (21b) recall that the formula for $\sigma(2+)$ entails the inequality

$$\sigma = r \sin \upsilon > e - e \cos \theta \tag{20b″}$$

This means that in order that equations (21b) and (20b″) be compatible it is necessary that θ satisfy the inequality condition

$$e - e\cos\theta < 1/2\ e\ (1 - \cos\theta) \pm \sqrt{r^2 - e^2 \sin^2 1/2\ \theta}\cos 1/2\ \theta \qquad (21b')$$

wherein the identity

$$\sin^2 1/2\ \theta = 1/2\ (1 - \cos\theta)$$

is used.

Recall that Case 2 places θ in the range $90^\circ + \alpha \leqq \theta \leqq 180^\circ - 2\alpha$ so that $1/2\ \theta$ is in the range

$$45^\circ + 1/2\ \alpha \leqq 1/2\ \theta \leqq 90^\circ - \alpha,\ \alpha = \arcsin\ (1/2\ e/r) < 90^\circ \qquad (21b'')$$

On the other hand, note from a simple adjustment of equation (21b) that

$$\pm\sqrt{r^2 - e^2 \sin^2 1/2\ \theta}\cos 1/2\ \theta > e \sin^2 1/2\ \theta \qquad (21b''')$$

But $\cos 1/2\ \theta > 0$ for $1/2\ \theta$ in the range specified by equations (21b'') and (21b'''). Hence the positive sign has to be used in front of the radical sign.

The implication is that the intersection V: (2, 3) is determined by a value of υ which is the same as that used in Case 1:

$$\upsilon \equiv \upsilon(V) = \arcsin\ [e/r \sin^2 1/2\ \theta + \sqrt{1 - e^2/r^2 \sin^2 1/2\ \theta}\cos 1/2\ \theta]$$

wherein the restriction imposed on $\sigma(2+)\ r \sin \upsilon(V) > e - e\cos\theta$, at V : (2, 3), is satisfied*

* A discussion of the applicability of the formula $\sigma(2-)$, listed in equation ($20b_2'$), is not taken up in these current remarks abour Case 2.

Finally, in regard to equation (21c), it is evident from an inspection of Figure 34 that

$$\upsilon = 180^{\circ} - \alpha \quad \text{at} \quad W : (1, 3) \tag{21c'}$$

The formulas for the brightness function $\sigma = \sigma(\eta, r, \theta)$ for Case 2 are identical with those for Case 1 for all values of υ in the region of definition U, V, W of $\sigma(\eta, r, \theta)$.

3. Case 3: $180^{\circ} - 2\alpha \leqq \theta \leqq 180^{\circ} - \alpha$, $\alpha = \arcsin(1/2\ e/r$

Reference is made to Figure 35 and the rotation used in Cases 1 and 2.

Note in Figure 35 that a diametrically opposite circular arc region U', V', W' is introduced in this Case 3 in addition to the customary U, V, W region of the previous two cases, Case 1 and Case 2.

The U', V', W' region is associated with positive values of η_1 $\eta > 0$, wherein υ is in the range $\alpha \leqq \upsilon \leqq 90^{\circ}$; the U,V,W region is associated with negative values of η_1 $\eta < 0$, wherein υ is in the range $90^{\circ} < \upsilon \leqq 180^{\circ} - \alpha$.

An inspection of the U', V', W' region of Figure 35 reveals that

$$\sigma(1) = e - r \sin \upsilon \tag{22a}$$

$$\sigma(2-) = e - e \cos \theta - \sqrt{r^2 - (r \cos \upsilon - e \sin \theta)^2} \tag{22b}$$

and

$$\sigma(3) = r \sin \upsilon \tag{22c}$$

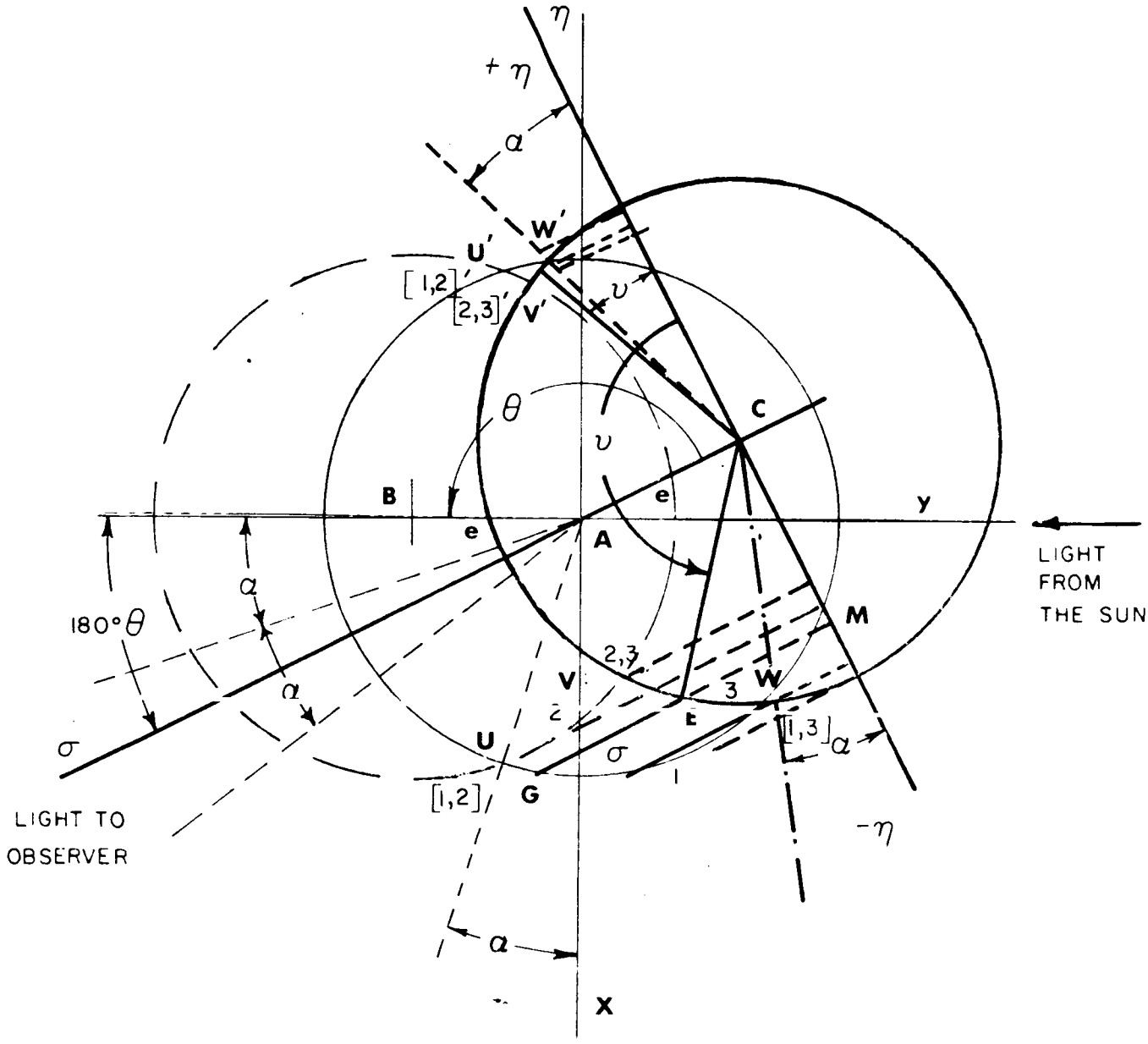

Figure 35. Scheme when θ is in the range $180^\circ - 2\alpha \leq \theta \leq 180^\circ - \alpha$.

The corners U' : $(1, 2)'$, V' : $(2, 3)'$, and W' : $(1, 3)'$ of the U', V', W' region are determined in the same manner as in the previous two cases:

$$U' : (1, 2) \rightarrow \sigma(1-) - \sigma(2-) \rightarrow e = 2r \sin (\upsilon + \theta) \tag{23a}$$

so that

$$\upsilon = 180^{\circ} - \theta - \alpha \quad \text{at} \quad U' : (1, 2)$$

Further,

$$W' : (1, 3)' \rightarrow \sigma(1-) = \sigma(3) \rightarrow e = 2r \sin \upsilon \tag{23b}$$

so that

$$\upsilon = \alpha \quad \text{at} \quad W' : (1, 3)'$$

Finally,

$$V' : (2, 3)' \rightarrow \sigma(2-) = \sigma(3) \tag{23c}$$

which implies that

$$e(1 - \cos \theta) = r \sin (\theta - \upsilon) + r \sin \upsilon \tag{23c'}$$

or that

$$2 e \sin^2 1/2 \theta = \eta \sin \theta + 2\sigma \sin^2 1/2 \theta \tag{23c''}$$

for the η, σ coordinates of the point V' on the circle C,

$$\eta = r \cos \upsilon , \quad \sigma = r \sin \upsilon \tag{17d}$$

Since V' : $(\eta_1\ \sigma)$ at $(2,\ 3)'$ is on the circle C of radius r_1

$$r^2 = \eta^2 + \sigma^2 \qquad (23c''')$$

Further, from (23c")

$$\eta = (e - \sigma) \tan 1/2\ \theta \qquad (23c_1''')$$

Eleminating η between equations (23c"') and ($23c_1$"') results in the equations

$$\sigma = e \sin^2 1/2\ \theta \pm \sqrt{r^2 - e^2 \sin^2 1/2\ \theta} \cos 1/2\ \theta \qquad (23c''')$$

for $\sigma = r \sin \upsilon$ at the point V' : (2, 3).

An examination of the conditions at the point V' : $(2,\ 3)'$ shows that the negative sign is required in the definition of υ at V' : $(2,3)'$ accordingly.

$$\upsilon = \upsilon(V') = \arcsin \left[e/r \sin^2 1/2\ \theta - \sqrt{1-\frac{e^2}{r^2} \sin^2 1/2\ \theta \cos 1/2\ \theta}\right]$$

at V' : (2, 3) $\qquad (23c^V)$

In regard to the U, V, W region in Figure 35 it is readily demonstrated that

$$\sigma(1+) = e + r \sin \upsilon \quad \text{for} \quad 90^\circ < \upsilon < 180^\circ - \alpha \qquad (24a)$$

and

$$\sigma(1+) = e + r \sin \upsilon$$
$$\sigma(1-) = e - r \sin \upsilon \quad \text{for} \quad 180^\circ - \alpha \leqq \upsilon \leqq 180^\circ$$

Further

$$\sigma(2+) = e - e\cos\theta + \sqrt{r^2 - (r\cos\upsilon - e\sin\theta)^2} \qquad (24b_1')$$

$$\sigma(2-) = e - e\cos\theta - \sqrt{r^2 - (r\cos\upsilon - e\sin\theta)^2} \qquad (24b_2')$$

and, as usual,

$$\sigma(3) = r\sin\upsilon \qquad (24c)$$

The corners U, V, and W of the u, V, W region have the following definitions:

$$U : (1, 2) \leftrightarrow \sigma(1+) = \sigma(2+) \rightarrow e = -2r\sin(\upsilon-\theta) \qquad (25a)$$

so that

$$\upsilon - 90^\circ + \alpha = 90^\circ - (180^\circ - \theta) \rightarrow \upsilon = \theta - \alpha \text{ at } U : (1, 2) \qquad (25a')$$

further,

$$W : (1, 3) \rightarrow \sigma(1-) = \sigma(3) \rightarrow e = 2r\sin\upsilon \qquad (25b)$$

so that

$$\upsilon = 180^\circ - \alpha \quad \text{at} \quad W : (1, 3) \qquad (25b)$$

and, finally,

$$V : (2, 3) \rightarrow \sigma(2+) = \sigma(3) \qquad (25c)$$

which implies that

$$\upsilon = \upsilon(V) \doteq 180^{\circ} - \arcsin\left[e/r \sin^2 1/2\,\theta + \sqrt{1 - \frac{e^2}{r^2}\sin^2 1/2\,\theta \cos 1/2\,\theta}\right]$$

at V : (2, 3)

Consider now the brightness function $\sigma(\eta, r, \theta)$ and its definition as the length of chord across the boundary of the circular arc region when the chord has the σ-direction associated with the (η, σ) reference system of circle C.

The enlarged view in Figure 36 clearly points out the intricacy of the definition of the function $\sigma(\eta_1\ r_1\ \theta)$ because of the length and orientation of the chord of the boundary of the U, V, W, region.

Reading from Figure 36 it is seen that there are four regions: I, II, III, and IV of definition of the angle υ in the circular arc region U, V, W in Case 3:

$$\text{I:}\quad (2, 3) \leftrightarrow (1, 2) \tag{26a}$$

$$\text{II:}\quad (1, 2) \leftrightarrow (2, 2) \tag{26b}$$

$$\text{III:}\quad (2, 2) \leftrightarrow (1, 3) \tag{26c}$$

$$\text{IV:}\quad (1, 3) \leftrightarrow (1, 1) \tag{26d}$$

The rotation (1, 2), (1, 3), and (2, 3) as the intersection point of circles 1 and 2, 1 and 3, and 2 and 3, respectively, is familiar, where circle 1 has the point A as center (and is also referred to as circle A), circle 2 (= circle B) has point B as center, and circle 3 (= circle C) has point C is center, The rotation (1, 1) signifies the extremity of circle A relative to the η direction, etc.

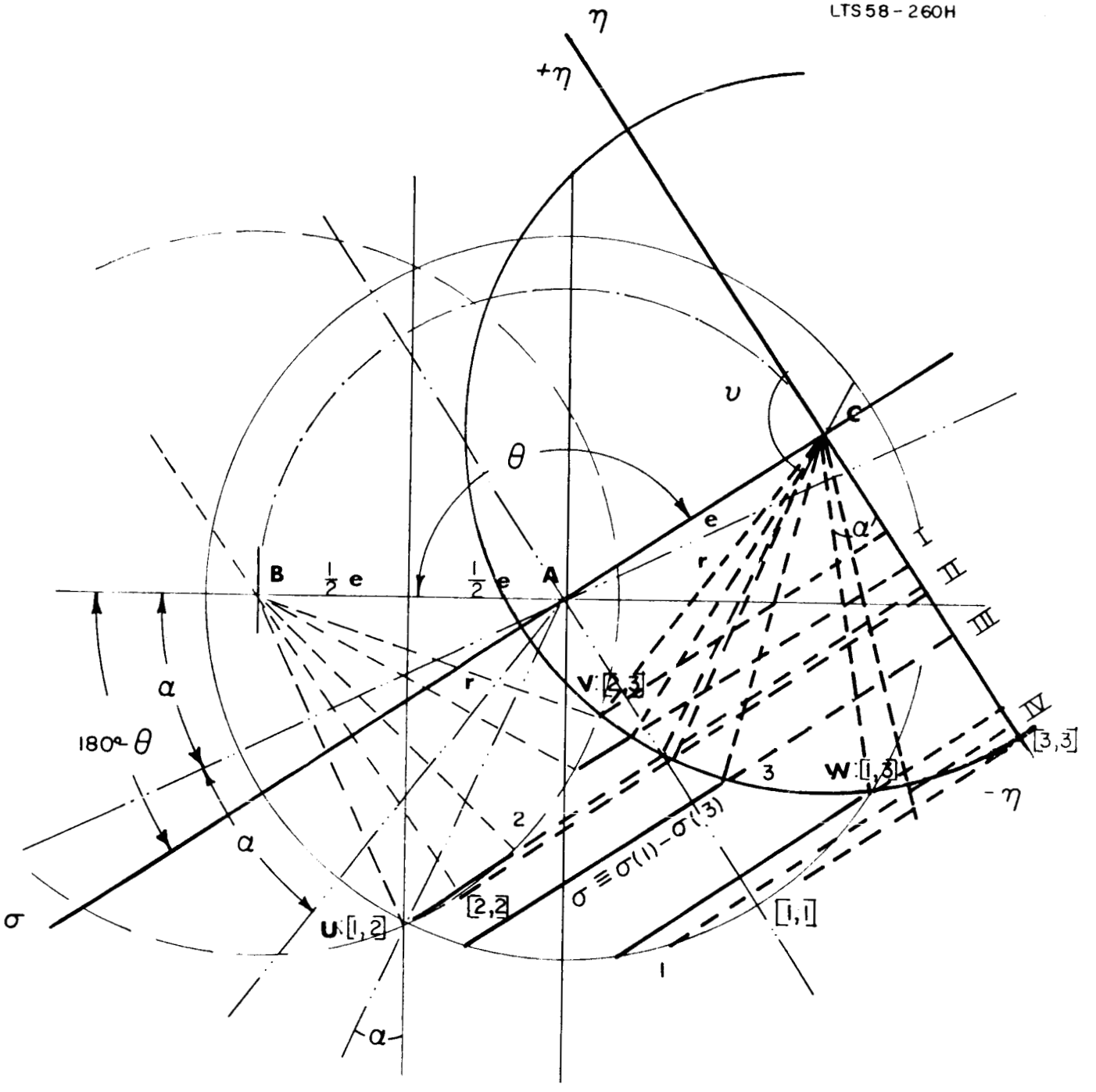

Figure 36. Enlarged view of region U, V, W for Case 3: $180^{\circ} - 2\alpha \leq \theta \leq 180^{\circ} - \alpha$.

The following distance formulas are read directly off Figure 36:

I: $\sigma(2-) = e - e\cos\theta - [r^2 - (r\cos\upsilon + e\sin\theta)^2]^{1/2}$

$\sigma(3) = r\sin\upsilon$

$\sigma(1+) = e + r\sin\upsilon$

$\sigma(2+) = e - e\cos\theta + [r^2 - (-r\cos\upsilon + e\sin\theta)^2]^{1/2}$

II: $\sigma(2-) = e - e\cos\theta - [r^2 - (-r\cos\upsilon + e\sin\theta)^2]^{1/2}$

$\sigma(3) = r\sin\upsilon$

III: $\sigma(1+) = e + r\sin\upsilon$

$\sigma(3) = r\sin\upsilon$

and

IV: $\sigma(1+) = e + r\sin\upsilon$

$\sigma(1-) = e - r\sin\upsilon$

The end points of the regions I, II, III, and IV are defined by the following conditions:

$$(2,\ 3) \rightarrow \sigma(2+) = \sigma(3)$$

so that

$$\upsilon = \arcsin\left[e/r\ \sin^2 1/2\,\theta + \sqrt{1 - \frac{e^2}{r^2}\sin^2 1/2\,\theta\cos 1/2\,\theta}\right] \text{ at } (2,3)$$

$$(2,\ 2) \rightarrow \sigma(2+) = \sigma(2-)$$

so that

$$r^2 - (-r\cos\upsilon + e\sin\theta)^2 = 0$$

or

$$(r + r \cos \upsilon - e \sin \theta)\ (r - r \cos \upsilon + e \sin \theta) = 0$$

This means that υ satisfies either of the following

$$r\ (1 + \cos \upsilon) = e \sin \theta \quad \text{or} \quad r\ (1 - \cos \upsilon) = - e \sin \theta \qquad (28b)$$

It is immediately evident that the e sin θ equation in (28b) is extraneous since $1 - \cos \upsilon \geqq 0$. Hence the angle υ at (2, 2) is determined by the condition

$$\alpha \cos^2 1/2\ \upsilon = e/r \sin \theta$$

that is,

$$\cos 1/2\ \upsilon = \sqrt{1/2\ e/r \sin \theta} \equiv \sqrt{\sin \alpha \sin \theta} \text{ at } (2, 2)$$

The intersection

$$(1, 3) \rightarrow \sigma(1-) \neq \sigma(3) \rightarrow 2r \sin \upsilon = e$$

so that

$$\upsilon = 180^\circ - \alpha \quad \text{at} \quad (1, 3)$$

finally,

$$(1, 1) \rightarrow \sigma(1+) = \sigma(1-) \rightarrow \sin \upsilon = 0$$

so that

$$\upsilon = 180^\circ \quad \text{at} \quad (1, 1)$$

With these definitions of the end-points of the four regions of U, V, W in hand one can set down the following definitions of the brightness function $\sigma = \sigma(\eta, r, \theta)$ relative to the U,V,W region of Case 3:

I: $\sigma(\eta_1\ r_1\ \theta) \equiv \sigma(2+) - \sigma(3)$

so that

$$\sigma(\eta_1\ r_1\ \theta) = e - e\cos\theta - r\sin\upsilon - [r^2 - (r\cos\upsilon - e\sin\theta)^2]^{\frac{1}{2}}$$

II: $\sigma(\eta_1\ r_1\ \theta) \equiv [\sigma(1+) - \sigma(3)] - [\sigma(2+) - \sigma(2-)]$

so that

$$\sigma(\eta_1\ r_1\ \theta) = e - 2[r^2 - (r\cos\upsilon - e\sin\theta)^2]^{1/2}$$

III: $\sigma(\eta_1\ r_1\ \theta) \equiv \sigma(1+) - \sigma(3)$

so that

$$\sigma(\eta_1, r, \theta) = e$$

and

IV: $\sigma(\eta_1\ r_1\ \theta) \equiv \sigma(1+) - \sigma(-) = 2r\sin\upsilon$

4. Case 4: $180^\circ - \alpha \leq \theta \leq 180^\circ$, $\alpha = \arcsin(1/2\ e/r)$

When θ is in the range $(180^\circ - \alpha, 180^\circ)$, so that the observer is looking at the photoluminescent cloud in the near direction of the sun, there are two regions of definition U′, V′, W′ and U, V, W for the brightness function $\sigma = \sigma(\eta_1\ r_1\ \theta)$, as shown in Figure 37.

Following the rotation and descriptive scheme used in Case 3 (where there were also two main regions U′, V′, W′ and U, V, W), it is possible to write down the following statements after an inspection of Figure 37:

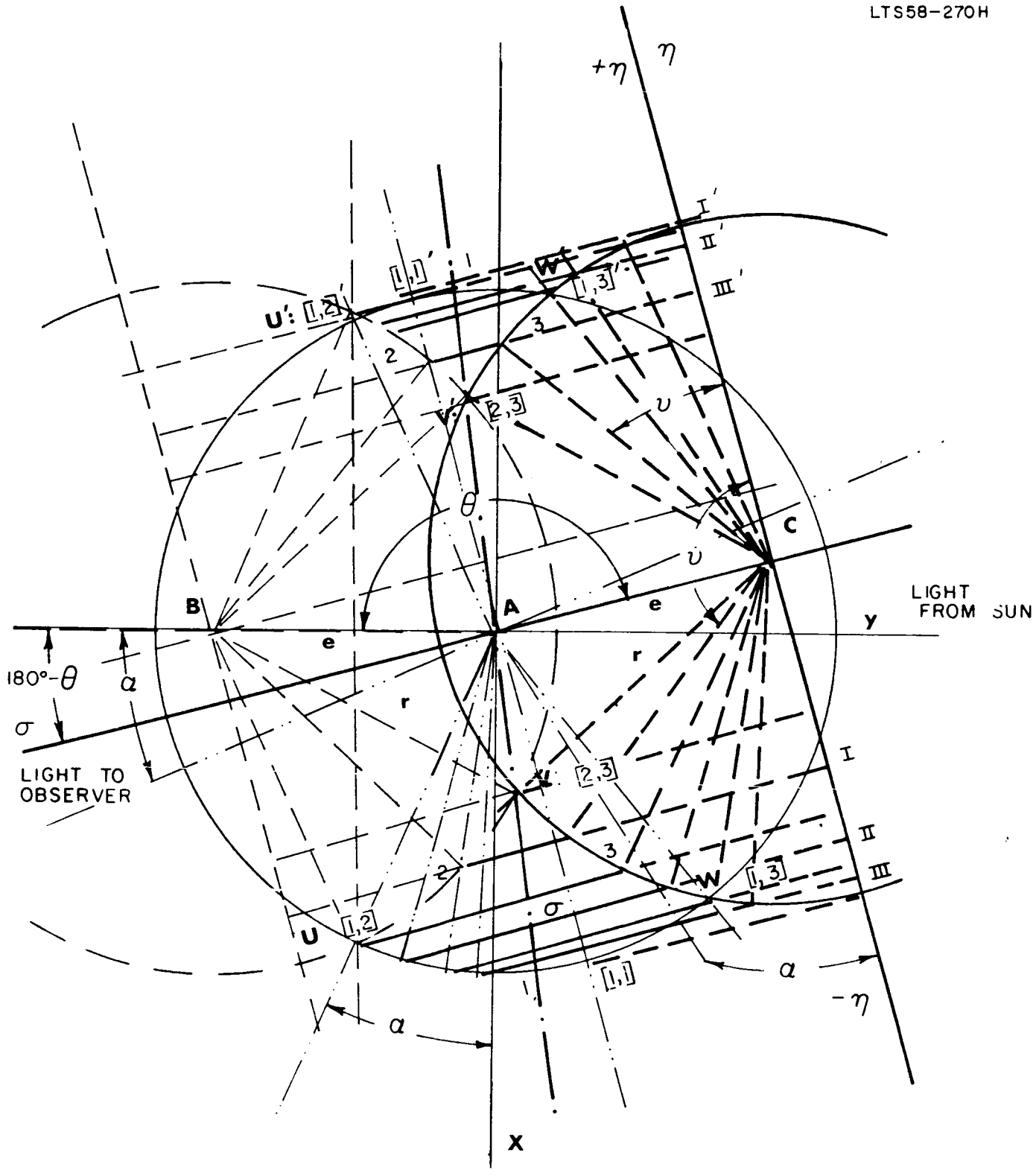

Figure 37, Plane section circular arc regions U', V', W' and U, V, W when $180^\circ - \alpha \leq \theta \leq 180^\circ$.

For $\eta > 0$,

$$I': \quad (1, 1)' \leftrightarrow (1, 2)'$$

$$II': \quad (1, 2)' \leftrightarrow (1, 3)'$$

$$III': \quad (1, 3)' \leftrightarrow (2, 3)$$

where

$$(1, 1)' \rightarrow \sigma(+) = \sigma(1-) \rightarrow \upsilon = 0$$

$$U': \ (1, 2)' \rightarrow \sigma(1+) = \sigma(2)$$

$$V': \ (2, 3)' \rightarrow \sigma(2) = \sigma(3)$$

and

$$W': \ (1, 3)' \rightarrow \sigma(1-) = \sigma(3)$$

In this case,

$$\sigma(1+) = e + r \sin \upsilon$$

$$\sigma(1-) = e - r \sin \upsilon$$

$$\sigma(2) = e - e \cos \theta - [r^2 - (r \cos \upsilon - e \sin \theta)^2]^{1/2}$$

and

$$\sigma(3) = r \sin \bar{\upsilon}$$

The intersection points U', V', and W' require the folowing conditions on the angle υ:

$$U': \ (1, 2)' \rightarrow e = -2r \sin (\upsilon - \theta) \equiv 2r \sin [180^\circ - \theta + \upsilon]$$

so that

$$\bar{\upsilon} = \alpha - (180^\circ - \theta) \quad \text{at} \quad U': \ (1, 2)$$

$$W' : (1, 3)' \rightarrow e = 2r \sin \upsilon$$

so that

$$\upsilon \text{ , } \alpha \quad \text{at} \quad W' : (1, 3)$$

and, finally,

$$V' : (2, 3)' \rightarrow 2e \sin^2 1/2\ \theta - \sigma = \eta \sin \theta - \sigma \cos \theta$$

or

$$\eta = (e - \sigma) \tan 1/2\ \theta$$

so that

$$\sigma = e \sin^2 1/2\ \theta - \sqrt{r^2 - e^2 \sin^2 1/2\ \theta} \cos 1/2\ \theta$$

since $r^2 = \eta^2 + \sigma^2$ on circle C. It follows from and the definition $\sigma = r \sin \upsilon$, that

$$\upsilon = \arcsin \left[e/r \sin^2 1/2\ \theta - \sqrt{1 - \frac{e^2}{r^2} \sin^2 1/2\ \theta} \cos 1/2\ \theta\right] \text{ at } V': (2,3)$$

With the endpoints of the regions I′, II′, and III′ determined by the foregoing formulas, the parameter υ is adequately defined in the following formulas for the brightness function $\sigma(\eta_1\ r_1\ \theta)$ in the U′, V′, W′ region:

$$I': \quad \sigma(\eta_1\ r_1\ \theta) = 2r \sin \upsilon$$

$$II': \quad \sigma(\eta_1\ r_1\ \theta) = r \sin \upsilon - e \cos \theta - \left[r^2 - (\cos\ \upsilon - e \sin \theta)^2\right]^{1/2}$$

and

$$III': \quad \sigma(\eta_1\ r_1\ \theta) = e - \cos \theta - r \sin \upsilon - \left[r^2 - (r \cos \upsilon - e \sin \theta)^2\right]^{1/2}$$

For $\eta < 0$,

$$\text{I:} \quad (2, 3) \leftrightarrow (1, 2)$$

$$\text{II:} \quad (1, 2) \leftrightarrow (1, 3)$$

and

$$\text{III:} \quad (1, 3) \leftrightarrow (1, 1)$$

where

$$(1, 1) \rightarrow \sigma(1+) = \sigma(1-) \rightarrow \upsilon = 180^{\circ}$$

and

$$U : (1, 2) \rightarrow \sigma(12) = \sigma(2)$$

$$V : (2, 3) \rightarrow \sigma(2) = \sigma(3)$$

$$W : (1, 3) \rightarrow \sigma(-) = \sigma(3)$$

wherein

$$\sigma(1+) = e + r \sin \upsilon$$

$$\sigma(1-) = e - r \sin \upsilon$$

$$\sigma(2) = e - e \cos \theta - \sqrt{r^2 - (r \cos \upsilon - e \sin \theta)^2}$$

$$\sigma(3) = r \sin \upsilon$$

The U, V, and W intersection points are defined by the following values of υ:

$$U : (1,2) : \upsilon = \theta - \alpha$$

$$V : (2,3) : \upsilon = 180^{\circ} - \arcsin \left[e/r \sin^2 1/2\, \theta + \sqrt{1 - \frac{e^2}{r^2} \sin^2 \frac{1}{2} \theta \cos \frac{1}{2} \theta} \right]$$

and

$$W : (1,3) : \upsilon = 180^{\circ} - \alpha$$

The brightness function $\sigma(\eta_1\ r_1\ \theta)$ has the representations:

I: $\sigma(\eta_1\ r_1\ \theta) = e - e\cos\theta - r\sin\upsilon - [r^2-(r\cos\upsilon - e\sin\theta)^2]^{1/2}$

II: $\sigma(\eta_1\ r_1\ \theta) = e$

III: $\sigma(\eta_1\ r_1\ \theta) = 2r\sin\upsilon$

5. Concluding Remarks

This concludes the exploratory analytic investigation of the brightness function proposed at the start of paragraph C. This investigation of the function $\sigma(\eta_1\ r_1\ \theta) = \sigma$ centered on the variation of σ with varying θ.

The variation of $\sigma(\eta_1\ r_1\ \theta)$ relative to the magnitude of the ratio e/r is left as a further task to be done (see Figure 15).

Before an analytic formulation of the brightness function $\sigma = \sigma(\eta_1\ r_1\ \theta)$ can be reduced to a numerical procedure whereby values of $\eta = \eta(\sigma_1\ r_\sigma\ \theta)$ for $\sigma = 1/10\ S$, S = 0, 1, ..., 9, 10, say, can be groundout, it is absolutely necessary to examine in further detail all the possible subdivisions of the regions U', V', W' and U, V, W for all possible values of η in $-R \leqq \eta \leqq R$, of r in $0 \leqq R \leqq R$, and of θ in $0 \leqq \theta \leqq 180^\circ$.

In those cases where the cloud radius R is very large compared to the optical depth of penetration, e, so that e/r can be quite small, $0 < r < R$, compared to unity, it might be possible to cut through the intricacies of branch cut decisions (inherent in the analytic approach), on the basis of some physical argument, so as to be able to sketch out the full isophote curves in the image plane, in some easy manner.

D. EXPERIMENTAL CHECK

It is the function of this section to check in a gross manner the general nature of the results calculated earlier. As an example the chemical release "Lily" of the Firefly program was selected. In this experiment 8 kilogram of 0.2 - 2.0μ aluminum oxide was released at 140 km under twilight conditions at 0408 CST, 21 July 1960. The initial diameter was 0.1 kms and grew slowly to a little over 1/2 kilometer at the end of one record. For the Mie scattering function at an $\alpha \sim 1.2$ the phase function is not too asymetric. This release was selected because of the availability of reasonable photographs of the early period before the cloud was optically thin. Moreover, the mathemetical and geometrical analysis although developed originally for isotropic scattering is also valid for assymetric scattering in the approximative model used. This is so because the demarcation involving the cross-cutting of two circular arcs with the original circle has for its scale in both directions the forward scattering optical depth. Consequently, the geometrical construction remains the same. However, the absolute brightness of the image would vary with the phase angle in a manner dependent upon the nature of the scattering function. All of the discussion assumes that the photographic set-up is adequate to picture the brightness level.

Figure 38 gives pictures of the early time history of the growth where the phase angle is estimated at (not given) between 70 and 130 degrees. The pictures resemble very closely some of the theoretical curves of the preceeding section. It is not considered appropriate to make exact calculations as of this time. However, it is pointed out that

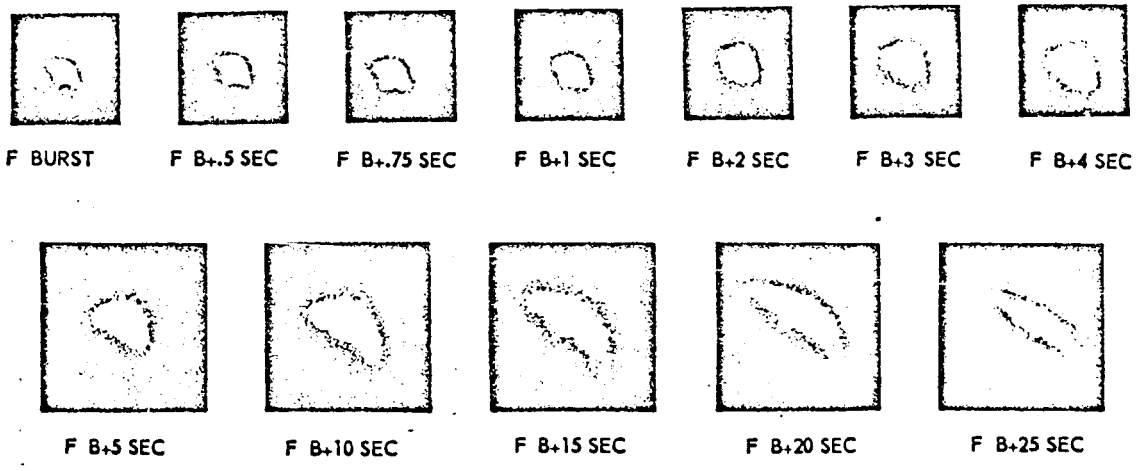

Figure 38. LILY

the shapes depicted in these photographs have previously been attributed to uneven bursting of the canister. The simplified analysis of this section would indicate that the morphology of such shapes is due purely to the scattering process and not to the anisotropy of the release. Moreover, a judgement can be made as to the optical depth of the cloud from the geometrical shape of the visible sector. From this the rate of growth can be deduced.